A MULTI-PHASE APPROACH TO TISSUE ENGINEERING OF THE TEMPOROMANDIBULAR JOINT

by

Catherine Hagandora

Bachelor of Science, Presbyterian College, 2009

Submitted to the Graduate Faculty of

Swanson School of Engineering in partial fulfillment

of the requirements for the degree of

Doctor of Philosophy

University of Pittsburgh

2014

UNIVERSITY OF PITTSBURGH

SWANSON SCHOOL OF ENGINEERING

This dissertation was presented

by

Catherine Kunkle Hagandora

It was defended on

July 11, 2014

and approved by

Stephen Badylak, D.V.M, Ph.D., M.D., Professor, Department of Surgery

Charles Sfeir, D.D.S., Ph.D., Associate Professor, Department of Oral Biology

Yadong Wang, Ph.D., Professor, Department of Bioengineering

Dissertation Director: Alejandro J. Almarza, Ph.D., Assistant Professor, Department of Oral Biology, Department of Bioengineering

A MULTI-PHASE APPROACH TO TISSUE ENGINEERING OF THE TEMPOROMANDIBULAR JOINT

Catherine Kunkle Hagandora, PhD

University of Pittsburgh, 2014

It is estimated that 10 million Americans are affected by temporomandibular joint (TMJ) disorders, a class of disorders encompassing symptoms such as jaw pain, functional disparities, and degenerative changes. In advanced cases, there is irreversible degradation of the articulating tissues of the joint. Due to the frequency and severity of these conditions, and the inadequacies of current replacement options, it is necessary to formulate tissue engineering strategies in order to restore TMJ anatomy and function. The objectives of this thesis were to further characterize the native TMJ fibrocartilage and identify effective methods and materials for tissue regeneration. As a first step, characterization of the native goat TMJ disc and condylar cartilage was performed. Bioactive magnesium ions and poly (glycerol sebacate) (PGS) were then investigated for their in-vitro potential to increase fibrocartilage production of goat costal fibrochondrocytes. Then, the response of human progenitor cells seeded in ECM scaffolds to mechanical stimulation was explored to better understand the in-vivo effectiveness of these scaffolds. Biomechanical, biochemical, and histological assessments were made to characterize both native and regenerated tissues. Gene expression analysis was also performed to determine the cellular response to mechanical stimulation within ECM scaffolds. The collagen content of the TMJ disc was found to be significantly greater than the condylar cartilage, while the opposite held for the glycosaminoglycan (GAG) and DNA content. The mandibular condylar cartilage, despite having significantly higher GAG content, is significantly less stiff than the TMJ disc

under compression. At high concentrations, magnesium ions allowed for fibrocartilage regeneration in-vitro, with constructs cultured in $MgSO_4$ exhibiting a significantly higher collagen type II/I ratio than the control. PGS was investigated as a mechano-transductive scaffold material for TMJ tissue engineering. It was shown that PGS is a substrate conducive to fibrochondrocyte infiltration and ECM regeneration, with scaffolds exhibiting near-native compressive properties after a culture period of 4 weeks. The mechanical properties of PGS also allowed for the transmission of compressive forces from the scaffold to the cells, impacting the patterning of collagen type I deposition. Similarly, within the bioactive environment of ECM scaffolds, compressive mechanical loading resulted in increased fibrochondrogenic gene expression of human bone marrow stromal cells. The results demonstrate that there is a set of culture conditions, including bioactive ions and/or compressive loading, and scaffolds that will stimulate cells to produce fibrocartilage, providing the foundation for tissue-engineered solutions to TMJ disorders.

TABLE OF CONTENTS

LIST OF TABLES

LIST OF FIGURES

PREFACE

I would like to gratefully acknowledge funding from the National Science Foundation for providing the financial support needed to complete this research.

This work would not have been possible without the contributions of several people. I would like to thank my committee: Drs. Badylak, Sfeir, and Wang for their knowledge and guidance in developing this thesis. To my mentor, Alejandro Almarza, it has been a privilege working with you. I am so appreciative of the time, energy, and enthusiasm you have devoted to guiding me in my research. I am inspired by your dedication to teaching and commitment to your students.

To my fellow students, faculty, and staff of the Center of Craniofacial Regeneration I thank you for providing such a supportive research environment throughout the course of my studies.

To my parents, Charles and Carol, I thank you for your constant encouragement and genuine interest in my scientific endeavors.

Finally to my husband, Nicholas, I am forever grateful for your unwavering support and commitment to my success. Our family is my constant source of inspiration and motivation.

1.0 INTRODUCTION

The objectives of this thesis are to further characterize the native temporomandibular joint (TMJ) fibrocartilage and identify effective methods and materials for tissue regeneration. As a first step, characterization of the properties of the articulating tissues of the joint is a necessary prequel to tissue engineering suitable constructs for replacement of damaged joint fibrocartilage. For regeneration, bioactive molecules and scaffolding choice are major players in improved outcomes. Magnesium has surfaced as a powerful ion to drive bone and cartilage regeneration, yet its effect on fibrocartilage is unknown. In order to understand fibrocartilage formation in-vitro, a good choice of synthetic scaffold is critical. In-vivo, extracellular matrix (ECM) scaffolds have shown great promise for fibrocartilage regeneration, but the interplay between cells and mechanical environment remains to be elucidated. These materials should have the potential to be utilized in tandem to understand and enhance fibrocartilage regeneration. Thus, four specific aims are used to characterize and engineer the fibrocartilage tissues of the joint:

Specific Aim No. 1: ***Characterization of goat TMJ fibrocartilage*****.** The objective of this aim is to characterize and compare the biomechanical and biochemical properties of the intermediate zone, medial, and lateral regions of the goat TMJ disc and mandibular condylar cartilage. The hypothesis is that there is a one-to-one correlation between the biomechanical and biochemical properties of the disc and condylar cartilage. Tissue cores are tested in unconfined compression,

and mechanical data are examined using the transversely isotropic biphasic model. The total collagen, glycosaminoglycan (GAG), and DNA content of the tissue regions are then determined.

Specific Aim No. 2: ***Exploring magnesium as a bioactive ion for fibrocartilage regeneration of the mandibular condyle*****.** While magnesium shows promise for bone and cartilage regeneration, its effect on fibrocartilage remains unexplored. The hypothesis is that magnesium will enhance fibrocartilage regeneration. This aim is an in-vitro approach to determining the effect of magnesium ion concentrations on fibrocartilage regeneration using goat fibrochondrocytes.

Specific Aim No. 3: ***Assessing poly (glycerol sebacate) (PGS) polymer as a synthetic fibrocartilage scaffold material for in-vitro fibrocartilage formation.*** Scaffolds for in-vitro tissue engineering, which act as substrates for cell infiltration and provide the necessary microenvironment to stimulate matrix deposition, are essential for understanding fibrocartilage formation. It is hypothesized that the elastomeric properties of poly (glycerol sebacate) PGS could potentially allow for the transmission of forces applied from the scaffold to seeded cells, which may promote not only the deposition of large quantities of ECM but also organization of the collagen ultrastructure. The first part of this aim is to assess the effect of cell seeding density of goat fibrochondrocytes in PGS scaffolds on the ECM production and biomechanical properties of the tissue-engineered constructs. The effect of mechanical stimulation and increased nutrient transport of cell-seeded PGS scaffolds on ECM production is also explored.

Specific Aim No. 4: ***Assessing porcine small intestinal submucosa (SIS) extracellular matrix (ECM) as a biologic TMJ disc scaffold for in-vivo regeneration.*** Porcine ECM scaffolds have shown exceptional fibrocartilage regeneration potential in-vivo. However, there is a lack of understanding of the effect of the mechanical environment on the regeneration potential of cells

migrating in the healing environment. In a simplified model of loading, uniaxial unconfined compression will be applied to scaffolds seeded with stem cells. It is hypothesized that compressive mechanical stimulation causes an increase in fibrochondrogenic gene expression of human stem cells seeded on ECM scaffolds.

The second chapter of this thesis discusses the current scientific and clinical evidence regarding TMJ disc removal both with and without graft replacement. After reviewing the literature from well-established animal studies to clinical findings published in the past 10 years, it was found that the results of animal models for discectomy corresponded to the clinical findings seen in patients at the longest follow up of 10 years. Overall, there is adaptive remodeling or degeneration of the TMJ following discectomy. Additionally, there is some reduction in pain but with variable amounts of dysfunction remaining following disc removal. Autogenous graft replacements reduce crepitus but have not demonstrated long term efficacy. These findings motivate further research into tissue engineering strategies for damaged TMJ fibrocartilage.

The third chapter describes Specific Aim 1, characterization of the native goat TMJ fibrocartilage. The goat is a feasible model for TMJ regeneration approaches, but its native properties have not been fully characterized. Samples taken mediolaterally from three regions of the TMJ disc and mandibular condylar cartilage are tested in unconfined compression at strain levels ranging from 10-50% and then assessed for biochemical content. Both tissues are tested to observe any possible regional correlations in mechanical or biochemical properties between the two tissue types. Due to the transverse arrangement of collagen fibers in both the TMJ disc and the surface of the mandibular condylar cartilage, the transversely isotropic biphasic model is applied to describe tissue behavior in unconfined compression.

Chapter 4 describes Specific Aim 2. In chapter 4, the in-vitro effect of pure magnesium on TMJ fibrocartilage regeneration is investigated. Goat costal fibrochondrocytes, which have produced the highest in-vitro collagen per wet weight ratio to date for fibrochondrocytes, are used in a scaffoldless tissue engineering model to determine the effect of magnesium on ECM production. Magnesium ions, both $MgCl_2$ and $MgSO_4$, are tested at three concentrations: 20, 50, and 100 mM in order to determine how a broad range of magnesium ion concentrations affect the fibrocartilage regeneration process.

Chapters 5 and 6 describe Specific Aim 3, examining the potential of PGS, a biocompatible, biodegradable elastomer, as a porous scaffold material for TMJ fibrocartilage. In chapter 5, the ideal seeding density of goat fibrochondrocytes on PGS scaffolds is investigated. Three concentrations of 25, 50, and 100 cells/ml of scaffold are investigated at 3 time points: 24 hours, 2 weeks, and 4 weeks in order to determine how initial seeding density affects ECM production over time. In chapter 6, spinner flask culture and dynamic compressive mechanical stimulation are explored as methods of improving cellular distribution and ECM organization within PGS scaffolds. The spinner flask bioreactor system is utilized to help improve nutrient diffusion throughout the scaffold during the culture period. Dynamic stimulation is applied to help improve the patterning of collagen deposition into a structure more closely resembling that of the native TMJ disc.

Chapter 7 describes the in-vivo behavior of both pure magnesium and PGS in the porcine condyle. A defect is created in the posterior aspect of the mandibular condyles of 3 month old female pigs. The defects are packed with either pure magnesium rods or PGS. At 1 month post-implantation, micro-computed tomography (micro-CT) analysis is performed in order to visualize both magnesium degradation and new bone formation.

Chapter 8 describes Specific Aim 4. Human bone marrow stromal cells are seeded on porcine SIS-derived ECM scaffolds and subjected to both biochemical and biomechanical stimulation. Basal passage media and chondrogenic media were used to determine the chemical effect on fibrocartilage gene expression. Both constant and dynamic loading mechanisms are also investigated in order to further elucidate the effect of the interaction between cells, scaffolds, chemical stimulants, and loading mechanism on the expression of fibrochondrogenic genes.

In summary, the following chapters describe the potential of various scaffolding materials to help regenerate fibrocartilage of the TMJ. These materials are tested using both in-vitro model systems and in-vivo. The mechanical and biochemical results are compared against the native values established in Specific Aim 1. The central hypothesis of this thesis is that there is a set of culture conditions, including bioactive ions and/or compressive loading, and scaffolds that will stimulate cells to produce fibrocartilage.

2.0 TMJ DISC REMOVAL: COMPARISON BETWEEN PRECLINICAL STUDIES AND CLINICAL FINDINGS[1]

2.1 INTRODUCTION

TMJ pathology and treatments

The clinical necessity for investigation stems from the fact that temporomandibular joint disorders (TMDs) may affect over 10 million Americans [1], with up to 70% of people with TMJ disorders suffering from displacement of the TMJ disc, or 'internal derangement' of the TMJ [2]. Internal derangement can be described as an abnormal positional relationship of the disc relative to the mandibular condyle and the articular eminence, in which the disc is generally anteriorly displaced, possibly resulting in pain, joint clicking, locking of the joint, and degeneration of the surrounding tissues.

Patients with severe TMDs, or joint pain and dysfunction that does not respond to nonsurgical treatments, resort to surgical interventions including disc repositioning, disc removal, and replacement of the condylar, fossa, or both components with a prosthetic device.

---

[1]Hagandora, C.K. and A.J. Almarza, *TMJ disc removal: comparison between pre-clinical studies and clinical findings*. J Dent Res, 2012. **91**(8): p. 745-52.

When the TMJ disc is too damaged to be repositioned, and there is no apparent condylar degeneration, surgeons will choose to perform a discectomy (disc removal).

The effectiveness of discectomy in alleviating the symptoms of TMDs remains controversial. The crux of the debate is whether or not discectomy is a safe long-term treatment option for patients suffering from TMDs, or if surgical removal of the disc creates an environment more susceptible to joint degeneration. The implementation of animal models has been a critical step in examining this process, but the comparability of joint remodeling observed in animals following discectomy to that seen in humans merits further investigation. While comprehensive reviews exist regarding the use of animal models for TMJ degeneration [3] as well as general clinical outcomes of discectomy [4], this review will examine established animal models for discectomy and critically assess the validity of these models in light of recent longer term clinical results in patients. In the first part of this review, animal models will be discussed in sequence of mid-sized (rabbit, guinea pig) and large (sheep, primate) models, focusing on the results of both. (**Table** 1) The second part of this review will focus on clinical findings in patients receiving discectomy alone or with biologic graft materials in the past 10 years. We will then focus on a broader range of investigations that use imaging as an assessment tool following discectomy. The implications of all sets of findings will then be evaluated. The methodology utilized in our literature search is outlined in **Figure 1.**

Table 1. Animal models for discectomy describing the animal model size, graft material used, age/weight, total number of animals used, last time point assessed, and whether or not a bilateral/unilateral surgery was performed.

Size	Graft	Animal	Age/weight	n=	Last Time Point	Bilateral/ Unilateral	Authors	Year
Medium	None	Rabbit	3-3.5kg	12	3 months	Unilateral	Sato *et al*.	2002
Medium	None	Rabbit	3-3.5kg	12	3 months	Unilateral	Sato *et al*.	2002
Medium	None	Rabbit		15	20 weeks	Unilateral	Dimitroulis *et al*.	2006
Medium	Auricular Cartilage	Rabbit	14 weeks (3-4 kg)	30	24 weeks	Unilateral	Takatsuka *et al*.	1996
Medium	Collagen/Dermal Graft	Rabbit	Adult	20	36 weeks	Bilateral	Feinberg *et al*.	1995
Medium	Lyophilized Auricular Cartilage	Guinea Pig	Adult	6	24 weeks	Unilateral	Ioannides *et al*.	1988
Medium	Sternal and Auricular Cartilage	Guinea Pig	Adult	15	3, 6, 12, 24 weeks	Unilateral	Ioannides *et al*.	1988
Large	None	Monkey	Adult	5	12 months	Unilateral	Yaillen *et al*.	1979
Large	None	Monkey	A least 48 months (1970-3100g)	14	6 months	Unilateral	Bjornland *et al*.	1999
Large	Auricular Cartilage	Monkey	Adult	4	24 weeks	Bilateral	Tucker *et al*.	1990
Large	Fascia Lata graft	Monkey	Adult	8	18 months	Unilateral	Tong *et al*.	2000
Large	Auricular cartilage and pedicled temporalis myofascial	Monkey	Adult	8	18 months	Unilateral	Tong *et al*.	2000
Large	Temporalis Muscle	Sheep	Adult (2 years)	24	24 weeks	Bilateral	Thyne *et al*.	1992

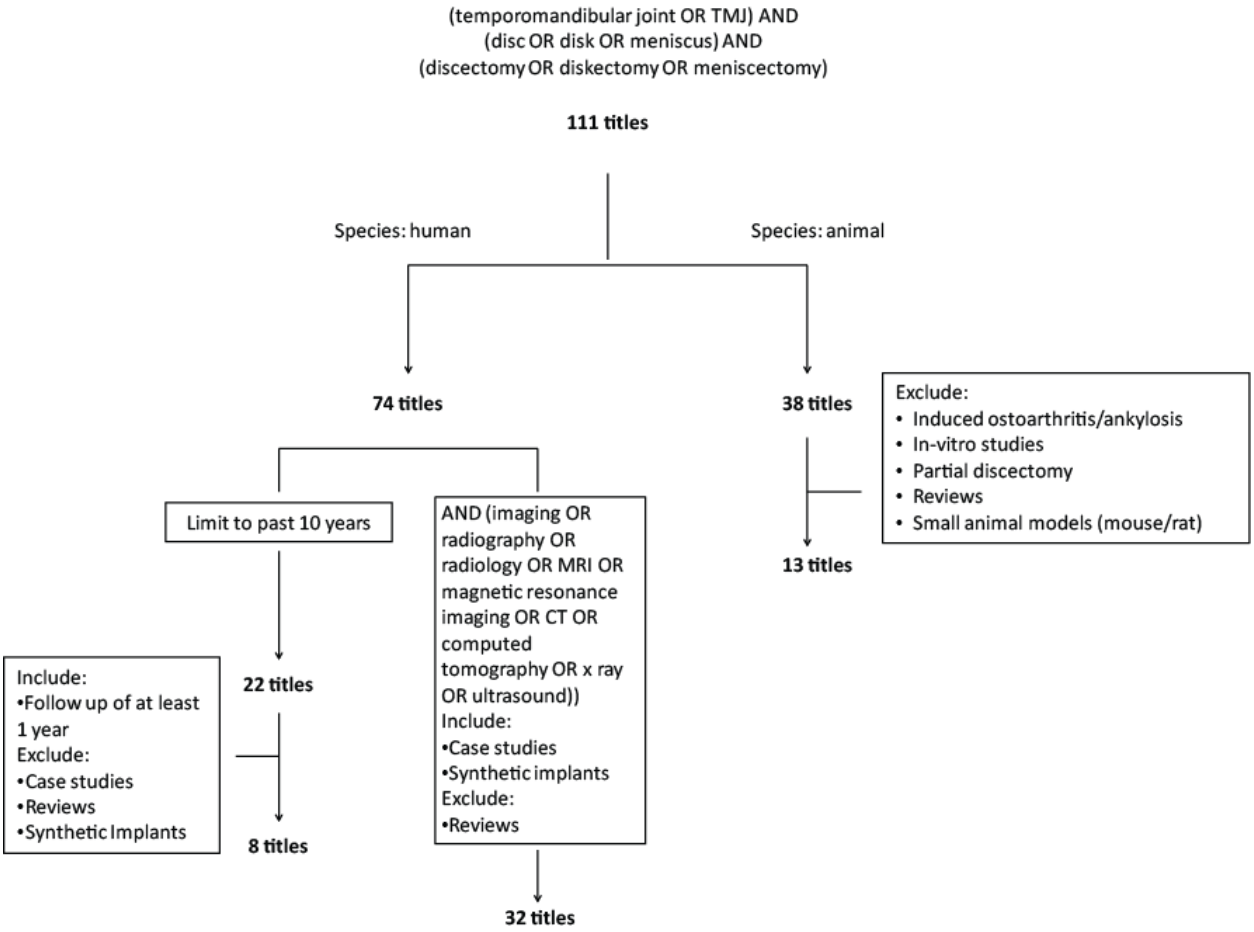

Figure 1. Schematic of manuscript inclusion and exclusion criteria. All searches were performed using PubMed.

2.2 MID-SIZE ANIMAL MODELS

Mid-size animal models, such as rabbit and guinea pig, have been used to further explore the effects of discectomy on the remaining joint tissue [5-7] (**Table 1**). The results of the mid-size animal discectomy studies show that disc removal alone can result in thickening of the fibrous layer of the condyle and articular eminence, changes in collagen fiber density, and flattening of the condyle on the unoperated joint [5-7]. The general response is remodeling of the articulating surfaces, such as thickening of the condylar cartilage, to compensate for the loss of the disc. While these studies show, qualitatively, the changes that take place following discectomy, they lack evidence of change of function of the tissue, which could be verified using mechanical testing.

Mid-size animal models have also been used to been used to examine the effect of discectomy with graft replacement [8-11] (**Table 1**). In a rabbit model, it has been shown that although auricular cartilage grafts developed perforations or fragmentations, animals that did not receive a graft showed more intense degenerative changes with flattening of the condyle and the eminence compared to the rabbits that did receive the graft [8]. The rabbit model has also been used to investigate the effectiveness of dermis and collagen graft replacements, and, although they were resorbed by 8 weeks, the authors concluded that both grafts seemed to prevent early degenerative changes in the joint [9]. The effect of auricular cartilage grafting was also investigated in a guinea pig model and it was found that at 24 weeks post surgery, most of the implant had been resorbed and replaced by young fibrous connective tissue completely separated from the surface of the condyle and fossa, with newly formed cartilage observed at the rostral part of the new fibrous structure. The articulating surfaces exhibited either slight or no major changes in the histological structure [10]. The use of fresh autogenous sternal grafting was also

examined in adult female albino guineas pigs with the authors concluding that autogenous sternal cartilage should not be recommended as a replacement material due to a difficulty in cutting to shape and tendency to warp [11].

The mid-size animal models discussed provide important information regarding the joint tissue response to discectomy with graft replacement. While certain graft materials appear to protect against degeneration when compared to discectomy alone, it is unclear if fibrous tissue formation around implants could lead to fibrous ankylosis or other functional problems at later time points. Additionally, the remodeling that takes place in response to discectomy could be an indicator of adaptation and not degeneration. If so, the necessity of using graft materials, which could lead to unwanted side effects, should be validated. The clear limitations of the use of the rabbit and guinea pig models are the distinct differences in anatomy and masticatory frequency [12]. **(Figure 2**) However, use of a mid-size model is a critical springboard for studies using larger, more relevant animal models to investigate the effect of discectomy alone and with graft replacement.

2.3 LARGE ANIMAL MODELS

Larger animal models have also been employed to study the effect of discectomy [13, 14] (**Table 1**). Yaillen *et al.* studied the effect of discectomy in five mature *Macaca fascicularis* monkeys and found that at 12 months, the operated joints exhibited severe degenerative changes signified by bone resorption, broadening and flattening of the condylar head, and ankylosis between the condyle and temporal bone [13]. The effect of discectomy on primate joints was further evaluated by Bjornland *et al.* and at 6 months post surgery a variety of joint changes were

observed including fibrous ankylosis, condylar flattening, absence of cartilage on the condyle or fossa, absence of cartilage lining of the condyle and fossa, formation of fibrous tissue, newly formed bone, and increased cartilage thickness [14]. The findings in this primate model correspond with those of the mid size animal models where discectomy results in substantial destruction of the articulating cartilage surfaces.

The discussed discectomy studies provide valuable insight into the process of joint degradation following disc removal in a relevant animal model [13, 14]. The non-human primate studies demonstrate that disc removal does result in joint tissue remodeling, which does not seem to result in a significant change in joint function. The sex of the experimental animals in these studies is not specified or discussed. Clarifying differences, if any, in joint response to discectomy with regard to sex is a vital step in understanding the gender polarity of the disease and propensity for females treated with disc removal to develop osteoarthritis.

Primate models have been utilized to determine the effect of biologic grafts on the TMJ [15-17] (**Table 1**). Tucker *et al.* [15] investigated the effect of discectomy and autogenous auricular cartilage implantation in four adult *Macaca fascicularis* monkeys. Both sides of the joint underwent discectomy and condylar shaving but only one side received the cartilage graft. At 24 weeks, the control side exhibited layers of dense fibrous connective tissue disrupted in areas along with projections of bone into the joint space. In the graft group, the condylar surface appeared smooth with a covering of fibrous connective tissue and the grafts were closely adapted to the fossa showing viable chondrocytes. The study shows that auricular graft might be a viable option for patients with degradation of both the articulating cartilage and TMJ disc.

In a study by Tong *et al.* [16], the effect of discectomy with and without replacement with a *fascia lata* graft was observed in 8 adult *Macaca mulatta*. The graft did not survive after

implantation. At 18 months, the graft did not protect against morphological changes of the condyle and glenoid fossa, thickening of the articular surface tissue, osteoarthritic changes, or fibrous ankylosis. A follow up study by Tong *et al.* compared auricular cartilage graft to pedicled temporalis myofascial graft in 8 rhesus monkeys [18]. At six months post surgery, the cartilage graft or remnants could not be identified. Auricular cartilage did not survive after grafting and did not induce reformation of the articular disc (except in 6 month old group). The pedicled temporalis muscle graft formed a band of fibrovascular tissue which appeared to remain intact under normal functional loads. The authors concluded that myofascial graft has the greatest potential to restore a "disc-like" structure while also protecting against osteoarthritic changes in the joint. The sheep model has been used to observe the effect of graft replacement following discectomy. Thyne *et al.* also investigated the use of the temporalis muscle flap as a replacement for the TMJ disc in sheep [17]. At 24 weeks, the joints were empty and the condyle and fossa were in close contact. The authors concluded that the temporalis muscle is not a good replacement material, and that replacement of the TMJ disc following discectomy is not necessary to prevent ankylosis.

The large animal discectomy studies utilizing graft replacement suggest that biologic grafts may provide some protection against the progression of osteoarthritis [15-17] (**Table 1**). However, the regeneration potential of many of these grafts is limited, suggesting that they might just serve to delay the remodeling that would occur in discectomy alone. Based on the current animal studies, there is little evidence to support the advantage of graft material to replace the TMJ disc when compared to discectomy alone. It should also be noted that the described large animal models are relatively dated (1979-2000), and the porcine model has recently been

regarded as the best model for the human TMJ and should be considered in future large animal studies [19]. (**Figure 2**)

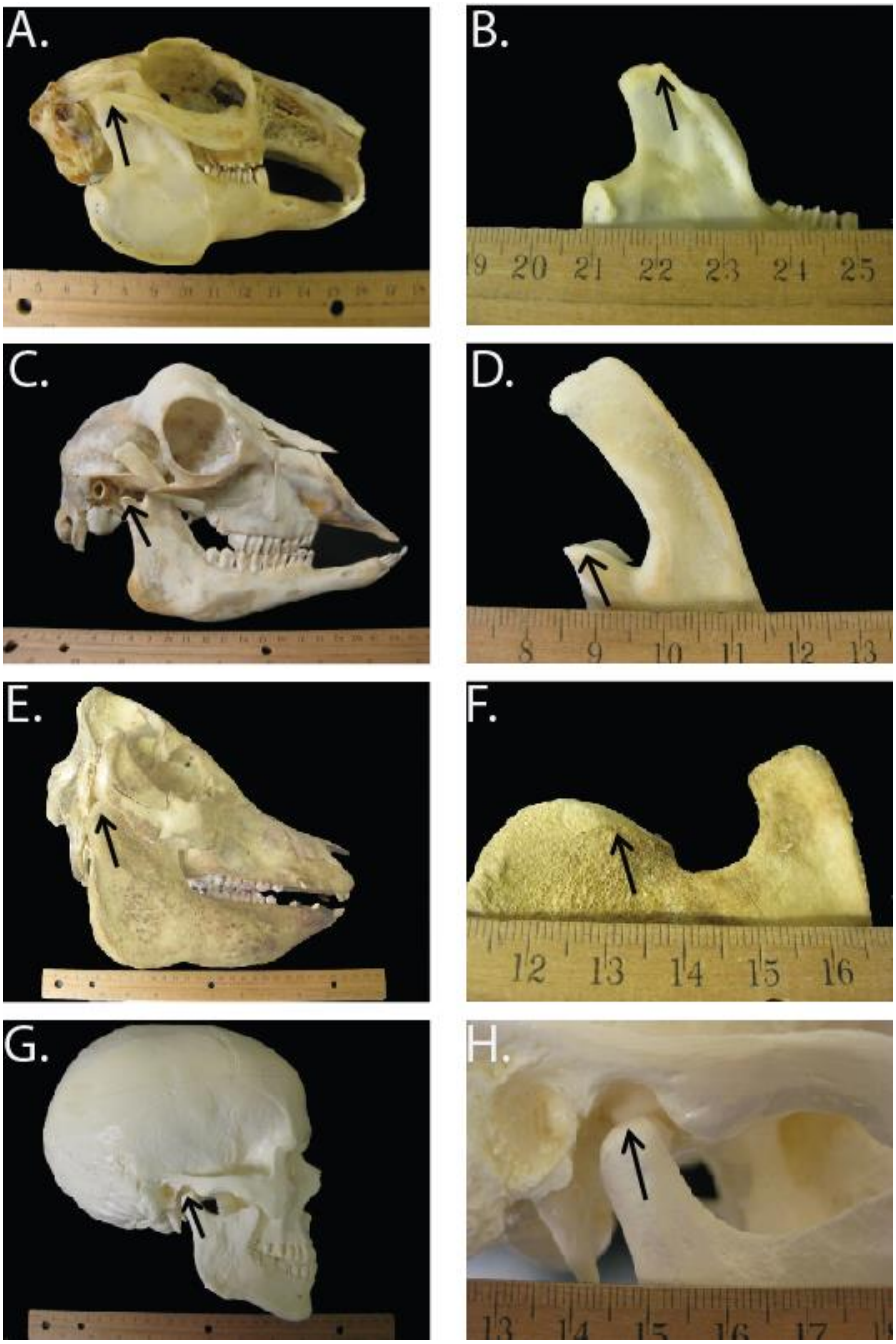

Figure 2. Anatomy of rabbit (a), goat (c), pig (e) and human (g) skulls. Mandibular condyles of the rabbit (b), goat (d), pig (f) and human (h) skulls. Arrows are pointing to the head of the mandibular condyle.

2.4 CLINICAL FINDINGS

2.4.1 Recent Investigations (past 10 years)

2.4.1.1 Discectomy alone

While notable findings have been published prior to 2002, such as comparisons between the effectiveness of discectomy and other surgical techniques [20], we will focus on the most up-to-date manuscripts for this portion of the review. Several longer term follow up studies have been performed to determine the impact of discectomy on joint pain and function since 2002 (**Table 2**). Prior to performing removal of the disc without graft replacement, magnetic resonance imagining (MRI), arthrography, and arthrotomography have been used to confirm disc displacement [21-23]. It has been shown that discectomy alone does result in an increase in chewing ability as well as a decrease in joint pain after 1-10 years follow-up [21-23]. A significant increase in maximal mouth opening ability following surgery has also been reported [22, 23]. The most notable negative finding following surgery has been crepitus, or joint noise [21-23]. Studies have also been performed comparing discectomy to other common surgical interventions. Hall *et al.* did a prospective comparison of four TMJ operations: arthroscopy, condylotomy, discectomy, and disc repositioning, revealing that pain relief was significant at 1 month post surgery and statistically indistinguishable between procedures [24]. The visual analogue scale chewing score as well as vertical range of motion (opening between the incisors) were improved at 1 year and indistinguishable by operation. The study calls into question the superiority of discectomy as a treatment method for painful TMD over less invasive procedures.

The discussed studies indicate an overall positive longer term response to discectomy in a majority of patients [21-24] (**Table 2**). However, a limitation of the clinical studies is the use of a small number of patients with varying clinical backgrounds. While the literature generally describes that the indication for surgery was internal derangement with pain and/or dysfunction unresponsive to nonsurgical treatments, specific details regarding the origin of the disorder are often unavailable. While exclusion criteria were used in these studies to help homogenize the patient population, there are inherent discrepancies in patient age and history which will impact the results. Using a small number of surgeons calls into question whether or not the findings were the result of the skill of the surgeon versus the effectiveness of the procedure itself.

Variations in postsurgical treatment (**Table 2**) can also have a substantial impact on the overall success of discectomy. In the discussed clinical studies, some form of physical therapy and/or soft food diet was always utilized following the discectomy procedure [21-24]. It is important to take into account the possibility that physical therapy as well as the implementation of a soft food diet immediately following surgery could impact the remodeling process, limiting the comparability of clinical results to animal studies where such post-surgical therapies are rarely employed.

Table 2. Clinical studies for discectomy describing the graft material used, sex, age, study size, longest time point assessed and whether or not a bilateral/unilateral surgery was performed.

Graft	Sex	Mean Age (years)	n=	Longest Follow Up Time	Indication for surgery	Bilateral/ Unilateral	Postoperative Treatment	First Author	Year
None	m=3 f=12	32	15	years	Disc displacement, unsuccessful nonsurgical treatment for at least 6 months	Unilateral	Physiotherapy	Nyberg *et al.*	2004
None	m=2 f=28	36.3	30	60 months	Pain, dysfunction, disc displacement, lack of improvement with nonsurgical therapies	Both	Soft food diet for 4-6 weeks, self-administered opening motion exercises at 1 week after surgery, Self-directed physical therapy	Miloro *et al.*	2010
None	m=5 f=24	37.2	29	10 years	Reduced mandibular motion, pain and dysfunction not alleviated by nonsurgical treatments, disc displacement with or without reduction	Both	Soft food diet 14 days postoperatively Physical therapy	Bjornland *et al.*	2003
None	92-100% female	30.8-41.7	54	1 year	Internal derangement and intolerable pain after standard medical treatment	Both	ROM exercises, splints, physical therapy, and/or home exercises depending on surgery	Hall *et al.*	2005

Table 2. (Continued)

Dermis	m=4 f=25	42	29	79 months	Severe internal derangement, pain and dysfunction not responding to at least 6 months of nonsurgical treatment	Both	Physiotherapy beginning 10 days after surgery	Dimitroulis *et al.*	2005
Dermis-fat	m=1 f=27	51.5	28	7 years	Severe internal derangement not responding to at least 6 months of preliminary treatment measures	Both	Physical therapy beginning 7 days after surgery	Dimitroulis *et al.*	2011
Dermis-fat	Post-surgical m=1 f=31 Pre-surgical m=3 f=26	Post-surgical 45.4 Pre-surgical 41.6	61	6 years	Intolerable joint pain and dysfunction not responding to at least 6 months of nonsurgical treatment	Unilateral		Dimitroulis, *et al.*	2010
Auricular Cartilage	m=1 f=32	41.1 Discectomy 27.6 Discoplasty	22 Discectomy 11 Discoplasty	1 year	Intra-articular pathology and unsuccessful nonsurgical treatment for at least 6 months	Both	Pharmacotherapy and physical therapy	Krug, *et al.*	2004

2.4.1.2 Discectomy and Graft

While many surgeons perform discectomy alone, several clinicians opt for the placement of autogenous grafts between the condyle and skull. Dimitroulis *et al.* examined the effect of discectomy with autogenous dermis used as an immediate interpositional graft in patients with advanced internal derangement of the TMJ [25] [26] [27]. Using the visual analogue scale, there was a 66% improvement in pain and 42% improvement in mandibular function following surgery [25]. Orthopantomograms were used to examine the morphology of the condylar head, revealing that the graft did not prevent remodeling of the joint, and that the only advantage of the graft is the elimination of crepitus when compared to discectomy alone [4, 25]. However, it was shown that discectomy with dermis graft replacement does result in a statistically significant improvement in pain, diet and chewing, mood, anxiety, and general health in the postsurgical group when compared to the presurgical group [27]. Discectomy with auricular cartilage graft replacement has also resulted in a significant reduction in pain and a significant increase in maximum interincisal distance at 1 year post surgery [28].

These studies show that the use of autogenous graft material may help to reduce the onset of crepitus resulting from discectomy alone while also delaying degeneration. However, there is still little evidence to support the long-term benefit of these interpositional materials when compared to discectomy alone. This should be further examined to validate the use of these grafts and justify the additional donor site morbidity. Furthermore, imaging modalities should be utilized more frequently and consistently to observe joint remodeling in response to discectomy with and without graft replacement, and not solely for diagnosis.

2.4.2 Imaging to assess surgical outcomes

2.4.2.1 Discectomy alone

Unfortunately, none of the recent studies describing discectomy alone use imaging for assessing the joint response following surgery. In order to more effectively compare the results from animal studies to clinical findings this section will focus on discectomy studies published since the year 1985 using imaging as an assessment tool to investigate structural changes that occur in the TMJ after discectomy. These imaging techniques include radiography, arthrography, tomography, and MRI. MRI has gained popularity as a diagnostic tool for TMD patients [29-31]. Studies have shown that MRI is useful at predicting certain pathologies in the joint such as degeneration [32], bone remodeling [25, 33], internal derangement [34], synovial chondromatosis [35], exostosis [36], hard tissue changes [37], disc perforation [33, 38], osteochondritis dissecans or avascular necrosis [39] and risk factors for surgery [40]. However the use of MRI still requires careful interpretation when used as a diagnostic tool since tissues can easily be misrepresented [41]. Case studies also demonstrate the usefulness of imaging techniques for more atypical diagnoses such as identifying metallic foreign bodies in the joint [42], ossified discs [43], or synovial chondromatosis [44].

There is conflicting evidence regarding the effect of discectomy on degenerative changes in the TMJ. While it has been reported that discectomy alone results in no radiographic changes in the joint [45], there are many studies describing radiographic evidence of joint remodeling following discectomy. These results are consistent with the changes in morphology observed in the discussed animal studies. This remodeling often presents itself as flattening of the condyle and/or fossa, sclerosis, and the presence of osteophytes [46-51]. It has also been shown that new tissue formation occurs between the condyle and fossa following discectomy, possibly acting as

a “pseudodisc” [36]. There are conflicting results regarding the correlation between radiographic changes in the joint structure and pain following surgery. While there is generally a reduction in pain following the surgical removal of the disc, patients with pain after discectomy exhibited signs of fibrous adhesions on MRI [52, 53]. Similarly, while it has been reported that discectomy alone results in adaptive remodeling of the joint that does not interfere with overall surgical success in terms of pain and function, a positive correlation between patients’ overall pain and radiographic scores has also been observed [47]. Changes such as narrowing of the joint space and osteophyte formation are accompanied by increased aggrecan/cartilage oligomeric matrix protein, indicating that this remodeling process may lead to osteoarthritis of the joint [37]. Furthermore, conflicting results also exist as to whether or not unilateral discectomy results in morphological changes in the opposing joint. Widmark *et al.* found moderate to severe osteoarthrotic changes mostly confined to the operated side of the joint [48]. However, Takaku *et al.* found that bony changes were present in non-operated joints at an average follow up of 20 years post surgery [49]. The overall impact of discectomy on the development of pain and osteoarthritis remains controversial.

2.4.2.2 Discectomy and Graft

While a majority of the discectomy studies using imaging as an assessment focus on discectomy without graft replacement, synthetic graft replacements, such as silicone sheets [54], have been used and resulted in little improvement in joint function following surgery. Polytetrafluoroethylene disc replacements resulted in severe radiographic changes in the joint as well as foreign body giant cell reaction [55]. The use of Proplast Teflon interpositional implants also resulted in symptomatic joints with condylar resorption [56] as well as implant migration and fragmentation accompanied by severe condylar, glenoid fossa, and eminence remodeling

changes [57]. Similarly, Dacron-reinforced silicone caused bone destruction and foreign body response [58].

Fewer studies using imaging as an assessment tool are available to describe morphological changes in the joint following discectomy with autograft replacement. Dermis grafting has shown to result in a reduction of pain, increase in function, decrease in crepitus and increase in quality of life following surgery [25] [27]. However, dermal grafts were unable to be detected using MRI at 6-23 months post surgery [59]. Due to the wide use of autografts for TMJ disc replacement, more studies using imaging as an assessment tool are needed to validate the use of these materials and their ability to prevent osteoarthritis in the joint.

2.5 INFERENCES FROM ANIMAL MODELS TO HUMAN FINDINGS

The discussed discectomy and discectomy with graft replacement studies provide insight into the predictive power of animal models for projecting changes in human joints. Many of the studies using imaging to assess the TMJ after discectomy are consistent with the findings observed in animal models with both exhibiting adaptive remodeling of the articulating surfaces of the joint, mainly destruction or resorption of the cartilage, with changes in joint function.

The recent clinical studies showed that the mean age in years of patients receiving discectomy was in the 30s and early 40s, with the majority being female. Although the authors of the longer term clinical studies state generally positive outcomes to discectomy with and without graft replacement, it is important to note that many of the patients still suffered from different degrees of pain and joint dysfunction and no imaging was performed to assess the

healing of the TMJ. The lack of imaging makes it hard to compare the recent results to the animal models.

The discussed discectomy models in rabbit, sheep, and monkey have focused on gross morphological/histological assessments, and were not designed to characterize the fundamental altered joint movement (kinematics) driving degeneration nor the functional consequences. While clinical results provide relevant information regarding pain and end of range motion, more radiographic evidence is needed to more closely examine changes in joint structure and path of joint movement that occur especially with the use of grafting material. Imaging modalities should be utilized more consistently in both animal and human studies to help quantify changes in joint kinematics.

The discectomy and use of graft replacement results seen in animals tend to mirror those seen in humans. There is a general consensus that the use of graft material does retard the onset of degenerative changes in the joint. However, the currently used graft materials in both animals and humans have a short lifespan, and there is little evidence to support the long term benefit of these interpositional materials. The limited success of autogenous graft material as well as the additional site morbidity required by their use reaffirms the need for tissue engineered devices to regenerate the lost disc, restore mobility, reduce pain, and eliminate the onset of crepitus. In conclusion, animal models provide valuable insight into the joint changes that occur as a result of discectomy, and should be considered as an essential step in the validation of tissue engineered disc replacements to treat patients requiring a discectomy.

3.0 A COMPARISON OF THE MECHANICAL PROPERTIES OF THE GOAT TEMPOROMANDIBULAR JOINT DISC TO THE MANDIBULAR CONDYLAR CARTILAGE IN UNCONFINED COMPRESSION[2]

3.1 INTRODUCTION

The temporomandibular joint (TMJ) is a synovial, bilateral joint formed by the articulation of the condyle of the mandible and the articular eminence and glenoid fossa of the temporal bone. It is estimated that 10 million Americans are affected by TMJ disorders (TMDs), a term encompassing a variety of conditions which result in positional or structural abnormalities in the joint [1]. Indications of TMDs can include pain, clicking, locking, headaches, joint pain/tenderness, restricted range of motion, and painful mastication [60]. While in many instances the cause is unknown, 11% of individuals with TMJ disorders have symptoms of TMJ osteoarthrosis [61], a pathology which can lead to a cascade of problems resulting from functional and morphological changes in the joint. [62] Additionally, up to 70% of people with TMJ disorders suffer from displacement of the TMJ disc, or 'internal derangement' of the TMJ

[2] Hagandora, C.K., T.W. Chase, and A.J. Almarza, *A comparison of the mechanical properties of the goat temporomandibular joint disc to the mandibular condylar cartilage in unconfined compression.* J Dent Biomech, 2011. **2011**: p. 212385.

[2]. Due to the frequency and severity of these conditions, it is necessary to formulate a more comprehensive understanding of the role of healthy articulating tissues in TMJ function.

The primary function of the TMJ is to facilitate mandibular motion. The fossa remains stationary throughout jaw movement, while the mobile portions of the joint include the condyles of the mandible. A fibrocartilage disc is positioned between the inferior surface of the articular eminence and the superior surface of the mandibular condyle. The TMJ disc helps joint motion by distributing compressive, tensile, and shear forces [63]. The TMJ disc has a biconcave geometry and the primary extracellular matrix (ECM) components of the disc are collagen, proteoglycans, and elastic fibers. The mandibular condyles consist of bone with a fibrocartilage layer on the articulating surface. The mandibular condylar cartilage (MCC) is considerably thinner than the TMJ disc [64-67], lies adjacent to subchondral bone, and possesses a distinct zonal organization.

Characterization of the properties of the articulating tissues of the joint is a necessary prequel to understanding the process of pathogenesis as well as tissue engineering suitable constructs for replacement of damaged joint fibrocartilage. In tissue engineering approaches for fibrocartilage, goat costal chondrocytes have proven to be a viable cell source for scaffoldless tissue engineering constructs, due to their production of high quantities of collagen and GAG [68, 69]. These studies show the potential for the goat as a tissue engineering model. However, a comprehensive mechanical characterization has not been performed. Furthermore, the current literature lacks a one-to-one comparison of the regional compressive behavior of the goat MCC to the TMJ disc. Since these tissues work synchronously during mandibular movement, a comparison of their properties is necessary to provide insight into how the articulating surfaces of the joint work as a unit.

To date, a phenomenological model has not been utilized to describe the unconfined compressive behavior of the goat TMJ tissues. The TMJ disc and MCC in other species have been characterized as highly organized hydrated, porous, and permeable solid extracellular matrix tissues [70-72]. The biphasic theory has been shown to successfully model the behavior of articular cartilage, a similar tissue to the disc and MCC, by applying two distinct fluid and solid phases [73]. However, it is known that the fibers of the TMJ disc run anteroposteriorly in the medial, lateral, and intermediate zones [74]. Furthermore, the most superior zone of the MCC has also been shown to possess a transverse collagen arrangement [75]. Taking into account this fiber alignment, the transversely isotropic biphasic model may provide an accurate account for the mechanical behavior of TMJ fibrocartilage when exposed to compressive forces [76].

The aim of this study was to characterize and compare the intermediate zone, medial, and lateral regions of the goat TMJ disc and MCC under unconfined compression. A simple mechanical analysis was used to calculate the percent relaxation and tangent modulus of the various tissue regions. Additionally, curve fitting the experimental data to the transversely isotropic biphasic model allowed for determination of transverse and axial Young's moduli, transverse and axial Poisson's ratios, and tissue permeability. Additionally, biochemical analysis was performed to determine the comparative collagen, GAG and DNA content of the various regions. We hypothesized that the transversely isotropic biphasic model can be used to describe the stress relaxation behavior of both the TMJ disc and MCC in unconfined compression. The results will provide for a more comprehensive understanding of the mechanical behavior of the articulating tissues of the TMJ.

3.2 METHODS

3.2.1 Mechanical testing

Eight skeletally mature Boer goat heads were obtained from a local abattoir and dissected to isolate the disc and MCC within 24 hours of death. A 4 mm circular biopsy punch was used to obtain the medial, lateral, and intermediate sections from the disc and condylar cartilage. (**Figure 3**) Specimens were wrapped in gauze, wetted in phosphate buffered saline (PBS) and stored at -20˚C until testing. This method of storage was utilized because it has previously been shown to have no effect on the material properties of the porcine TMJ disc [77]. Prior to testing, samples were allowed to equilibrate for 1 hour in PBS. The tissue punches were then attached to a compression platen using cyanoacrylate with the inferior surface of the disc and the superior surface of the condyle facing up. The specimen diameter was measured prior to testing using digital calipers. To estimate specimen height, force was applied to the sample until reaching 0.05 N, at which point the crosshead position was noted and the platen was immediately removed. The water bath was then filled with PBS and the thermocouple was set to 37˚C prior to testing. The MTS Insight® was used to measure changes in force throughout the test. The upper platen was lowered within 0.1 mm of the determined specimen height and a preload of 0.05 N was applied for 30 min. The height at the end of the preload was taken to be the height of the specimen and was utilized in subsequent calculations. The specimens then underwent 10 cycles of preconditioning at 9%/min until 10% strain was reached. The strain rate parameter was determined by Sergerie *et al.* for applying the transversely isotropic biphasic model to cartilage [78]. Immediately following preconditioning, a series of five stress relaxation tests were

performed. The samples were compressed in 10% increments until 50% strain was reached, and were allowed to relax for thirty minutes between increments.

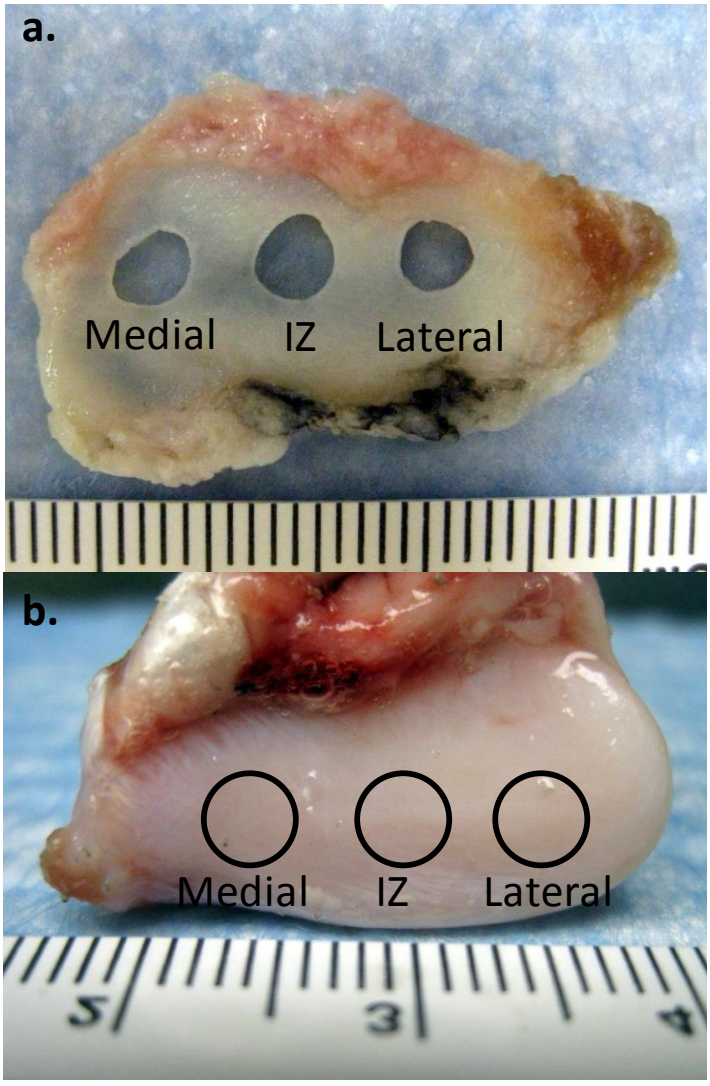

Figure 3. a.) TMJ disc and b.) MCC. The three test sites are indicated on each specimen.

3.2.2 Compression Analysis

A simple analysis was first used to evaluate the data. A tangent modulus was fit to the linear portion of the stress strain curve using Matlab®. The linear portion was defined as the last 2% strain of the ramping phase of each 10% increment. The percent relaxation was determined by evaluating the ratio of the stress of the relaxed specimen, with the specimen considered fully relaxed at 30 min, to the peak stress.

The transversely isotropic biphasic model [76] was used to assess the mechanical properties of the three sections of the disc and condylar cartilage. The model allows for the determination of Young's moduli in the transverse and axial planes (E_1, E_3), Poisson's ratios for the transverse and axial planes (ν_{21}, ν_{31}), and the transverse permeability coefficient (k). As previously described [78], a four-parameter optimization procedure was performed to find k, E_1, ν_{21}, and ν_{31}. Briefly, the Young's modulus in the axial plane (E_3) was derived from the experimentally obtained relaxation stress. Using Matlab® and the root mean square error method the experimental data was fitted to analytical curves provided by the model. In Equations 1-2, α_n are the roots of Equation 7, where J_0 and J_1 are Bessel functions of the first kind, and the numbers of summations (n) used was the number of convergences to 0 for values of x ranging from 0 to 20 (in increments of 0.01). The root equaling zero was programmed to be greater than -0.02 but less than 0.04. The constants Δ_1, Δ_2, Δ_3, and C_{11} (Equations 3-6) are calculated after Equation 7 [76]. These constants were then used to determine the loading force (Equation 1) and relaxation force (Equation 2).

The uniqueness of the curve-fits was tested using several sets of initial values. 81 different combinations of initial values were used to perform the fit, utilizing 3 guesses for each parameter. The initial guesses for each parameter ranged in equal increments from 0.1 to 0.5 for

ν_{21} and ν_{31}, 0.1 MPa to 10 MPa for E_1, and $1x10^{-14}m^4/Ns$ to $7x10^{-14}m^4/Ns$ for *k*. The final parameters were the resulting average of all solutions with an error less than 1.5 times the minimum error found for all 81 guesses that complied with thermodynamic restrictions for a transversely isotropic material (Equations 8-9). [79] The model was not fit to individual curves, but the average curve of each tissue per strain step. The average force response, thickness, and radius of all sections of the TMJ disc and MCC were used to obtain a set of parameters for each strain level.

$$f(t) = E_3\dot{\epsilon}_0 t + E_1\frac{\dot{\epsilon}_0 a^2}{C_{11}k}\Delta_3\left[\frac{1}{8} - \sum_{n=1}^{\infty}\left\{\frac{\exp\left(-\alpha_n^2 C_{11}\left(\frac{kt}{a^2}\right)\right)}{\alpha_n^2\left[\Delta_2^2\alpha_n^2 - \frac{\Delta_1}{1+\nu_{21}}\right]}\right\}\right], 0 < t < t_0 \quad (1)$$

$$f(t) = E_3\dot{\epsilon}_0 t_o - E_1\frac{\dot{\epsilon}_0 a^2}{C_{11}k}\Delta_3\sum_{n=1}^{\infty}\frac{\exp\left(-\alpha_n^2 C_{11}\left(\frac{kt}{a^2}\right)\right) - \exp\left[-\frac{\alpha_n^2 C_{11}k(t-t_0)}{a^2}\right]}{\alpha_n^2\left[\Delta_2^2\alpha_n^2 - \frac{\Delta_1}{1+\nu_{21}}\right]}, t > t_0 \quad (2)$$

$$\Delta_1 = 1 - \nu_{21} - 2\nu_{31}\left(\frac{E_1}{E_3}\right) \quad (3)$$

$$\Delta_2 = \frac{1-\nu_{31}^2\frac{E_1}{E_3}}{1+\nu_{21}} \quad (4)$$

$$\Delta_3 = (1 - 2\nu_{31}^2)\frac{\Delta_2}{\Delta_1} \quad (5)$$

$$C_{11} = \frac{E_1(1-\nu_{31}^2)\frac{E_1}{E_3}}{(1+\nu_{21})\Delta_1} \quad (6)$$

$$J_1(x) - \left(\frac{1-\nu_{31}^2 \frac{E_1}{E_3}}{1-\nu_{21}-2\nu_{31}^2 \frac{E_1}{E_3}} \right) x J_0(x) = 0 \tag{7}$$

$$\left(1 - \nu_{31}^2 \frac{E_1}{E_3}\right), (1 - \nu_{21}^2) > 0 \tag{8}$$

$$1 - \nu_{21}^2 - \nu_{31}^2, \frac{E_1}{E_3} - 2\nu_{21}\nu_{31}^2 \frac{E_1}{E_3} > 0 \tag{9}$$

3.2.3 Biochemistry

The mechanically tested specimens were allowed to equilibrate for one hour in phosphate buffered saline and the wet weights were measured. The specimens were lyophilized for 48 hours in order to obtain the dry weight. The samples were then digested in a papain solution, 125 μg/ml papain in 50 mmol phosphate buffer containing 5 mmol N-acetyl cystein overnight at 60˚C [80]. The total hydroxyproline content of the tissue sections was assessed using the modified protocol of reacting the samples with chloramine T and dimethylaminobenzaldehyde that allows for a colorimetric comparison [81]. The samples were run against both hydroxyproline and collagen standards and it was found that collagen is approximately 9% hydroxyproline. This value was used to calculate the collagen content of the samples. The DNA content was measured using a PicoGreen® dsDNA Quantitation Kit (Molecular Probes, Inc., Eugene, Oregon). The total amount of glycosaminoglycan was measured using a dimethymethylene blue colorimetric assay kit (Biocolor; Newtownabbey, UK).

3.2.4 Histology

Histological analysis with polarized light microscopy was performed to visualize any damage to the collagen network from the high strains imposed. Samples from tested (right, intermediate zone) and untested (left, intermediate zone) goat TMJ discs were embedded in OCT freezing medium and flash frozen in -80°C. The samples were cryo-sectioned to 12 μm in the transverse and axial planes, stained with hematoxylin and eosin, and imaged using polarized light.

3.2.5 Statistical Analysis

A three-way ANOVA was used to assess differences between biomechanical values based on tissue type, region, and strain level for the following factors: peak stress, equilibrium stress, tangent modulus, and percent relaxation. The model utilized can be described as follows: region (*A*) is nested within tissue (disc or MCC) (*B*) and both region and tissue are crossed with strain level (*C*). (Equation 10) To determine the differences between biochemical values a two-way ANOVA was used based on tissue type and region for the following factors: collagen content per dry weight, GAG content per dry weight, DNA content per dry weight, and percent water per wet weight. Tukey's post hoc testing was used to examine differences between groups for both analyses. All statistical analysis was performed using Minitab.

$$AB(A)CA * CB * C \tag{10}$$

3.3 RESULTS

The results from the mechanical assessment showed no statistically significant differences between the three regions in both the MCC and TMJ disc for each strain level. Therefore, the results are expressed in terms of tissue type (TMJ disc and MCC) for each strain level in **Figures 4-5** and **Tables 3-4**.

3.3.1 Simple Analysis

The results from the simple compression analysis are shown in **Figure 4** for a comparison between the disc and MCC, and in Error! Reference source not found. for a further comparison across strain step. The differences in peak stress (**Figure 4a**) between the two tissue types becomes more profound after 20% strain with the TMJ disc reaching a peak stress that is significantly higher than the MCC ($p<0.05$). For example, at 30% strain the disc reaches a peak stress of 127±40 kPa which is significantly greater than the MCC at 71±30 kPa ($p<0.05$). There were also significant differences in peak stress between strain levels for both tissues (Error! Reference source not found.). For example, at 30% strain the peak stress of the disc is 127±40 kPa which is significantly greater than the peak stress of 61±26 kPa at 20% strain. For the MCC, at 40% strain the peak stress is 132±52 kPa, which is significantly greater than the peak stress of 71±30 kPa at 30% strain ($p<0.05$). Conversely, with the equilibrium stress (**Figure 4c**), the differences between tissues were not significant. The equilibrium stress at 50% strain was significantly higher than all other strain steps ($p<0.05$) for both the disc and the MCC at values of 122±75 kPa and 152±92 kPa, respectively (Error! Reference source not found.). The percent

stress relaxation (**Figure 4c**) remained consistent between tissues at all strain levels until 40% strain when the MCC relaxed 62±18%, significantly less than the TMJ disc which relaxed 79±12% ($p<0.05$). The differences between strain levels for percent relaxation were significant at high strain levels for both the disc and the MCC (Error! Reference source not found.). For instance, the disc relaxed 61±17% at 50% strain, significantly less than 79±12% at 40% strain. The MCC relaxed 62±18% at 40% strain, significantly less than 78±10% at 30% strain ($p<0.05$). The TMJ disc showed a significantly higher tangent modulus than the MCC at all levels beyond 10% (**Figure 4d**). For example, at 20% strain the tangent modulus of the TMJ disc was 729±267 kPa, significantly greater than the MCC which was 363±169 kPa. There were also significant differences between strain level for the tangent moduli of both the disc and MCC (Error! Reference source not found.). For instance, the tangent modulus for the disc significantly increases from 304±141 kPa at 10% strain to 2413±406 kPa at 50% strain ($p<0.05$). The tangent modulus for the MCC significantly increases from 205±107 kPa at 10% strain to 1677±538 kPa at 50% strain ($p<0.05$).

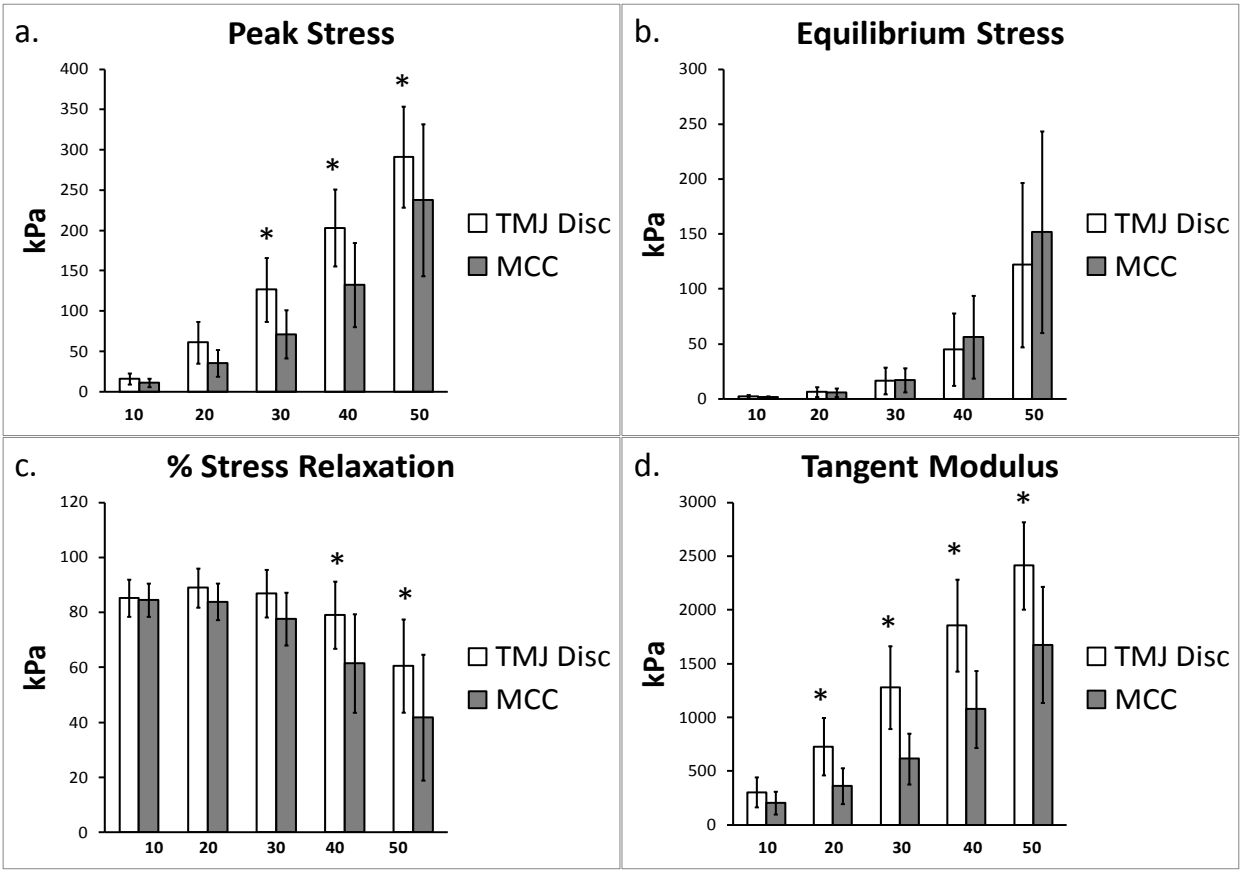

Figure 4. Simple compression analysis of the TMJ disc (*n*=8 goats x *n*=3 regions) and MCC (*n*=8 goats x *n*=3 regions) at 10, 20, 30, 40, and 50% strain. a.) Peak stress b.) Equilibrium stress c.) Percent stress relaxation d.) Tangent modulus. The symbol (*) indicates significance ($p<0.05$) between the TMJ disc and MCC at each strain step. Error bars indicate S.D.

Table 3. Peak stress, equilibrium stress, percent relaxation, and tangent modulus (mean±standard deviation) of the TMJ disc and MCC (regions combined). Means within a column that do not share a letter have a difference that is statistically significant ($p<0.05$).

Tissue	***Strain Level***	***Peak Stress (kPa)***	***Equilibrium Stress (kPa)***	***% Relaxation***	***Tangent Modulus (kPa)***
TMJ Disc	10	16±7 E	2±1 D	85±7 A	304±141 F
	20	61±26 D	6±4 CD	89±7 A	729±267 D
	30	127±40 C	17±12 CD	87±9 A	1278±85 C
	40	203±48 B	45±33 BC	79±12 A	1856±429 B
	50	291±63 A	122±75 A	61±17 B	2413±406 A
MCC	10	11±5 E	2±1 D	85±6 A	205±107 F
	20	35±17 DE	6±4 CD	84±7 A	363±169 EF
	30	71±30 D	17±11 BCD	78±10 A	616±237 DE
	40	132±52 C	56±38 B	62±18 B	1077±359 C
	50	238±94 B	152±92 A	42±23 C	1677±538 B

3.3.2 Transversely Isotropic Biphasic Model

It was determined that the transversely isotropic biphasic model provided a good fit for the stress response of the TMJ disc and MCC up to 30% strain. Since the relaxation profile for 40% and 50% strain changed, this data was not fitted to the model. The average stress response and curve fit for the TMJ disc and MCC at 10, 20, and 30% strain is shown in **Figure 5**. The results predicted by the transversely isotropic biphasic model are shown in **Table 4**. The model provided a better fit for the relaxation portion of the curve due to the fact that more data points were collected and utilized from the 30 minute relaxation period compared to the short ramping period. The results show an increase in E_1, E_3, and ν_{31} from 10-30% strain in both the TMJ disc and MCC. Conversely, there is a decrease in *k* with increasing strain level in both tissues. The TMJ disc had a greater E_1 and E_3 than the MCC at all strain levels. For example, at 10% strain E_1 of the disc is 0.18 MPa while that of the MCC is 0.14 MPa. Overall, the MCC exhibited a greater tissue permeability than the TMJ disc at all strain levels. For example, the permeability of the MCC at 10% strain was $5.48 \times 10^{-14} m^4/Ns$ while the TMJ disc was $4.47 \times 10^{-14} m^4/Ns$.

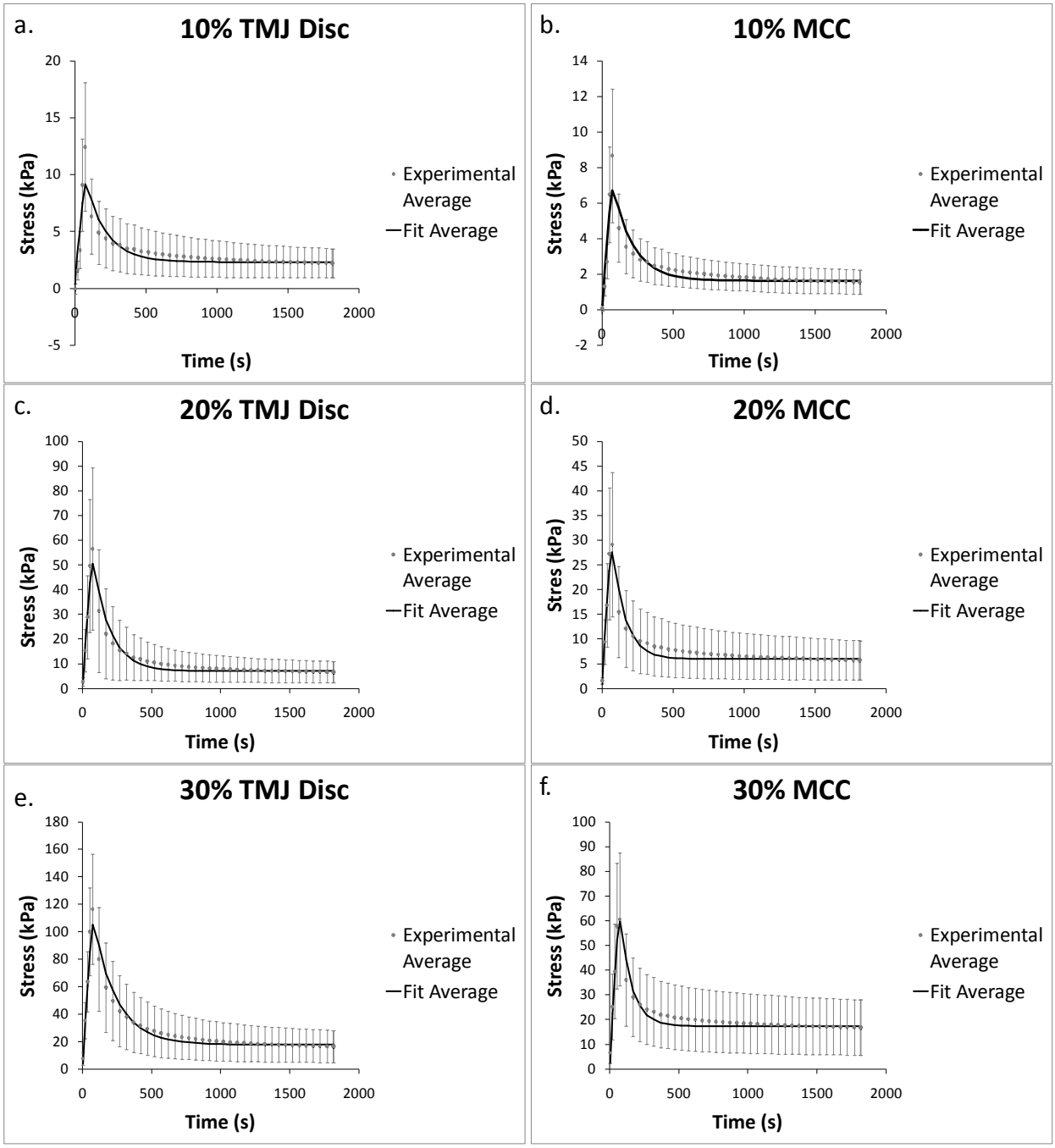

Figure 5. Average stress response of TMJ disc (a, c, e) and MCC (b, d, f) to 10, 20, and 30% strain and curve fit. The experimental average is the average stress response of all specimens with the error bars indicating standard deviation. The fit average was obtained by determining the best fit parameters for the average stress response.

Table 4. Average transverse Young's modulus (E_1), axial Young's modulus (E_3), transverse Poisson's ratio (v_{21}), axial Poisson's ratio (v_{31}), and tissue permeability (k) of the TMJ disc and MCC (regions combined).

Tissue	***Strain Level***	E_1 **(MPa)**	E_3**(MPa)**	v_{21}	v_{31}	k (10^{-14}m^4/Ns)
TMJ Disc	10	0.18	0.02	0.10	0.02	4.47
	20	0.97	0.07	0.23	0.05	0.78
	30	1.93	0.17	0.17	0.06	0.31
MCC	10	0.14	0.01	0.10	0.00	5.48
	20	0.61	0.06	0.21	0.02	1.70
	30	1.22	0.17	0.23	0.03	0.90

3.3.3 Biochemical and Histological Analysis

The results from the biochemical assessment also showed no statistically significant differences between the three regions in both the MCC and TMJ disc. Therefore, the regions were combined and results are presented by tissue type (**Figure 6a-d**). The percent collagen content per dry weight of the disc was 45.7 ±19.6% which was significantly higher than the MCC with a collagen content of 18.6 ±6.9% ($p<0.05$) (**Figure 6a**). The GAG content per dry weight of the disc was 2.1±1.2% which was significantly lower than that of the MCC with a dry weight of 4.2±2.1% ($p<0.05$) **(Figure 6b**). The DNA content per dry weight of the disc was 0.1±0.05% which was also significantly lower than the MCC with a DNA content of 0.3±0.1% ($p<0.05$) (**Figure 6c**). The percent water content of the TMJ disc was found to be 79±8%, which was significantly lower than that of the MCC with a water content of 84±7% ($p<0.05$) (**Figure 6d**).

The results from the histological assessment are shown in **Figure 7**. There is no conclusive evidence of change in collagen fiber organization, orientation, integrity, or packing between the mechanically tested to 50% strain and untested TMJ disc.

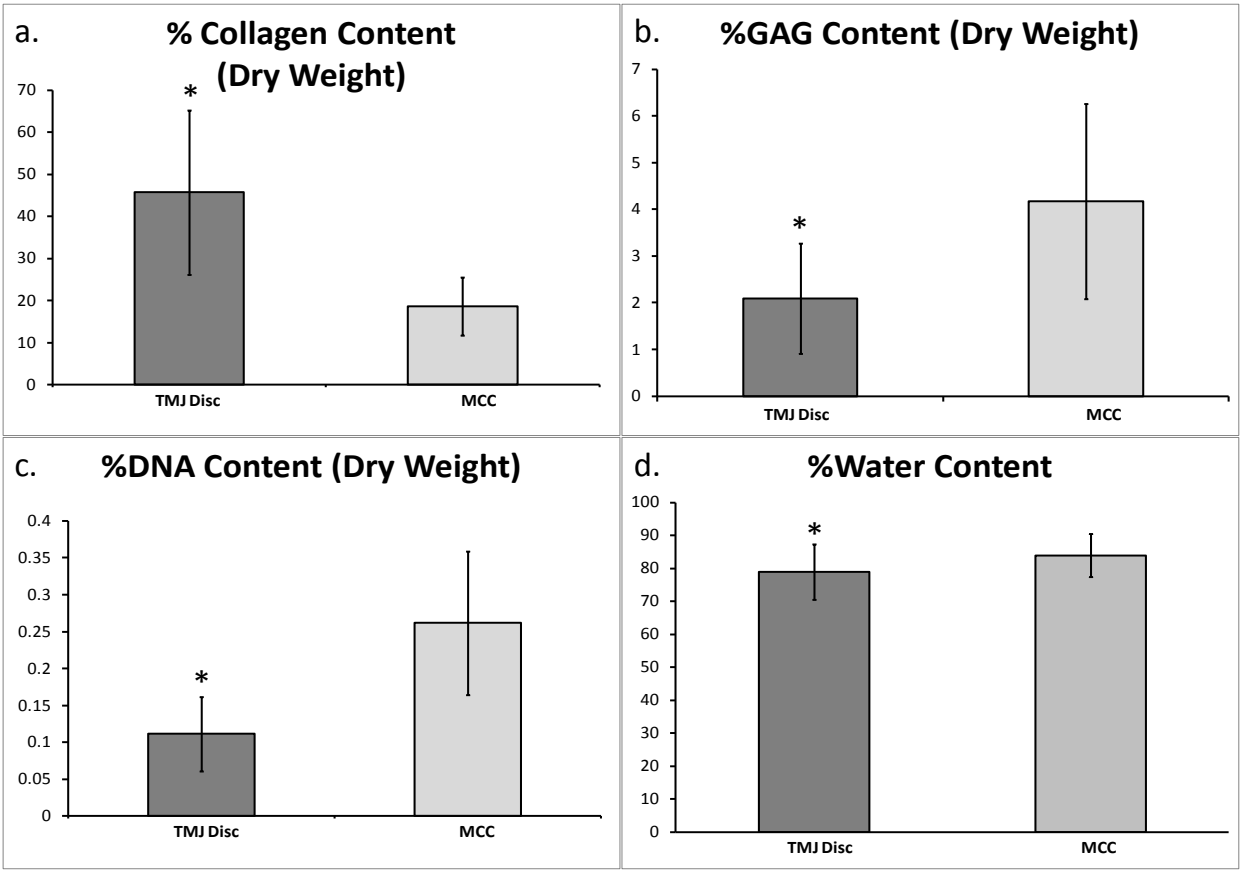

Figure 6. Biochemical analysis of the TMJ disc (*n*=8 goats x *n*=3 regions) and MCC (*n*=8 goats x *n*=3 regions). a.) Percent collagen content per dry weight b.) Percent GAG content per dry weight c.) Percent DNA content per dry weight and d.) Percent water content of the tissue. The symbol (*) indicates significance ($p<0.05$) between the TMJ disc and MCC. Error bars indicate S.D.

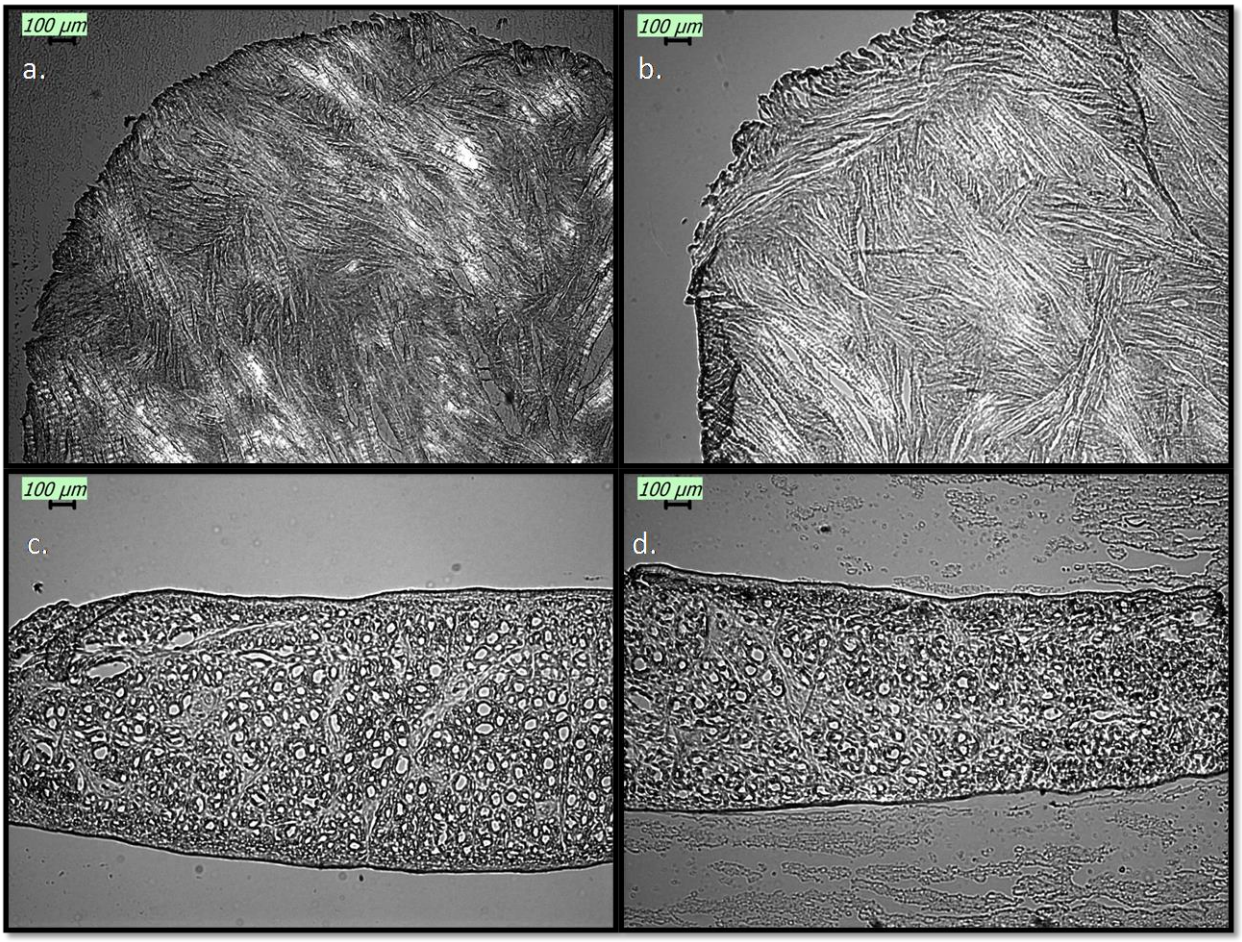

Figure 7. Polarized light image of the TMJ disc. A. Transverse section of untested TMJ disc. B. Transverse section of mechanically tested TMJ disc. C. Axial section of untested TMJ disc. D. Axial section of mechanically tested TMJ disc.

3.4 DISCUSSION

The goal of this study was to compare the mechanical and biochemical properties of the goat TMJ disc to the MCC. The results indicated that the TMJ disc exhibits a significantly greater tangent modulus and peak stress than the MCC. There were strain level dependencies in peak stress, equilibrium stress, percent relaxation, tangent modulus, Young's moduli, Poisson's ratio, and tissue permeability for both tissue types. The transverse isotropic biphasic model provided a good fit for the stress-relaxation behavior of both the TMJ disc and MCC up to 30% strain. Due to the change in relaxation behavior at 40% and 50% strain, this data was not applied to the model. Coinciding with previous findings, the current assessment showed that the goat TMJ disc is stiffer than the MCC, albeit using different testing methods [82]. This study showed that, unlike a regional analysis of the porcine disc by Athanasiou and co-workers [83], the goat disc does not seem to exhibit regional variations in mechanical properties with this testing protocol. Conversely, the lack of significant differences in the middle regions of the goat MCC corresponds with previous findings using the porcine model by Detamore and co-workers [84]. Significant differences between the mechanical properties of the tissues at different strain levels shed light on the function of these tissues *in vivo*, suggesting a change in tissue behavior at higher strains.

The biphasic theory derived by Mow [73] can be used to describe the behavior of the fibrocartilagenous tissues of the TMJ under compression by assuming that the solid matrix may be linearly elastic and isotropic or anisotropic, and that interstitial fluid are intrinsically incompressible, or that compression is only possible due to fluid exudation. Viscous dissipation is assumed to be a result of interstitial fluid flow relative to the porous permeable solid matrix, and frictional drag is directly proportional to the relative velocity and it may be strain dependent.

Biphasic approaches have been utilized which require confined compression chambers [85] or indentation testing for the TMJ disc [86, 87]. In another study, using biphasic indentation creep analysis, Athanasiou and co-workers found that the intermediate zone of the porcine TMJ disc exhibits an aggregate modulus of 18.6 ± 5.2 kPa and a permeability of 22.8 ± 9.8 $x10^{-15}$ m^4/Ns [88]. In contrast, an additional study found that in confined compression, the average aggregate modulus of the intermediate, lateral, and medial regions of human TMJ disc is 69.75 ± 11.47 kPa and the permeability is 3.75 ± 0.72 $\times 10^{-15}$ m^4/Ns [89]. The values obtained using biphasic models do not deviate greatly from what was obtained for the axial Young's modulus of the goat TMJ disc (20 kPa) at 10% strain. However, the tissue permeability of the goat TMJ disc was found to be 4.47 $\times$ 10^{-14} m^4/Ns at 10% strain, which is greater than the previously reported findings.

The group from Dr. Athanasiou also showed that, using a viscoelastic model, and a high strain rate, the instantaneous modulus for the TMJ disc was found to be around 500 kPa [83]. Additionally, when Dr. Detamore's group investigated the porcine MCC using a high strain rate it, Singh *et al.* demonstrated that the average elastic modulus ranged from about 0.8 to 1.5 MPa [84]. While these values exceed what was observed in the goat TMJ, it is likely that these differences are largely attributed to differences in strain rate, along with species variation, testing protocols, and modeling.

The collagen content of the goat TMJ disc is less than that of the previously reported porcine (68.2 ± 14.5%) and human TMJ disc (62.0 ± 11.4) [72, 89]. We did validate our collagen assay with porcine samples, and obtained results comparable to literature [90]. Additionally, corresponding to our lack of significant differences in mechanical behavior between regions, there was no significant difference in biochemical content between regions.

Further studies need to be performed to determine the remaining biochemical content of the goat disc and MCC. As for GAGs, the common concept of the role of GAGs is that they act to retain water molecules providing an added "cushion" under compression. However, this did not correspond to our findings where the TMJ disc, containing fewer GAGs than the MCC, had a higher tangent modulus. This seems to indicate that the collagen has an influence on mechanical support which outweighs that of the GAG, since GAG content might be too low to have a significant impact in force bearing.

A limitation of the transversely isotropic biphasic theory is that it assumes the solid matrix is homogenous and behaves linearly. It is known that the extracellular environment of both the disc and the MCC is inhomogeneous and it is more likely that the solid part of the tissue exhibits viscoelastic behavior. Additionally, the theory assumes the application of low strain rates and lower applied strain, which was pushed well pass 10% in this study. In the future, the use of alternate models, such as a finite element model, should be used to address the limitations of applying the transversely isotropic biphasic model to fibrocartilage when subject to high strain. Similarly, the application of a model that considers the compression-tension non-linearity of tissues in unconfined compression stress relaxation, such as a fiber-reinforced model, may also provide for a more accurate depiction of the tissue behavior *in vivo*. The MCC, in general, provided for a better fit to the model than the disc. This difference was expected considering that the structure and composition of the disc and MCC are dissimilar. The TMJ disc consists of collagen arranged in tight bundles of anteroposteriorly oriented fibers in the zones that were tested [91]. In contrast, the MCC has a zonal organization of cartilage consisting of significantly less collagen and more GAG (**Figure 7a-b**). These structural differences affect the porosity of the solid matrix component and the ability to allow water flow. This is further supported by the

finding that the water content of the disc is significantly lower than that of the MCC. **(Figure 6d**) These differences between the two tissues help explain why using a permeable, solid matrix model such as the transversely isotropic biphasic model is more appropriate for the MCC. A viscoelastic model may prove more appropriate for the TMJ disc, especially at higher strain rates [83]. Another limitation might be the shorter relaxation time of 30 minutes. However, on average, in the last minute of the stress relaxation period, there was never a change of force greater than 0.01 N at all strain levels for both tissues. Lastly, this study did not quantify and characterize the various types of collagen and proteoglycans found in both the TMJ disc and MCC, which could further explain the differences in behavior.

Establishing the differences in composition and function of the disc and MCC is necessary for understanding the way these tissues interact *in vivo*. While both tissues are classified as fibrocartilagenous, this study elucidated important distinctions between the two joint tissues. As the joint tissues become better characterized, the appropriate design criteria for tissue engineered constructs can be established. The information from this study provides a necessary framework for the development of devices that alleviate the symptoms of TMDs.

4.0 THE EFFECT OF MAGNESIUM ION CONCENTRATION ON THE FIBROCARTILAGE REGENERATION POTENTIAL OF GOAT COSTAL CHONDROCYTES[3]

4.1 INTRODUCTION

It is estimated that temporomandibular joint (TMJ) disorders (TMDs) affect over 10 million Americans [1]. The TMJ is a synovial, bilateral joint formed by the articulation of the condyle of the mandible and the glenoid fossa and articular eminence of the temporal bone. The soft tissues of the joint include the TMJ disc and mandibular condylar cartilage. Both of these tissues are classified as fibrocartilage and consist mostly of collagen type I, elastic fibers, glycosaminoglycans (GAGs) and proteoglycans [92]. Clinical indications of TMD can include clicking, locking, headaches, joint pain and tenderness, restricted range of motion, painful mastication, and deterioration of the disc and articulating surfaces [60]. When symptoms become severe, patients resort to invasive surgical interventions such as disc repositioning, discectomy, and replacement of the condyle, fossa, or both components with a prosthetic device. Currently, two TMJ implants are used by clinicians: Techmedia/TMJ Concepts, and Walter Lorenz/Biomet [93]. The benefits of these total joint replacement systems include restored

[3] Hagandora, C.K., M.A. Tudares, and A.J. Almarza, *The effect of magnesium ion concentration on the fibrocartilage regeneration potential of goat costal chondrocytes.* Ann Biomed Eng, 2012. **40**(3): p. 688-96.

masticatory function and variable pain relief [93]. However, these prosthetics can harbor infections which require the removal of the device, debridement, antibiotic treatment, and implantation of a new device. Additionally, due to the mismatch between mechanical properties of prosthetic materials and bone leading to micro-motion [94], the lifetime of these devices in-vivo may be limited, making them less than ideal for a young patient population. This is a major insufficiency considering that 80% of patients treated for TMD symptoms are women in their reproductive years, between the ages of 20-40 [95, 96].

Recently, magnesium has been explored as a potential biomaterial for biodegradable orthopedic implants due to its similar mechanical properties to bone [97] and biocompatibility. Witte *et al.*[98] found that magnesium alloy rods implanted in guinea pig femurs resulted in a significant increase in mineralized bone area when compared to a control polymer group (SR-PLA 96) after 6 and 18 weeks of implantation. This suggests that magnesium could potentially be used as a coating material to enhance bone fixation to TMJ prosthetics, preventing micromotion and extending the lifetime of the implant. While magnesium shows promise as a biomaterial for enhancing bone regeneration, the effect of degrading magnesium on the surrounding soft tissue needs to be determined. In a study done by Feyerabend et al. [99], it was found that high concentrations of magnesium sulfate ($MgSO_4$) support chondrocyte proliferation and redifferentiation. Feyerabend et al. further showed that magnesium concentrations up to 10 mM resulted in increased chondrocyte proliferation while concentrations of 15-30 mM inhibited cell proliferation [99]. The authors also found that magnesium concentrations higher than 10 mM resulted in an increase in GAG production per DNA during the redifferentiation of chondrocytes in alginate [99]. However, during chondrogenesis of the cells in high density pellets, the introduction of magnesium had a detrimental effect on extracellular matrix (ECM)

production. While these findings demonstrate the effect of magnesium concentrations up to 30 mM on chondrocyte behavior, the degradation products of some magnesium alloys could result in higher concentrations. This generates the need to test for the effects of higher concentrations of magnesium on cell behavior. Magnesium chloride ($MgCl_2$), will also be tested to ensure that changes in tissue response are not attributed to increased sulfate concentration. Since the ultimate goal is to use biodegradable magnesium to enhance the fixation of devices for the TMJ, the effect of high concentrations of magnesium on the fibrocartilage interface needs to be investigated.

While degenerating magnesium has been shown to enhance bone in-growth, further exploration of the effect on the articulating surface is merited. In tissue engineering approaches for fibrocartilage, goat costal chondrocytes cultured using a scaffoldless approach have proven to be a viable cell source due to their production of high quantities of collagen and GAG [68, 69]. In the present study, scaffoldless costal chondrocyte constructs are used as a tissue engineering model to determine the effect of additional magnesium on fibrocartilage extracellular matrix production. Testing is performed at 4 weeks because scaffoldless constructs are mature enough at this point to be tested mechanically. The objective of this study was to assess the effect of concentrations of 20, 50, and 100 mM of magnesium chloride ($MgCl_2$) and magnesium sulfate ($MgSO_4$) on the matrix production of goat costal fibrochondrocytes and subsequent mechanical properties. Magnesium concentrations up to 100 mM were tested because preliminary studies show that goat fibrochondrocytes do not survive at concentrations beyond this point.

4.2 MATERIALS AND METHODS

4.2.1 Cell Culture

Goat costal cartilage was isolated from the ribs of three young (<1 year) female Boer goats obtained from a local abattoir within 4 hours of slaughter. The fibrocartilage was minced and digested in 2 mg/ml type II collagenase (Worthington) overnight at 37°C and 5% CO_2 with constant mechanical agitation on an orbital shaker. Isolated fibrochondrocytes were passaged three times in Dulbecco's modified Eagle medium (DMEM)/high glucose (Thermo Scientific) 10% fetal bovine serum (Atlanta Biologicals), 1% penicillin-streptomycin (Lonza), 1% MEM non-essential amino acid solution (Thermo Scientific) and 25 μg/ml L-ascorbic acid (Sigma-Aldrich). The cells were frozen after passage one in passage media with 5% DMSO and an additional 10% FBS and then thawed and passaged twice to allow for simultaneous seeding of the constructs. The passaged cells were seeded in 5 mm 2% agarose **(**SeaPlaque® Lonza**)** cylindrical wells at a density of 2 million cells/well using chondrogenic media consisting of DMEM/high glucose (Thermo Scientific) supplemented with 1% penicillin-streptomycin (Lonza), MEM 1% non-essential amino acid solution (Thermo Scientific), 1% insulin-transferrin-selenium + premix (BD Biosciences), 0.1 μM dexamethasone (MP Biomedicals), 40 ug/mL L-proline (Acros Organics) and 50 μg/mL ascorbate 2-phosphate (Sigma-Aldrich).[68] Additional concentrations of 20, 50, and 100 mM $MgCl_2$ (Fisher Scientific) and $MgSO_4$ (Acros Organics) were sterile filtered into the chondrogenic media. The baseline magnesium ion concentration of the DMEM/high glucose was 0.8 mM $MgSO_4$. The scaffoldless constructs were formed by the cell-cell interaction that takes place when the goat costal fibrochondrocytes are seeded in the agarose wells. Since the cells do not attach to agarose, they instead attach to each

other forming a spherical three-dimensional structure termed "construct". Constructs were visible inside the wells at approximately 8-12 hours after seeding. Constructs were cultured in 37° C and 5% CO_2 conditions at all times. Chondrogenic media was replenished every 48 hours. After two weeks, constructs were transferred to agarose coated plates for an additional 2 weeks.

4.2.2 Histology

Constructs (*n*=3 per group) were embedded in OCT freezing medium (Tissue-Teck) and flash frozen to -80°C. The samples were cryo-sectioned at 6 μm, fixed in cold acetone, and stained with picrosirius red for collagen staining and Safranin-O/Fast green for GAG staining. For the picrosirius red stain, the nuclei were first stained using Weigert's hematoxylin and then washed. The samples were then stained using picrosirius red to give near-equilibrium staining of collagen. For the Safranin-O/Fast green stain, the samples were first stained using Weigert's iron hematoxylin working solution and fast green solution. Then they were rinsed in 1% acetic acid solution and stained in 0.1% Safranin-O solution. This procedure stains the nuclei black, the cytoplasm gray or green, and the cartilage, mucin, and mast cell granules orange to red. Immunostaining for collagen types I and II was performed using a Vectastain® ABC kit (Vector Laboratories), monoclonal anti-collagen type I antibody produced in mouse (Sigma), and anti-human collagen type II produced in mouse (MP Biomedicals) [100]. Briefly, the procedure was performed as follows: samples were washed in 10 mM Na_3PO_4 0.9% buffer with a pH of 7.50, incubated in diluted normal horse serum (3 drops in 10 mL of sodium phosphate buffer) for 20 minutes, washed in buffer, incubated in diluted primary antibody (2 μL of Monoclonal Anti-Collagen Type I in 3 mL of sodium phosphate buffer), washed in buffer, incubated in diluted secondary antibody (1 drop of biotinylated antibody in 10 mL of sodium phosphate buffer),

washed in buffer, quenched in 1% methanol, washed in buffer, incubated with ABC reagent (kit) for 30 minutes, washed in buffer, incubated in diaminobenzidine (DAB) for 2 minutes, rinsed with water, and mounted with mounting medium (Richard-Allan Scientific). Negative stains were also performed without applying the primary antibody.

4.2.3 Biochemistry

Constructs (*n*=6 per group) were lyophilized for 48 hrs and digested as previously described [69]. Briefly, samples were digested at 4°C with constant mechanical agitation in 125 ug/mL papain (Sigma-Aldrich) for 10 days followed by 1 mg/ml elastase (Sigma-Aldrich) digestion for 3 days. All assays were performed using this digest. The total hydroxyproline content was assessed using the modified protocol of reacting the samples with chloramine T and dimethylaminobenzaldehyde that allows for a colorimetric comparison [72]. A conversion factor of 9% was used to calculate the collagen content of the samples [101]. The DNA content was measured using a PicoGreen® dsDNA quantitation kit (Molecular Probes). The formula for conversion from concentration of DNA to number of cells was 7.7 pg DNA/cell [72]. The total amount of glycosaminoglycan was measured using a dimethymethylene blue colorimetric assay kit (Biocolor). Collagen types I and II were quantified using an ELISA kit according to the manufacturer's instructions (Chondrex). All biochemical testing was performed on the constructs at 4 weeks.

4.2.4 Mechanical Testing

Unconfined compression testing and analysis was performed according to our published methods [101]. Prior to testing, samples (n=6 per group) were allowed to equilibrate for 1 hour in phosphate buffered saline. The construct diameter was measured prior to testing using digital calipers. The constructs were attached to a compression platen using cyanoacrylate. To estimate construct height, force was applied to the construct until reaching 0.05 N, at which point the crosshead position was noted and the platen was immediately removed. The water bath was then filled with PBS and the thermocouple was set to 37°C prior to testing. The MTS Insight® was used to measure changes in force throughout the test. The upper platen was lowered within 0.1 mm of the determined construct height and a preload of 0.05 N was applied for 30 minutes. The height at the end of the preload was taken to be the height of the construct and was utilized in subsequent calculations. The constructs then underwent 10 cycles of preconditioning at 9%/min until 10% strain was reached [78, 101]. immediately following preconditioning, the samples were compressed until 10% strain was reached, and were allowed to relax for 60 minutes.

A tangent modulus was fit to the linear portion of the stress strain curve using Matlab®, defined as the last 2% of 10% strain. The percent relaxation was determined by evaluating the ratio of the stress of the relaxed specimen, with the specimen considered fully relaxed at 60 minutes, to the peak stress.

The transversely isotropic biphasic model [76] was also used to assess the mechanical properties of the constructs. The model allows for the determination of Young's moduli in the transverse and axial planes (E_1, E_3), Poisson's ratios for the transverse and axial planes (ν_{21}, ν_{31}), and the transverse permeability coefficient (k). The average force response, thickness, and radius of each group of constructs were used to obtain a set of parameters.

4.2.5 Statistical Analysis

A one-way ANOVA was used to assess differences for biochemical and biomechanical values within magnesium concentration with $p<0.05$ defined as statistically significant. Tukey's post hoc testing was used to examine differences between groups. All statistical analysis was performed using Minitab. All data is reported as average ± standard error of the means.

4.3 RESULTS

4.3.1 Gross Morphology

Constructs at 4 weeks are shown in **Figure 8**. Constructs cultured in the 0.8 mM Mg^{2+} media had an average diameter and thickness of 2.7±0.1 mm and 2.1±0.05 mm, respectively **(Figure 8a**). There were no significant differences between construct diameter and thickness between 20, 50 mM $MgCl_2$ **(Figure 8b, 8c**) and 20 $MgSO_4$ (**Figure 8e**) groups and the 0.8 mM Mg^{2+} constructs, while the 50 mM $MgSO_4$ **(Figure 8f**) group had a significantly greater diameter of 3.3±0.1 mm. ($p<0.05$) The constructs in the 100 mM $MgCl_2$ (**Figure 8d**) and $MgSO_4$ (**Figure 8g**) groups were more gelatinous in consistency when compared to the solid constructs formed in the other groups, and accurate diameter measurements could not be performed.

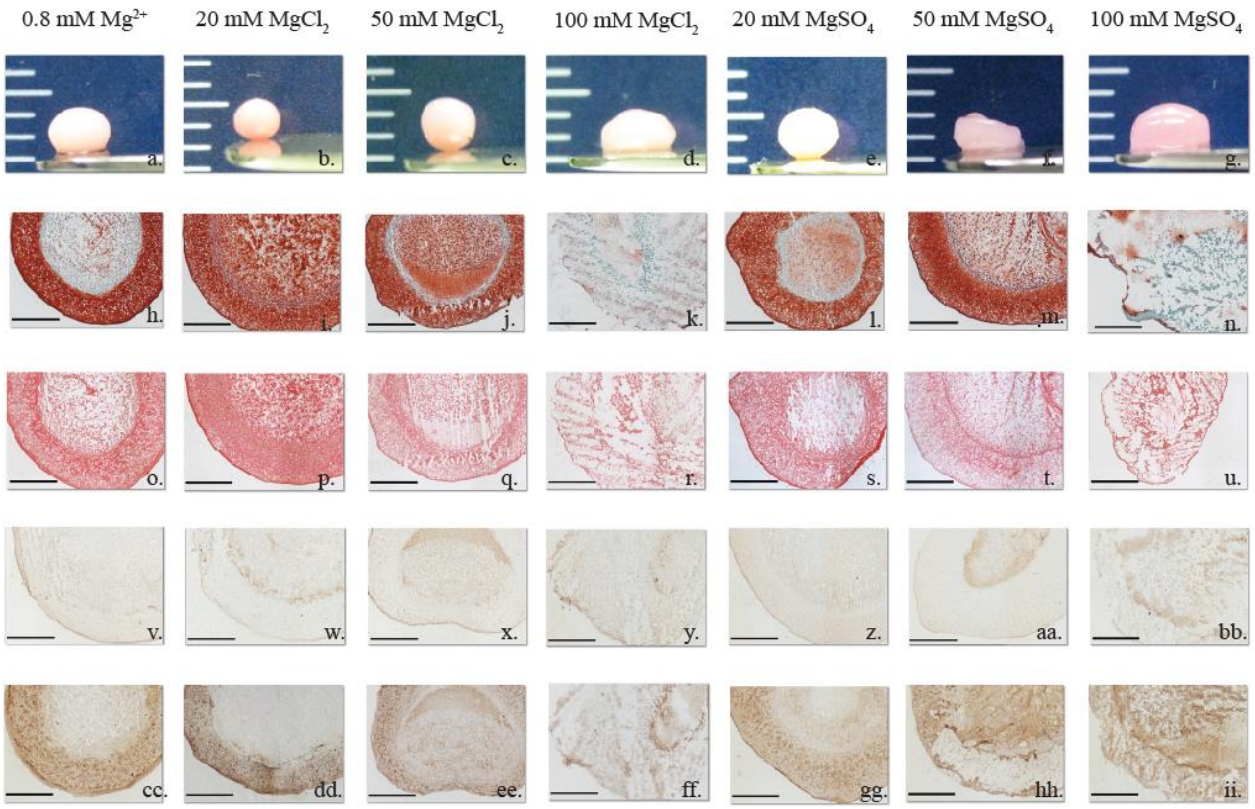

Figure 8. Morphological and histological images of constructs for 0.8, 20, 50, and 100 mM $MgCl_2$ and $MgSO_4$ at 4 weeks. a-g: gross morphology, h-n: safranin-o/fast green staining to visualize sulfated GAGs, o-u: picrosirius red staining to visualize collagen, monoclonal primary antibodies were used for v-bb: collagen type I IHC, cc-ii: collagen type II IHC. The negative control without primary is not shown. Scale bar = 0.5 mm

4.3.2 Histology

The results from the histological assessment are shown in **Figure 8**. The 0.8 mM Mg^{2+} constructs exhibited a well defined, highly concentrated GAG ring with trace amounts of GAG in the center (**Figure 8h**). A similar pattern was observed in the 20 mM $MgCl_2$ and $MgSO_4$ and 50 mM $MgCl_2$ and $MgSO_4$ groups, **Figure 8i, l, j, and m**, respectively. The 100 mM $MgCl_2$ (**Figure 8k**) and $MgSO_4$ (**Figure 8n**) constructs exhibited a sparse distribution of GAG throughout a poorly-defined structure.

Similar to the pattern seen in the Safrain-O stain, the 0.8 mM Mg^{2+} constructs again exhibited a concentrated ring of collagen with trace amounts of collagen in the center (**Figure 8o**). The 20 mM $MgCl_2$ and $MgSO_4$ and 50 mM $MgCl_2$ and $MgSO_4$ constructs maintained the same pattern as the 0.8 mM Mg^{2+} constructs**, Figure 8p, q, s, and t**, respectively. The 100 mM $MgCl_2$ and $MgSO_4$ constructs exhibited a lower concentration of collagen distributed throughout the construct (**Figure 8r, u**).

All constructs stained positive for collagen type I and II (**Figure 8v-ii**). Staining for collagen type I was more concentrated in the center of the scaffold in the 0.8 mM Mg^{2+} constructs and 20 mM $MgCl_2$ and $MgSO_4$ and 50 mM $MgCl_2$ and $MgSO_4$ constructs, **Figure 8w, z, x, and aa**, respectively. The 100 mM $MgCl_2$ (**Figure 8y**) and 100 mM $MgSO_4$ (**Figure 8bb**) constructs exhibited a meager distribution of collagen type I throughout the construct. Collagen type II was more concentrated in the outer ring of the constructs in the 0.8 mM Mg^{2+}, 20 mM $MgCl_2$ and $MgSO_4$ and 50 mM $MgCl_2$ and $MgSO_4$ constructs, **Figure 8cc, dd, ee, gg, and hh**, respectively. In the 100 mM $MgCl_2$ (**Figure 8ff**) and 100 mM $MgSO_4$ (**Figure 8ii**) constructs collagen type II was less concentrated and not localized to the outer ring.

4.3.3 Biochemistry

The results from the biochemical assessment are shown in **Figure 9.** The collagen content of the 0.8 mM Mg^{2+} constructs was 6.9±0.5% of the dry weight (**Figure 9a**). There was no difference between the 20 mM $MgCl_2$ and $MgSO_4$ constructs and the 0.8 mM Mg^{2+} control. The collagen content of the 50 and 100 mM $MgCl_2$ constructs was significantly lower than the 0.8 mM Mg^{2+} constructs (3.8±0.2% and 1.9±0.1%, respectively) (p<0.05). Similarly, the collagen content of the 50 and 100 mM $MgSO_4$ constructs was also significantly lower than the 0.8 mM Mg^{2+} constructs (4.5±0.2% and 2.0±0.1%, respectively). The collagen type II/I ratio of the control constructs was 1.6±0.1 (**Figure 9b**). The 50 and 100 mM $MgCl_2$ constructs were significantly lower than the 0.8 mM Mg^{2+} constructs (0.7±0.03 and 0.01±0.002, respectively) (p<0.05). The 20 mM $MgSO_4$ constructs had a significantly greater collagen type II/I ratio than the 0.8 mM Mg^{2+} constructs (3.0±0.03) while there was no difference between the 50 mM $MgSO_4$ constructs and the control (p<0.05). The 100 mM $MgSO_4$ constructs again had a significantly lower collagen type II/I ratio than the 0.8 mM Mg^{2+} constructs.

The GAG content of the 0.8 mM Mg^{2+} constructs was 16.5±1.3% of the dry weight (**Figure 9c**). There was no difference between the 20 mM $MgCl_2$ and $MgSO_4$ constructs and the 0.8 mM Mg^{2+} control. The GAG content of the 50 and 100 mM $MgCl_2$ constructs were significantly lower than the control (10.9±1.6% and 3.9±0.4%, respectively) (p<0.05). Again, the GAG content of the 50 and 100 mM $MgSO_4$ constructs was also significantly lower than the 0.8 mM Mg^{2+} constructs (10.8±0.7% and 3.6±0.4%, respectively) (p<0.05). All concentrations of magnesium resulted in a significant reduction in cell content of the constructs when compared to the 0.8 mM Mg^{2+} constructs (0.88±0.02 million cells) (p<0.05) (**Figure 9d**).

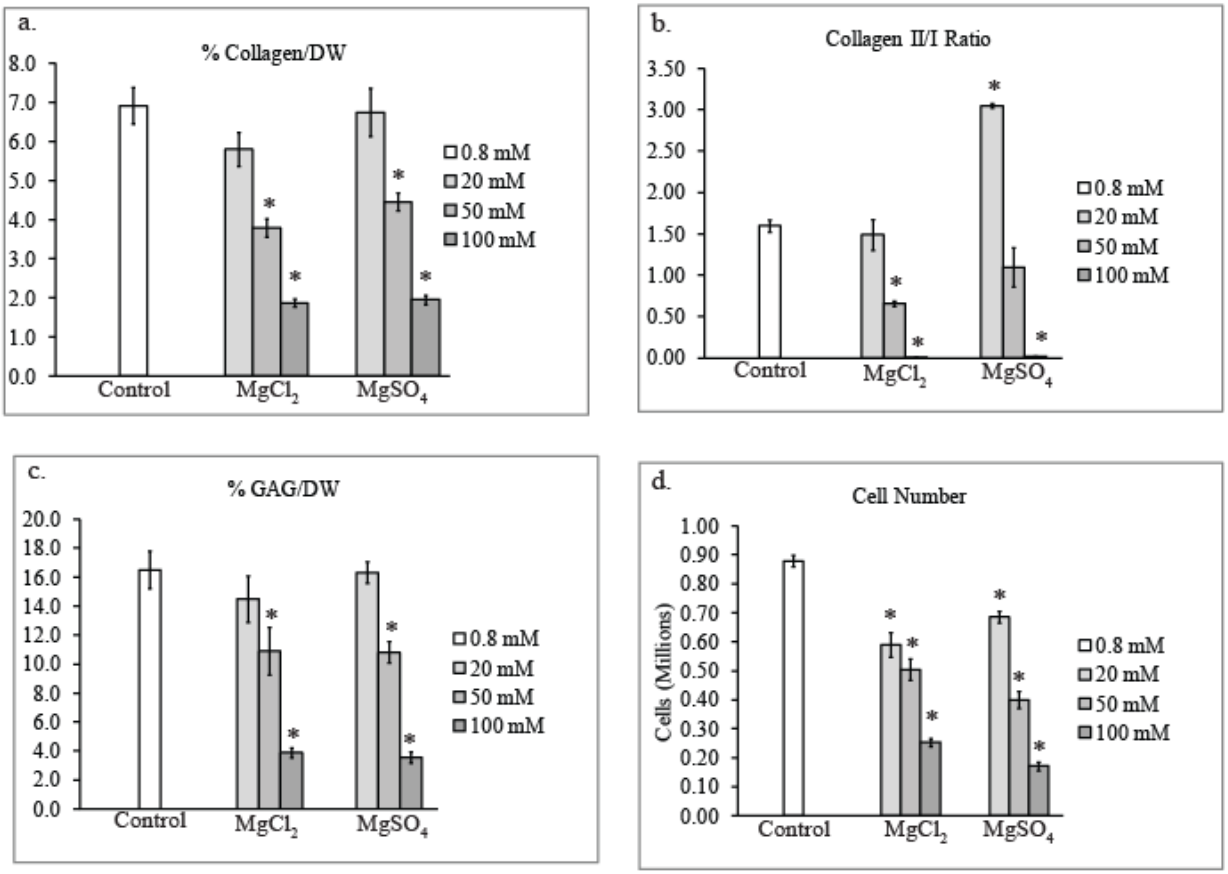

Figure 9. Biochemical analysis of the scaffoldless constructs (n=6) constructs for 0.8, 20, 50, and 100 mM $MgCl_2$ and $MgSO_4$ at 4 weeks. (a) Percent collagen content per dry weight. (b) Collagen type II/I ratio. (c) Percent GAG content per dry weight. (d) Cell content. The symbol (*) indicates significance ($p<0.05$) to the 0.8 mM Mg^{2+} constructs. Error bars indicate S.E.M.

4.3.4 Mechanical Properties

The results from the compression analysis can be seen in **Figure 10**. The constructs from the 100 mM $MgCl_2$ and 100 $MgSO_4$ groups did not have the structural integrity to withstand the 0.05 N preload and were therefore deemed un-testable. There were no statistically significant differences between the peak stress of the 0.8 mM Mg^{2+} constructs and the 20 and 50 mM $MgCl_2$ groups (**Figure 10a**). There was also no statistically significant difference between the peak stress of the 0.8 mM Mg^{2+} constructs and the 20 mM $MgSO_4$ groups. However, the 50 mM $MgSO_4$ group did have a statistically significant lower peak stress than the 0.8 mM Mg^{2+} constructs, 10.4±1.2 kPa and 33.9±2.1 kPa, respectively (p<0.05). The equilibrium stress of the control constructs was 14.2±1.6 kPa (**Figure 10b**). There was no statistically significant difference between the equilibrium stress of the 20 and 50 mM $MgCl_2$ constructs and the control. There was also no statistically significant difference between the 20 mM $MgSO_4$ group and the control. The 50 mM $MgSO_4$ group had a significantly lower equilibrium stress than the 0.8 mM Mg^{2+} constructs at 2.5±0.9 kPa (p<0.05). The percent stress relaxation of the 0.8 mM Mg^{2+} constructs was 55±0.4% (**Figure 10c**). There was a significant decrease in stress relaxation in the 20 mM $MgCl_2$ group (44.8±7.2%) and no difference between the 50 mM $MgCl_2$ group compared to the 0.8 mM control (p<0.05). There was also no significant difference between the stress relaxation of the 20 mM $MgSO_4$ group and the control but there was significant increase in the 50 mM $MgSO_4$ group (75.7±3.9%) (p<0.05). The tangent modulus of the control constructs was 434.8±46.8 kPa (**Figure 10d**). There was no statistically significant difference between the 20 mM $MgCl_2$ group and the 0.8 mM control. The results show a significant decrease in tangent modulus compared to the 0.8 mM Mg^{2+} constructs in the 50 mM $MgCl_2$ constructs (229.2±41.5) (p<0.05). Again, there was no significant difference in tangent modulus between the 20 mM

$MgSO_4$ constructs and the control. The 50 mM $MgSO_4$ constructs did have a significantly lower tangent modulus than the control at 126.2±6.3 kPa ($p<0.05$).

The results predicted by the transversely isotropic biphasic model are shown in **Table 5**. The model provided a good fit for the stress response of the tested constructs at 10% strain. (**Figure 11**) E_1 ranged from 99-295 kPa while E_3 ranged from 24-178 kPa across groups. The results show that E_1 and E_3 in the 50 mM $MgSO_4$ groups was the lowest. ν_{21} ranged from 0.21 to 0.29 while ν_{31} ranged from 0.00 to 0.05 across groups. While ν_{21} was similar across groups, ν_{31} in the 50 mM $MgSO_4$ group was the lowest. The permeability (k) ranged from $0.45x10^{-14}m^4/Ns$ to $2.26\ x10^{-14}m^4/Ns$ across groups. All groups exhibited higher tissue permeability when compared to the 0.8 mM Mg^{2+} group ($0.45\ x10^{-14}m^4/Ns$), with the most drastic increase observed in the 50 mM $MgSO_4$ group ($2.26x10^{-14}m^4/Ns$).

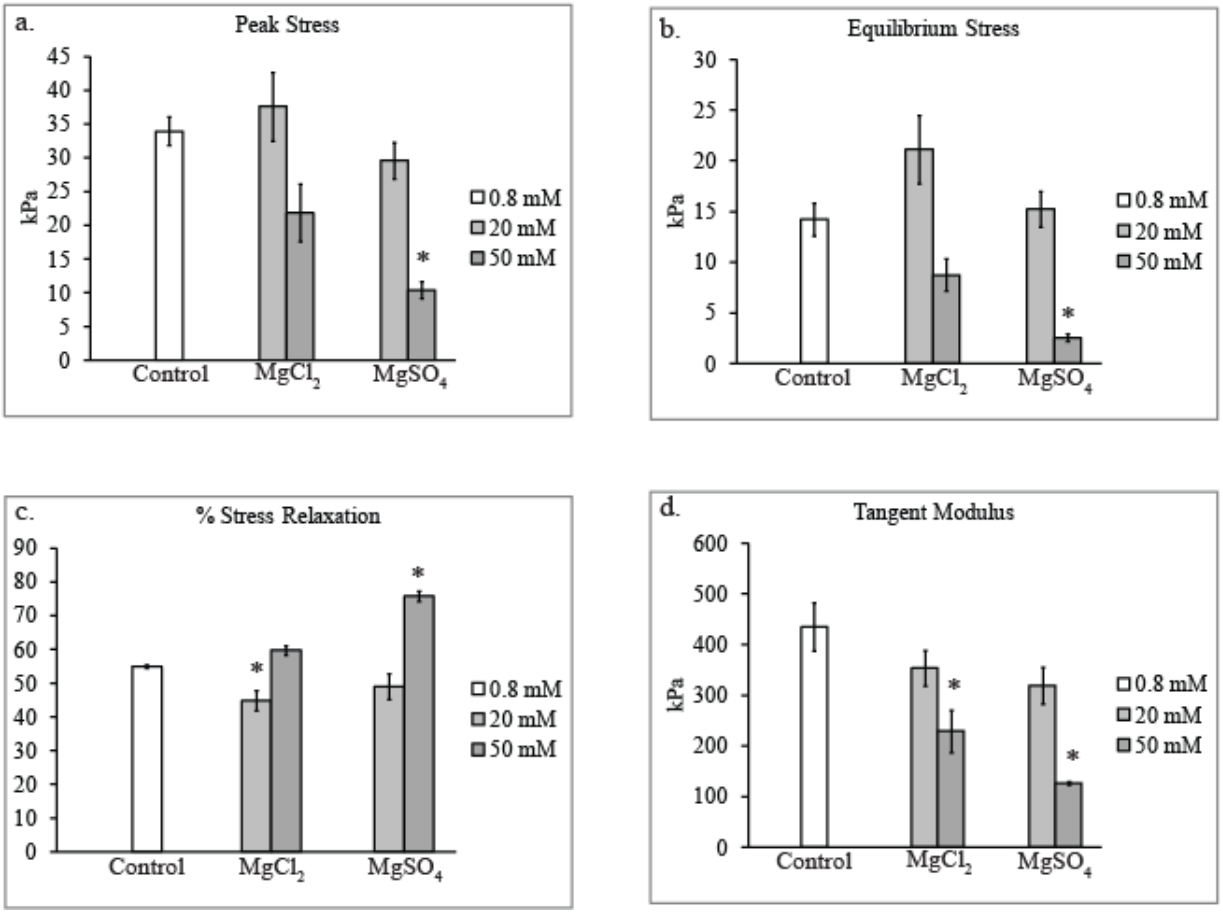

Figure 10. Simple compression analysis of the scaffoldless constructs (n=6) constructs for 0.8, 20, 50, and 100 mM $MgCl_2$ and $MgSO_4$ at 4 weeks. (a) Peak stress (b) Equilibrium stress (c) Percent stress relaxation and (d) Tangent modulus. The symbol (*) indicates significance ($p<0.05$) to the 0.8 mM Mg^{2+} constructs. Error bars indicate S.E.M.

Table 5. Average transverse Young's modulus (***E*$_1$**), axial Young's modulus (***E*$_3$**), transverse Poisson's ratio (***ν*$_{21}$**), axial Poisson's ratio (***ν*$_{31}$**), and tissue permeability (***k***) of the constructs.

	E_1 (kPa)	E_3 (kPa)	ν_{21}	ν_{31}	k (10^{-14}m^4/Ns)
0.8 mM (Control)	295	130	0.21	0.04	0.45
20 mM $MgCl_2$	285	178	0.29	0.05	0.52
50 mM $MgCl_2$	286	111	0.27	0.02	0.71
20 mM MgSO4	249	135	0.21	0.05	0.78
50 mM MgSO4	99	24	0.24	0.00	2.26

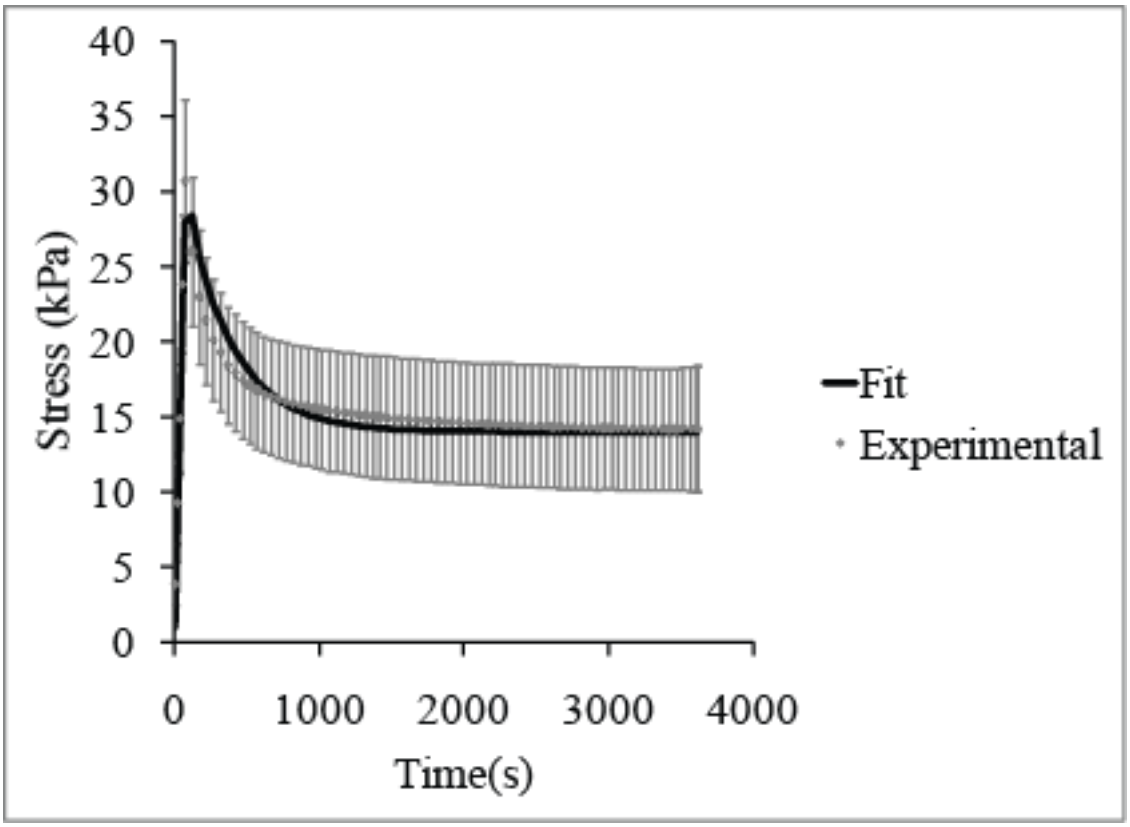

Figure 11. Average stress response of the 0.8 mM Mg^{2+} constructs at 10% strain and curve fit. The experimental average is the average stress response of all constructs in the group with the error bars indicating standard deviation. The fit average was obtained by determining the best fit parameters for the average stress response.

4.4 DISCUSSION

The results of this study demonstrate the histological, biochemical, and mechanical differences between scaffoldless constructs cultured in high concentrations of magnesium. The extracellular matrix components (GAG, collagen) and cell content of the 0.8mM Mg^{2+} fibrochondrocyte constructs were similar to what has previously been reported by Anderson et al [69] using the same tissue engineering approach. A vital dye assay was performed on our constructs prior to mechanical testing (results not shown), showing that a majority of the cells in the scaffoldless construct were alive, which is consistent with the results from the DNA assay. The amount of matrix produced per cell number was examined and it was found that there was an overall trend of increased GAG/DNA and collagen/DNA content from the addition of magnesium ions when compared to control. In comparison to chondrocyte behavior, Feyerabend et al. demonstrated that magnesium concentrations higher than 10 mM led to an increase in GAG production in human chondrocytes in the redifferentiation phase [99]. This finding corresponds with the results obtained from this study, where concentrations of magnesium of 50 mM were reached before finding a significant reduction in matrix production, albeit using different experimental conditions. This suggests that fibrochondrocytes have a high degree of resilience to increasing magnesium concentrations, as significant differences in collagen and GAG production were not observed between 0.8 mM Mg^{2+} and 20 mM Mg^{2+} constructs.

Interestingly, constructs cultured in 20 mM $MgSO_4$ exhibited a collagen II/I ratio of approximately twice that of the control. This suggests that the addition of 20 mM $MgSO_4$ may be beneficial for collagen type II production. This is consistent with the finding that magnesium cations support integrin-mediated chondrocyte attachment to type II collagen [102]. Additional interaction between the sulfate anion could explain why this effect was observed in the $MgSO_4$

constructs and not the $MgCl_2$ constructs. The therapeutic effects of $MgSO_4$ have been studied in an osteoarthtic rat model, and it was shown that intra-articular administration of $MgSO_4$ resulted in a significantly lower degree of cartilage degeneration [103]. Lee et al. [103] proposed the mechanism behind this response was the inhibition of N-methyl-D-aspartate (NMDA) receptors by Mg^{2+}, which prevents entry of extracellular calcium into cells and prevents chondrocyte damage

The collagen content of the constructs (~7% per dry weight) was less than what has been reported for the native goat TMJ disc and mandibular condylar cartilage (45.7 ±19.6% and 18.6±6.9%, respectively) [101]. Conversely, the GAG content of the 0.8 mM Mg^{2+}, 20, and 50 mM magnesium constructs (~15% per dry weight) was greater than what has been reported for the goat TMJ disc and mandibular condylar cartilage (2.1±1.2% and 4.2±2.1%).[101] The interaction between magnesium ions and growth factors should be examined to determine if there is an optimum combination for suppressing excess GAG while promoting collagen type I production.

Corresponding with the biochemical assessment, constructs cultured in concentrations of magnesium of 50 mM or higher also exhibited decreased mechanical properties. The tangent modulus for all tested groups (~350 kPa) was in a similar range to that which was obtained for the goat TMJ disc and mandibular condylar cartilage at 10% strain (304±141 kPa and 205±107 kPa, respectively) [101]. This demonstrates that the scaffoldless constructs do achieve compressive mechanical integrity which is comparable to that of TMJ native tissue. Additionally, the dissimilarities between the native tissue and the engineered constructs in regards to matrix organization would also have an impact on tensile properties of the tissue, as aligned collagen fibers exhibit high tensile strength axially. It is important to note that the

compressive tangent modulus reported in this study is greater than the compressive instantaneous modulus of scaffoldless constructs reported by Anderson *et al.* (55.0±14.7 kPa) [68].

A limitation of this study was the use of magnesium ions as opposed to potential magnesium implant materials. The effect of degrading magnesium alloys on magnesium ion concentration and fibrocartilage regeneration should be assessed to ensure that the products of degrading magnesium-based implant materials do not inhibit matrix production. While other alloying elements may also potentially have an impact on cells which needs to be investigated, testing the primary component, magnesium, is a crucial first step in determining the biological impact of these alloys. Furthermore, depending on the corrosive mechanism of the implant material, the concentration of degrading magnesium is likely to not be continuous over a four week period. Future studies should be performed to determine how fibrochondrocytes matrix production is altered in response to fluctuations in magnesium concentrations. Furthermore, the effect of osmolality on fibrochondrocytes biology should be controlled for in future studies, since Fischer et al. [104] demonstrated a linear increase in osmolality in relation to concentration of $MgCl_2$. Additionally, it is notable that $MgSO_4$ has a substantial impact on collagen type II where $MgCl_2$ does not, meriting a control experiment using $NaSO_4$ to determine if this effect is due to sulfate. Finally, in vivo testing is crucial since the in vitro corrosion does not necessarily reflect the in vivo corrosion behavior [105].

Understanding the effect of high concentrations of magnesium on fibrochondrocyte behavior in vivo is a vital step towards application of biodegradable magnesium-based implants to the TMJ. This study demonstrates that there are specific ranges of magnesium ion concentration that are optimum for cell survival, matrix production, and fibrocartilage

regeneration. As the role of magnesium in the regeneration process becomes further understood, the appropriate design criteria for tissue engineered devices can be established.

5.0 POLY (GLYCEROL SEBACATE): A NOVEL SCAFFOLD MATERIAL FOR TEMPOROMANDIBULAR JOINT DISC ENGINEERING[4]

5.1 INTRODUCTION

The temporomandibular joint (TMJ) is a bilateral joint consisting of the articulation of the condyle of the mandible against the glenoid fossa of the temporal bone. A fibrocartilage disc rests between the condyle and the fossa, acting as a distributer of compressive, tensile, and shear loads during mandibular movements [63, 106-108]. It is estimated that 10 million Americans suffer from temporomandibular joint disorders (TMDs) [1], with up to 70% exhibiting displacement of the TMJ disc [2], or an abnormal positional relationship of the disc relative to the mandibular condyle and the articular eminence. When the displaced disc becomes morphologically damaged, surgeons may perform discectomy with or without autograft replacement. While autografts have been demonstrated to prevent the onset of crepitus [109], or a grating noise during joint movement, which often occurs in discectomy alone [21-23], they are limited by their propensity to perforate and resorb in addition to increased donor site morbidity [16]. Since the TMJ disc is relatively avascular and does not spontaneously regenerate or repair itself in-vivo [110], it has become a target for tissue engineering.

[4] Hagandora, C.K., et al., *Poly (glycerol sebacate): a novel scaffold material for temporomandibular joint disc engineering.* Tissue Eng Part A, 2013. **19**(5-6): p. 729-37.

The ideal scaffold for engineering the TMJ disc should be biodegradable, sufficiently porous to allow for the diffusion of nutrients to cells [111], support matrix deposition, and provide adequate mechanical support throughout the regeneration process. Up to this point, TMJ fibrocartilage engineering techniques using alginate [112], poly glycolic acid (PGA) [112, 113], and poly-L-lactic-acid (PLLA) [114] have been attempted with varying success. The intrinsic challenge of regenerating a suitable TMJ disc replacement is engineering a structure that achieves levels of type I collagen and GAG comparable to the native TMJ disc [115].

Poly (glycerol sebacate) (PGS) is a biocompatible, biodegradable polymer [116] which has shown great potential as a scaffolding material for soft tissue engineering applications [117]. As a first step towards tissue engineering of the TMJ disc, we will determine whether PGS provides an acceptable environment for fibrochondrocyte attachment and matrix production. Furthermore, the optimum cell seeding density of fibrochondrocytes in porous PGS scaffolds must be evaluated.

Unlike TMJ disc cells, which are difficult to obtain and unlikely to provide a viable cell source from diseased tissues, costal cartilage, which is used clinically as an autogenous tissue graft for TMJ reconstruction, can be easily harvested. Additionally, previous studies have shown that costal chondrocytes, which become more like fibrochondrocytes with increased passage number, produce the highest collagen per wet weight to date in scaffoldless tissue culture [68, 69]. The objective of this study was to determine the effect of cell seeding density of goat fibrochondrocytes in PGS scaffolds on the extracellular matrix production and biomechanical properties of the tissue engineered scaffolds. Cells were seeded at concentrations of 25, 50, and 100 million cells/ml of scaffold (low, medium, and high seeding density groups) and were tested histologically and biochemically after 24 hours, 2 weeks, and 4 weeks of culture. The

mechanical properties of the scaffolds in unconfined compression were assessed at 24 hrs and 4 weeks. The selected range of low, medium, and high seeding densities: 25- 100 million cells/ml scaffold, was based off a study performed by Almarza *et al.*, in which a high seeding density of 120 million cells/ml of PGA scaffold resulted in the highest collagen production by porcine TMJ disc fibrochondrocytes [113]. Saturation effect was noted between medium (30 million cells/ml of scaffold) and high (120 million cells/ml of scaffold) density seeding and it was suggested that 75 million cells/ml of scaffold would likely be ideal for porcine TMJ disc cells seeded in PGA scaffolds. Therefore, we decided to test within a similar range of seeding densities for our goat fibrochondrocytes seeded in PGS scaffolds. The 24 hour time point was evaluated to determine the cell seeding efficiency as well as a way of measuring the initial compressive strength of the scaffold. Previous studies using goat costal fibrochondrocytes have not shown major ECM deposition beyond 4 weeks, and thus it was chosen as the last time point. The 2 week time point was evaluated in order to assess the behavior through time. In this study, we evaluated both time points to ensure that, despite degradation of the PGS scaffold, there continued to be an increase in extracellular matrix production.

5.2 METHODS

5.2.1 Cell Isolation and Culture

Goat costal cartilage was isolated from the ribs of three young (<1 year) female Boer goats within 24 hours of slaughter. The fibrocartilage was minced and digested in 2 mg/ml type II collagenase (Worthington) overnight at 37°C and 5% CO_2 with mechanical agitation. Isolated

fibrochondrocytes were passaged three times in Dulbecco's modified Eagle medium (DMEM)/high glucose (Thermo Scientific), 10% fetal bovine serum (Atlantic Biologicals), 1% penicillin-streptomycin (Lonza), 1% non-essential amino acid solution (Thermo Scientific) and 25 μg/ml L-ascorbic acid (Sigma-Aldrich). The cells were frozen after passage one in passage media with 5% DMSO and an additional 10% FBS and then thawed and passaged twice to allow for simultaneous seeding of the scaffolds.

5.2.2 Cell Seeding

PGS sheets were prepared as previously described, using salt particles of 75-150 μm, which have been shown to facilitate fibroblast attachment and diffusion [117]. Scaffolds were cut from a PGS sheet of approximately 1.3 mm thickness using a 5 mm biopsy punch. Scaffolds were seeded at 25, 50, and 100 million cells/ml of scaffold in 10 μl of chondrogenic media using a 25 gauge needle. Chondrogenic media consisted of DMEM/high glucose (Thermo) supplemented with 1% penicillin-streptomycin (Lonza), MEM 1% non-essential amino acid solution (Thermo Scientific), 1% insulin-transferrin-selenium + premix (BD Biosciences), 0.1 μM dexamethasone (MP Biomedicals), 40 μg/mL L-proline (Acros Organics) and 50 μg/mL ascorbate 2-phosphate (Sigma-Aldrich) [68]. Scaffolds were cultured in 24-well plates coated in 2% agarose. After seeding, the media was replenished every 48 hours (1 ml of media per well). Scaffolds were cultured in 37° C and 5% CO_2 on an orbital shaker (approximately 9 orbits per minute) for 24 hours, 2 weeks, and 4 weeks.

5.2.3 Histology

Scaffolds (*n*=3 per group) were embedded in OCT freezing medium (Tissue-Teck) and flash frozen to -80°C. The samples were cryo-sectioned at 6 μm, fixed in cold acetone, and stained with hematoxylin and eosin to visualize cell cellular content and distribution, picrosirius red for collagen staining and Safranin-O/Fast green for GAG staining. Immunostaining for collagen types I and II was performed, as previously described [118], using a Vectastain® ABC kit (Vector Laboratories), monoclonal anti-collagen type I antibody produced in mouse (Sigma), and anti-human collagen type II produced in mouse (MP Biomedicals) [100, 118]. Negative stains were also performed without applying the primary antibody. All images were obtained on a Nikon Eclipse TE2000E inverted light microscope.

5.2.4 Biochemistry

Scaffolds (*n*=6 per group) were dried on the Speed Vac (Thermo) overnight and digested as previously described [69]. Briefly, samples were digested at 4°C with constant mechanical agitation in 125 ug/mL papain (Sigma-Aldrich) for 8 days followed by 1 mg/ml elastase (Sigma-Aldrich) digestion for 3 days. All scaffolds were dried and stored in -20°C until digestion was ready to be performed on all samples at once. All assays were performed using this digest. The DNA content was measured using a PicoGreen® dsDNA quantitation kit (Molecular Probes, Inc., Eugene, Oregon). The total hydroxyproline content was assessed using the modified protocol of reacting the samples with chloramine T and dimethylaminobenzaldehyde that allows for a colorimetric comparison and compared against collagen standards [72]. The total amount

of GAG was measured using a dimethymethylene blue colorimetric assay kit (Biocolor; Newtownabbey, UK).

5.2.5 Compression Testing

Unconfined compression testing and analysis was performed per our published methods (n=6 per group) [119]. Scaffolds were tested at 2 time points, 24 hours and 4 weeks, in order to compare changes in mechanical integrity as a result of matrix deposition over the 4 week period. The construct diameter was measured prior to testing using digital calipers. The scaffolds were attached to a compression platen using cyanoacrylate. To estimate construct height, force was applied to the construct until reaching 0.02 N, at which point the crosshead position was noted and the platen was immediately removed. The water bath was then filled with PBS and the thermocouple was set to 37°C prior to testing. The MTS Insight® was used to measure changes in force throughout the test. The upper platen was lowered within 0.1 mm of the determined construct height and a preload of 0.05 N was applied for 30 minutes. In the compression testing analysis, the estimated effect of buoyant force is not subtracted from the acquired force reading. However, by determining the construct height using the compression system prior to filling the water bath, we believe we are minimizing error that may be attributed to buoyant force. By zeroing the load at 0.1 mm above the sample, there is an average travel path of approximately 0.3 mm which would result in a buoyant force which is well below the accuracy of our load cell. The height at the end of the preload was taken to be the height of the construct and was utilized in subsequent calculations. The scaffolds then underwent 10 cycles of preconditioning at 9%/min until 10% strain was reached [78, 119]. Immediately following preconditioning, the

samples were compressed until 10% strain was reached, and were allowed to relax for 60 minutes.

A tangent modulus was fit to the linear portion of the stress strain curve using Matlab®, defined as the last 2% of 10% strain. The percent relaxation was determined by evaluating the ratio of the stress of the relaxed specimen, with the specimen considered fully relaxed at 60 minutes, to the peak stress.

5.2.6 Statistical Analysis

A two-way ANOVA was used to assess differences for biochemical and biomechanical values within culture time and seeding density with $p<0.05$ defined as statistically significant. Tukey's post hoc testing was used to examine differences between groups. Outliers were defined as observations with values exceeding 1.5 times the interquartile range and were excluded from the analysis. All statistical analysis was performed using Minitab. All data is reported as average ± standard deviation of the means.

5.3 RESULTS

5.3.1 Gross Morphology

The gross morphology of the PGS scaffolds at 24 hours and 4 weeks after cell seeding is shown in **Figure 12**. At all time points and seeding densities scaffolds were indistinguishable by size, shape and opacity of the cell seeded construct.

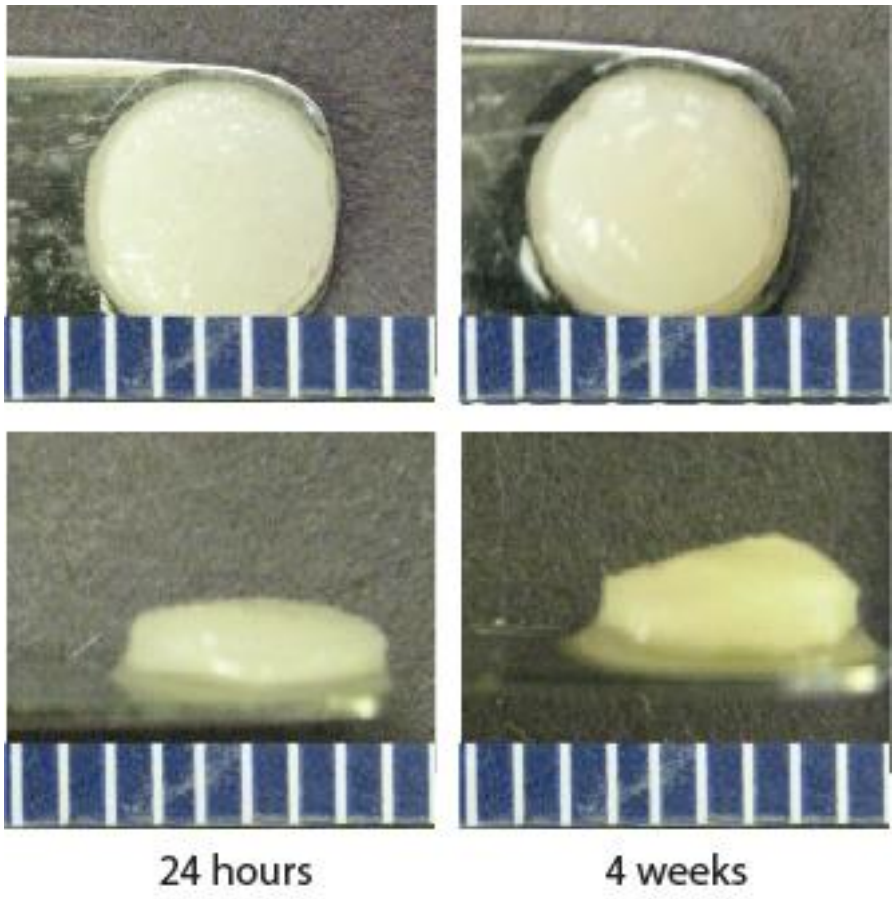

Figure 12. Gross morphology of the high seeding density PGS scaffolds at 24 hours and 4 weeks.

5.3.2 Histology

The PGS scaffolds stained with hematoxylin and eosin are shown in **Figure 13**. The images were magnified to show matrix deposition from the edge to the center of the PGS scaffolds. There was an increase in areas of staining with high seeding density and time. The staining reveals proliferation of fibrochondrocytes as well as an increase in extracellular matrix over time. At 4 weeks, the high seeding density group appeared to have more lacunae than the other groups, corresponding to an increase in cellular content over time.

The images from the histological assessment of specific matrix content are shown in **Figure 14**. The images show matrix deposition from the edge to the center of the PGS scaffolds. No specific staining for GAG or collagen was seen at 24 hours, thus images are not shown. All groups stained positively for GAG at weeks 2 and 4. There tended to be an increase in areas of staining with high seeding density and time. There was variability in the way matrix was deposited throughout the scaffolds with some scaffolds showing matrix deposition throughout and others with matrix deposition confined to the edges, not dependent on seeding density.

The picrosirius red stain revealed that all groups also stained positively for collagen at 2 and 4 weeks. (**Figure 14**) Corresponding with the biochemistry findings, there was an increase in areas of collagen staining at later time points. Similar to the GAG results, there was a random distribution of collagen throughout the scaffold with some scaffolds exhibiting collagen throughout and others with collagen on one or both edges of the scaffold, not dependent on seeding density.

The scaffolds demonstrated sparse staining for collagen type I that was indistinguishable from the negative control with the primary antibody removed. There was positive staining for collagen type II throughout the scaffolds at weeks 2 and 4. (**Figure 14**) A side-by-side

comparison of the positive and negative collagen type II stain is shown in **Figure 15**. At week 4, there were more areas of staining for collagen type II in the center of the scaffolds than in week 2, where collagen type II staining was confined to the outer edges of the scaffold.

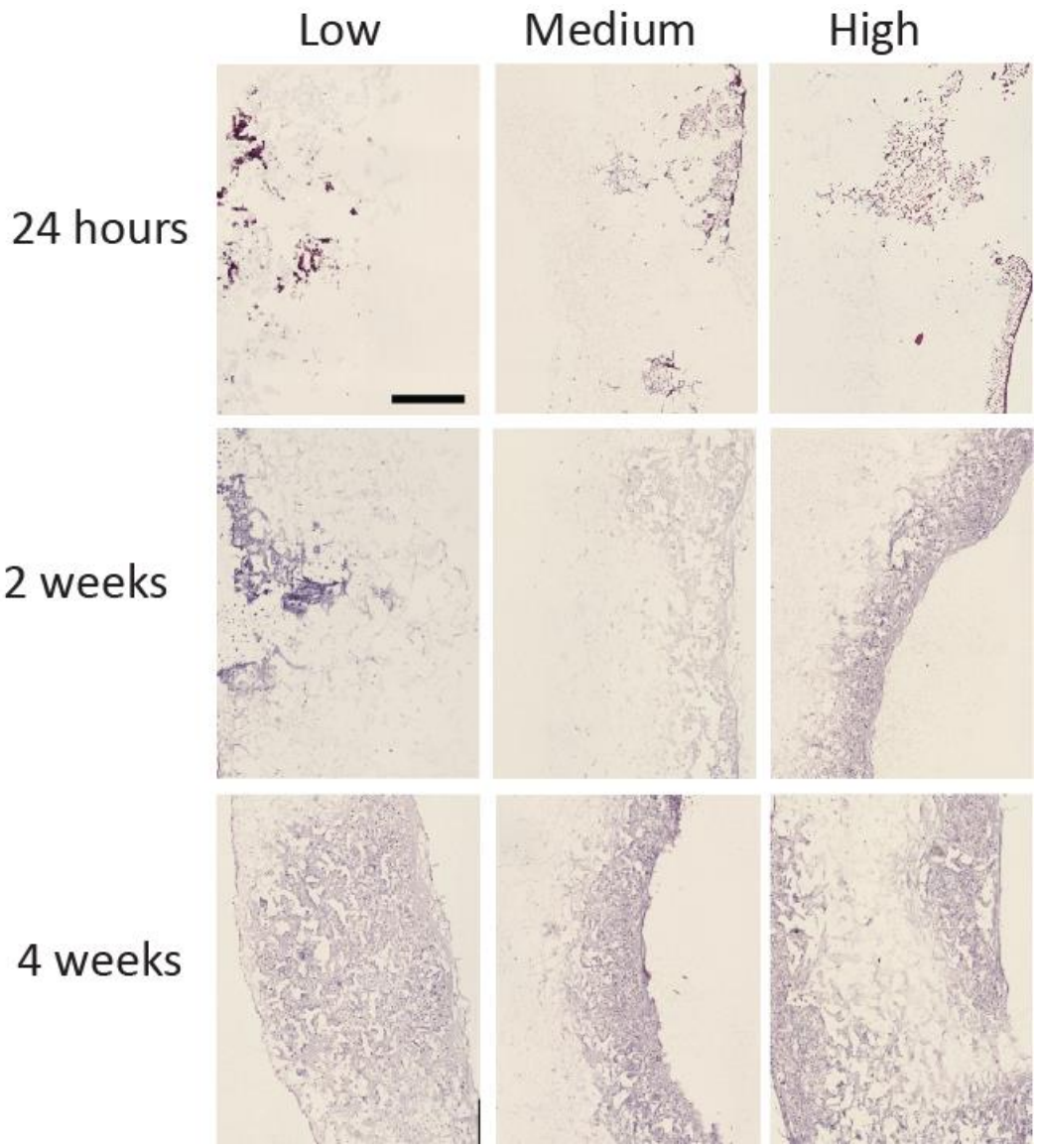

Figure 13. Hematoxylin and Eosin staining of the low, medium, and high seeding density PGS scaffolds at 24 hours, 2 weeks, and 4 weeks. Scale bar is 500 μm.

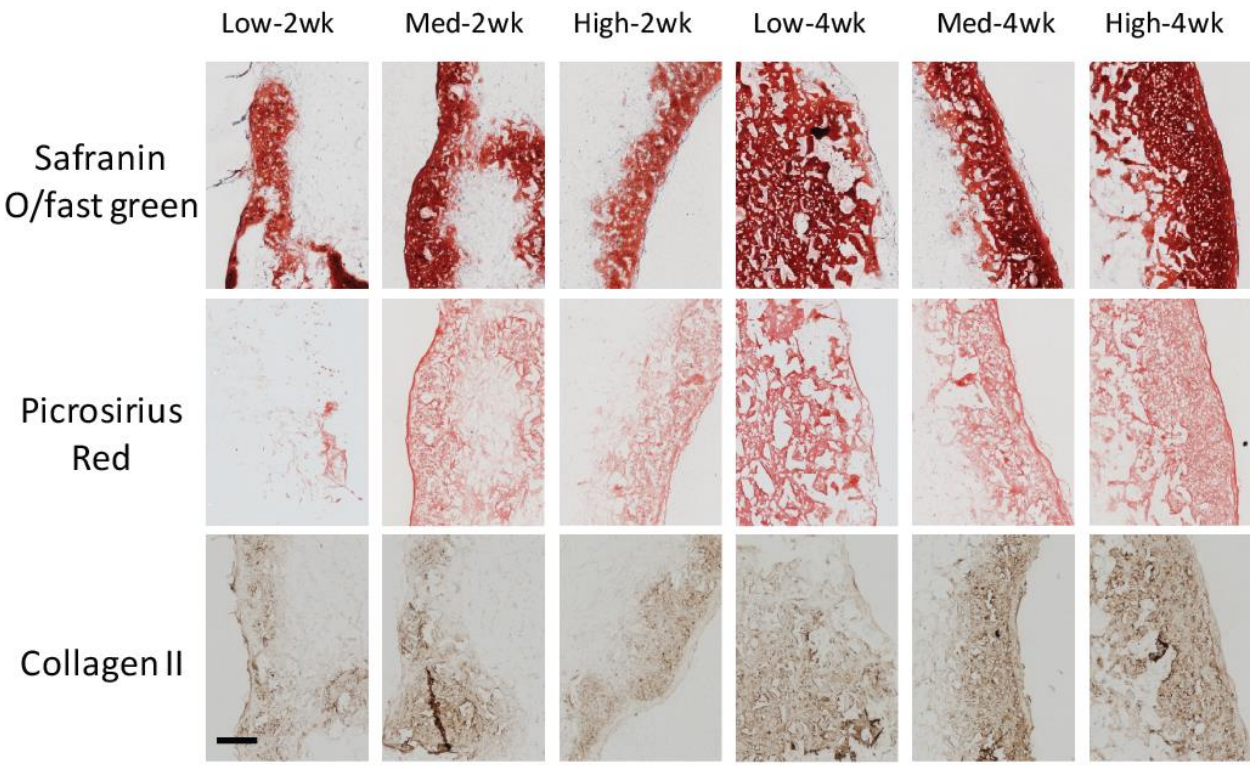

Figure 14. Histological staining of the PGS scaffolds. Row 1: Safranin o/fast green staining for GAG. Row 2: Picrosirius red staining for collagen. Row 3: Collagen type II immunostain. Scale bar is 250 μm.

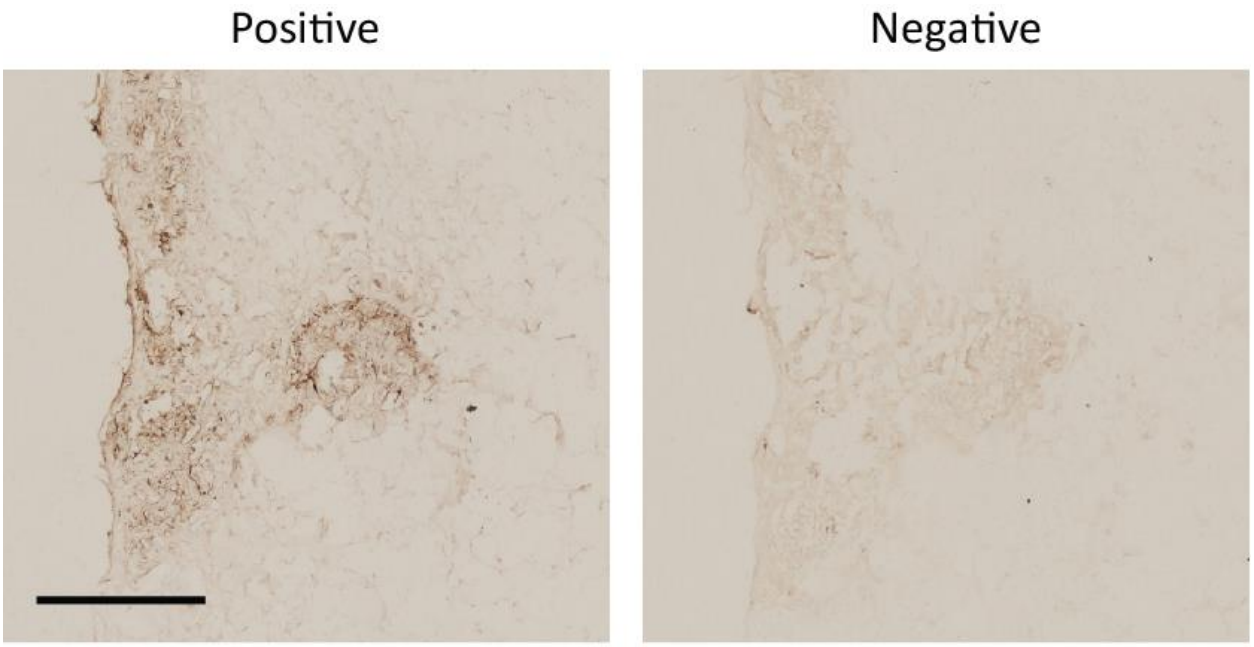

Figure 15. Example of collagen type II positive and negative stain. Scale bar is 500 µm.

5.3.3 Biochemical Content

The cell content of the scaffolds is shown in **Figure 16a**. There were no significant differences between seeding density groups within each time point. There was a significant increase in cellular content at 4 weeks when compared to 2 weeks and 24 hours ($6.7\pm1.8 \times 10^5$ compared to $4.6\pm0.9 \times 10^5$ and $3.7\pm1.0 \times 10^5$ cells/construct, respectively (low, medium, and high groups combined)) ($p<0.001$). Also, the low seeding density group had significantly lower cell content than the medium and high seeding density groups across all time points. ($4.0\pm1.3 \times 10^5$ compared to $5.5\pm2.1 \times 10^5$ and $5.6\pm1.7 \times 10^5$ cells/construct, respectively (24 hour, 2 week, and 4 week time points combined)) ($p<0.001$).

The collagen content of the scaffolds is shown in **Figure 16b**. There were significant differences in collagen content of the scaffolds between seeding density groups and time (Error! Reference source not found.) ($p<0.001$). In the low seeding density group there was a significant difference in collagen content between 24 hours and 2 weeks (24±3 μg and 72±19 μg of collagen per construct, respectively). In the medium seeding density group, there was a significant increase in collagen content at each time point (38±6 μg, 102±34 μg, and 181±46 μg of collagen per construct at 24 hours, 2 weeks, and 4 weeks, respectively) ($p<0.001$). Similarly, in the high seeding density group there was a significant increase in collagen content at each time point (36±7 μg, 100±22 μg, and 218±24 μg of collagen per construct at 24 hours, 2 weeks, and 4 weeks, respectively) ($p<0.001$). There were no significant differences between the low, medium, and high seeding density groups at 24 hours and 2 weeks. At 4 weeks, the low seeding density group had significantly lower collagen content per scaffold (105±28 μg) than the medium and high seeding density groups (181±46 μg and 218±24 μg of collagen per scaffold, respectively ($p<0.001$).

The GAG content of the scaffolds is shown in **Figure 16c**. There were significant differences in GAG content of the scaffolds between seeding density groups and time (Error! Reference source not found.) (p<0.001). In the low seeding density group, there was a significant increase in GAG content between 24 hours and 4 weeks (3±1 μg and 324±73 μg of GAG per scaffold, respectively) (p<0.001). In the medium seeding density group there was a significant increase in GAG content at each time point (9±2 μg, 362±125 μg, and 702±253 μg of GAG per scaffold at 24 hours, 2 weeks, and 4 weeks, respectively) (p<0.001). Similarly, in the high seeding density group there was also an increase in GAG content at each time point (10±3 μg, 338±57 μg, and 773±187 μg of GAG per scaffold at 24 hours, 2 weeks, and 4 weeks, respectively) (p<0.001). There were no significant differences between the low, medium, and high seeding density groups at 24 hours and 2 weeks. At 4 weeks, the low seeding density group had significantly lower GAG content per scaffold (324±73 μg) than the medium and high seeding density groups (702±253 μg and 773±187 μg of GAG per scaffold, respectively) (p<0.001).

Table 6. Differences in μg of collagen in response to time (24 hours, 2 weeks, and 4 weeks) and seeding density (low, medium, and high). Groups that do not share a letter are statistically significant (p<0.001).

Collagen (μg)	Low	Medium	High
24 hours	24±3	38±6	36±7
	D	CD	CD
2 weeks	72±19	102±34	100±22
	BC	B	B
4 weeks	105±28	181±46	218±24
	B	A	A

Table 7. Differences in μg of GAG in response to time (24 hours, 2 weeks, and 4 weeks) and seeding density (low, medium, and high). Groups that do not share a letter are statistically significant (p<0.001).

GAG (μg)	Low	Medium	High
24 hours	3±1	9±2	10±3
	C	C	C
2 weeks	199±27	362±125	338±57
	BC	B	B
4 weeks	324±73	702±253	773±187
	B	A	A

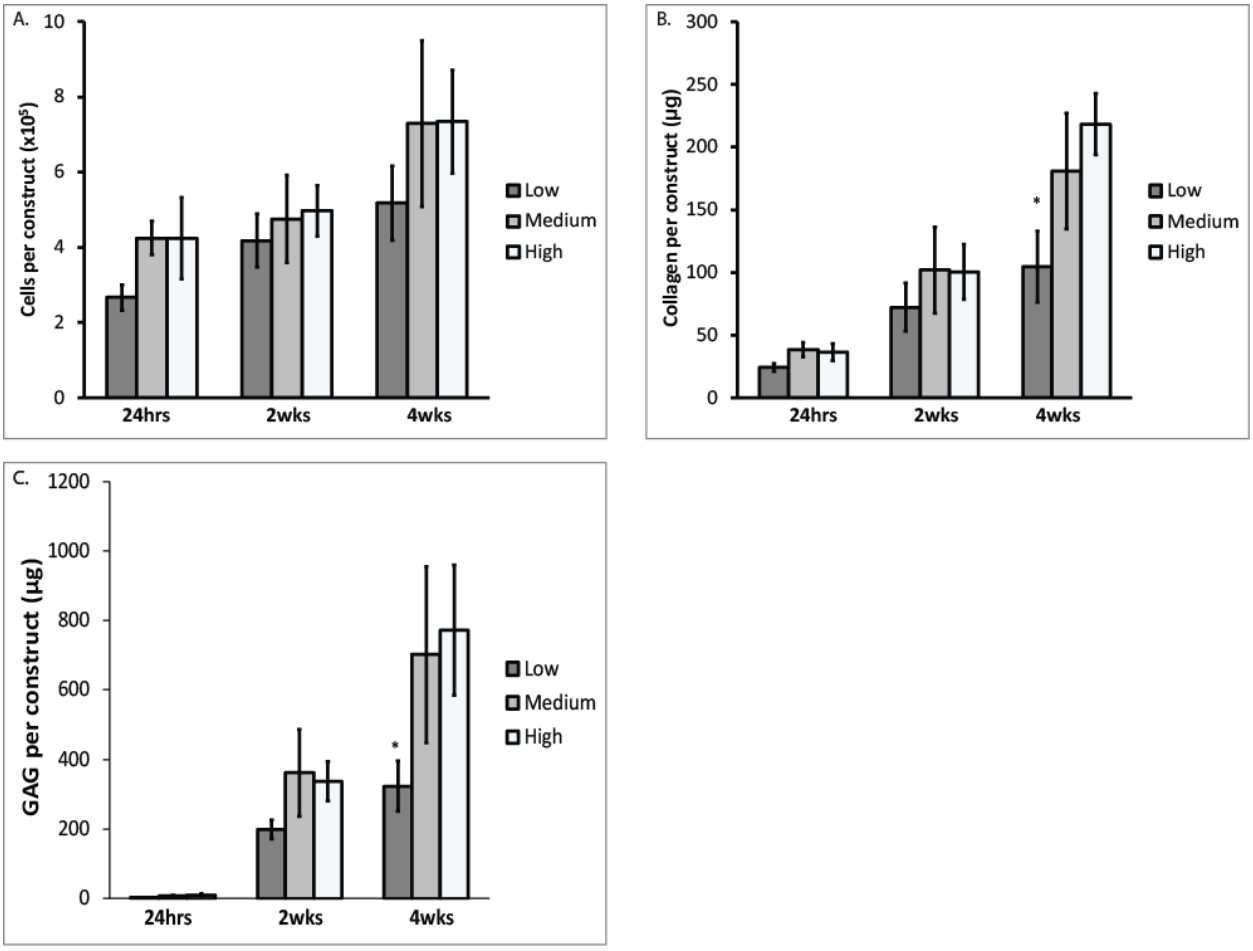

Figure 16. Biochemical content of PGS scaffolds at 24 hours, 2 weeks, and 4 weeks: a. cell content per construct, b. collagen content per construct, and c. GAG content per construct. Error bars indicate average ± standard deviation. The symbol (*) indicates statistical difference between groups at each time point $p<0.001$.

5.3.4 Compression

The results from the compression analysis are shown in **Figure 17**. There was a significant increase in peak stress of the cell-seeded PGS scaffolds at 4 weeks (4.1±0.7 kPa at 24 hours and 10.3±6.1 kPa at 4 weeks) (p<0.001). (**Figure 17a**) There were no significant differences in peak stress between seeding density groups at each time point. Similarly, there was a significant increase in equilibrium stress over the 4 week period (3.6±0.7 kPa at 24 hours and 5.4±1.4 kPa at 4 weeks) (p<0.001) with no differences between seeding density group at each time point. (**Figure 17b**) The percent stress relaxation of the 4 week scaffolds was significantly greater than the 24 hour scaffolds (38.3±11.5% and 14.5±4.2%, respectively) (p<0.001). (**Figure 17c**) There were no significant differences in stress relaxation between seeding density group at each time point. The tangent modulus was significantly greater at 4 weeks than 24 hours (123.6±86.0 kPa and 26.2±5.0 kPa, respectively) (p<0.001). **(Figure 17d**) Again, there were no significant differences between the seeding density groups at each time point.

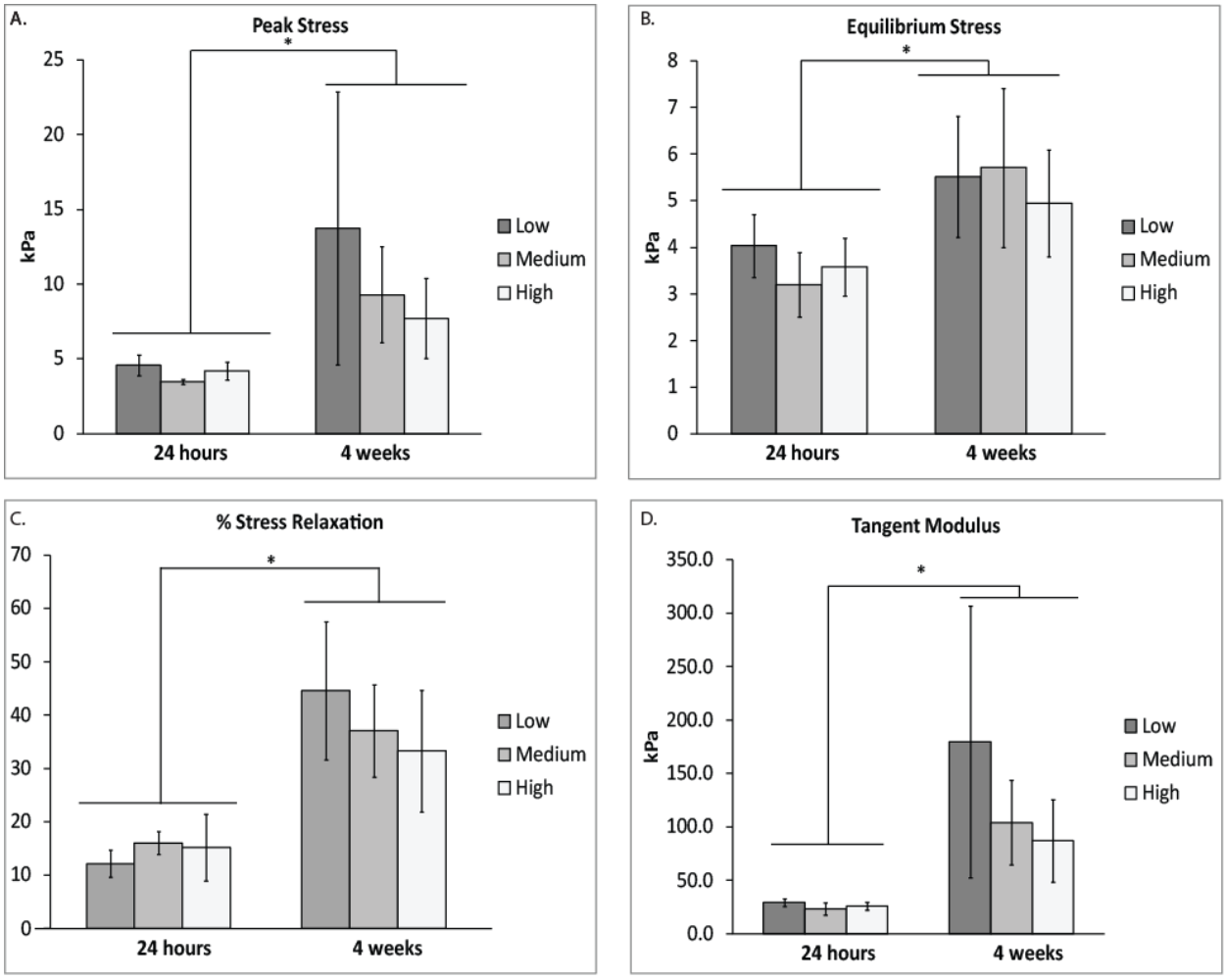

Figure 17. Biomechanical properties of PGS scaffolds at 24 hours and 4 weeks. a. peak stress, b. equilibrium stress, c. percent stress relaxation, and d. tangent modulus. Error bars indicate average ± standard deviation. The symbol (*) indicates $p<0.001$ for all groups between time points.

5.4 DISCUSSION

The results show that PGS shows great potential as a substrate for fibrocartilage regeneration. Cell seeding density and culture time did have an effect on both the biochemical and biomechanical properties of the scaffolds. The histological results confirm the biochemistry findings, indicating an increase in matrix deposition both with time and cell seeding density. Histology also indicated that cells did migrate and deposit matrix throughout the scaffold. This demonstrates that the PGS scaffolds are of a sufficient porosity to support both the migration of cells and diffusion of nutrients. The immunostaining revealed a sparse distribution of type I collagen throughout the scaffold and positive staining for type II collagen. This is consistent with what has been reported when using the same cell type and media formulation [68, 69]. Increasing the collagen type I/II ratio remains a critical challenge in fibrocartilage tissue engineering. It is possible that cyclic compression or *in vivo* mechanical environment is necessary to achieve the proper collagen type I/II ratio.

There was an increase in cellular, GAG, and collagen content over the four week period and an increase in ECM deposition at higher seeding densities. The average amount of collagen produced by goat costal chondrocytes in PGS at four weeks in the high cell seeding density group (218±24 μg collagen per construct) exceeded that which has been reported previously using porcine TMJ disc cells and PGA scaffolds for TMJ disc engineering [113]. In the high seeding density group, there was 3.5±0.5% collagen and 12.1±2.3% GAG per dry weight at 4 weeks which is comparable to scaffoldless constructs which have shown to achieve 6.9±0.5% collagen and 16.5±1.3% GAG per dry weight at 4 weeks [118]. In contrast, the native goat TMJ disc is 45.7±19.6% collagen and 2.1±1.2% GAG per dry weight [119]. Additionally, there was an increase in cell density over time, indicating that, even at high seeding densities, the scaffolds

did not reach saturation, and there was sufficient diffusion of nutrients into the scaffold to support cell proliferation.

The tangent modulus of the low seeding density group at 4 weeks (180±127 kPa) was in the range of what has been reported for the goat TMJ disc (304±141 kPa) [119]. There was a wide range of maximum stress obtained in the low seeding density group at 4 weeks ranging from 5-14 kPa, which, based on histological evidence, was likely due to variations in the way matrix was deposited throughout the scaffold (edges vs. middle). Similarly, there was a significant increase in percent stress relaxation between 24 hours and 4 weeks which ranged from 33±11% to 45±13% in all three seeding density groups, compared to 85±7% which was reported in the goat TMJ disc [119]. The increase in tangent modulus of the PGS scaffolds over the 4 week period provides evidence that the degradation rate of the material is slow enough to allow for the regeneration of ECM and restoration of mechanical integrity. The change in stress relaxation behavior is a positive indicator that the tissue engineered constructs are becoming more viscoelastic, and better emulating the mechanical behavior of the native TMJ disc.

In this study, the amount of collagen and GAG per scaffold exceeded that which has been reported using TMJ disc cells on PLLA scaffolds with exogenous growth factors [114]. A noteworthy advantage to using the PGS scaffold material is avoidance of scaffold contraction observed in PGA non-woven meshes, which have shown to reduce in volume by over 50% in 4-6 weeks [120]. In this study, the dimensions of the unseeded PGS scaffolds were indistinguishable from the 4 week cell-seeded scaffolds. In contrast, scaffoldless constructs using the same cell type and media formulation exhibit varying morphology dependent on the culture time [69]. Furthermore, scaffoldless constructs fail to support cell viability and matrix production in the center of the construct, likely due to limitations in nutrient diffusion [118]. However, the

fibrochondrocytes utilized in the study were able to successfully deposit matrix throughout the PGS scaffold, indicating that using scaffolding materials with sufficient porosity is key to supporting cell growth and ECM production. A limitation in this study was the non-homogenous cell and matrix distribution within the PGS scaffolds, which could be ameliorated by using smaller scaffolds, multiple injections of cells during seeding, cyclic compression, and/or spinner flasks [112]. Additionally, in order to make the engineered tissue more fibrocartilagenous, steps must be taken to adjust the collagen type I and GAG content closer to the native tissue. In order to increase the collagen type I/II ratio, the incorporation of combinations of growth factors such as insulin-like growth factor-I, transforming growth factor-β1, or basic fibroblast growth factor could be employed [121]. Chondroitinase could also be utilized to deplete the excess GAG production, allowing more space for the production of additional collagen. It has also been shown that the application of mechanical stimuli during culture could potentially enhance type I collagen production and organization of fibrochondrocytes [122]. In future studies, the effect of mechanical stimulation on collagen production will be assessed by analyzing gene expression. Finally, the use of co-culture with costal chondrocytes and TMJ disc cells could also be used to increase collagen type I production [123].

This study demonstrated the potential of PGS as a scaffold material for fibrocartilage engineering, with the highest seeding density and longest time point producing the greatest amount of extracellular matrix. It has been shown that fibrochondrocytes respond to the application of mechanical forces by producing elevated amounts of extracellular matrix [122]. It is hypothesized that the elastomeric properties of PGS will allow for the transduction of force to cells seeded on the scaffold, enhancing both the production and organization of collagen. Therefore, a future aim is to test the effect of the application of both static and cyclic

compression on the matrix production of fibrochondrocytes seeded on PGS scaffolds. Additionally, the ability of autologous cell-conditioned scaffolds to promote the regeneration of TMJ fibrocartilage *in vivo* will also be assessed.

6.0 EXPLORING THE EFFECTS OF SPINNER FLASK CULTURE AND MECHANICAL STIMULATION ON TMJ FIBROCARTILAGE ENGINEERING

6.1 INTRODUCTION

The articulating surfaces of the temporomandibular joint (TMJ) include the fibrocartilage-covered condyle of the mandible and articular eminence of the temporal bone. A fibrocartilage disc is situated between the articulating surfaces, acting as a distributor of loads during mandibular movement. Ten million Americans are affected by TMJ disorders (TMDs), which can be defined as a group of conditions which cause pain and dysfunction in the jaw joint [1]. Mechanical damage in the joint is often characterized by displacement of the disc relative to the mandibular condyle and degeneration of the joint surfaces. Patients with severe symptoms resort to invasive surgical interventions such as disc repositioning, discectomy, and replacement of the condyle, fossa, or both components with a prosthetic device [124]. The insufficiencies of commercially available devices drive the need to further explore tissue engineered alternatives.

In the past ten years, attempts have been made to tissue engineer TMJ fibrocartilage using poly glycolic acid [112, 113], poly-L-lactic acid [114], and alginate [112] scaffolds with variable successes. Poly(glycerol sebacate) (PGS) is a biocompatible, biodegradable polymer which has recently shown potential for TMJ tissue engineering applications [125]. Goat costal fibrochondrocytes seeded on PGS scaffolds via injection produced both collagen and

glycosaminoglycans (GAGs) [125]. However, extracellular matrix (ECM) production may be further enhanced by improving cell seeding efficiency and distribution, based on the postulation that a homogenous distribution of cells throughout a porous scaffold would allow more space for matrix regeneration per cell. It has been shown that spinner flask cell seeding on PGA scaffolds resulted in higher collagen production of porcine TMJ disc cells when compared to orbital shaker and pellet culture [112]. Based on this finding, we believe that culturing fibrochondrocytes on PGS in a spinner flask bioreactor environment will allow for increased ECM production.

Two major challenges unique to TMJ fibrocartilage tissue engineering are increasing the amount of collagen production and mimicking the structural organization of the native tissue. It has been shown that TMJ disc cells subjected to mechanical forces produced greater amounts of collagen type I when compared to static culture [122]. PGS is an elastomeric material which may allow seeded cells to sense and respond to mechanical forces in a three-dimensional environment. Applying compressive forces to cells seeded on PGS scaffolds may help recapitulate a loaded joint environment and improve collagen production and organization. However, it is unknown at what maturation point during *in vitro* culture that fibrochondrocytes benefit most from applied mechanical stimulation.

The goals of this study were twofold: first, to explore spinner flask culture as a way of improving cell seeding efficiency, distribution, and survival in PGS scaffolds; and second, to determine the effect of length of mechanical stimulation on fibrochondrocyte ECM production. Costal cartilage is used clinically as a TMJ graft material [126], so goat costal fibrochondrocytes were chosen as a relevant cell source for TMJ fibrocartilage tissue engineering. A compression culture system was utilized to determine the effect of long and short periods of dynamic compressive loading on the biochemical and biomechanical properties of PGS scaffolds seeded

with fibrochondrocytes. We hypothesize that allowing scaffolds to mature for six weeks in a spinner flask environment prior to application of mechanical stimulation will result in higher ECM production and greater mechanical properties when compared to the control. This is based on pilot studies which demonstrate that a longer culture time allows for the development of a more robust neocartilage.

6.2 MATERIALS AND METHODS

6.2.1 Cell Isolation and Expansion

Goat costal cartilage was isolated from the ribs of three young (<1 year) female Boer goats within 24 hours of slaughter. The fibrocartilage was minced and digested in 2 mg/ml type II collagenase (Worthington) overnight at 37°C and 5% CO_2 with mechanical agitation. Isolated fibrochondrocytes were passaged four times in Dulbecco's modified Eagle medium (DMEM)/high glucose (Thermo Scientific) 10% fetal bovine serum (Atlantic Biologicals), 1% penicillin-streptomycin (Lonza), 1% non-essential amino acid solution (Thermo Scientific), and 25 μg/ml L-ascorbic acid (Sigma-Aldrich).

6.2.2 Spinner Flask Culture

PGS sheets were prepared as previously described [117], using salt particles of 75-150 μm. Scaffolds were cut from a PGS sheet of approximately 1.5 mm thickness using a 4 mm biopsy punch. 50 scaffolds were seeded in chonodrogenic media at 75 million cells/ml of scaffold (70.7

million cells total) in one 250 ml spinner flask at 60 rotations per minute. Chondrogenic media consisted of DMEM/high glucose (Thermo) supplemented with 1% penicillin-streptomycin (Lonza), MEM 1% non-essential amino acid solution (Thermo Scientific), 1% insulin-transferrin-selenium + premix (BD Biosciences), 0.1 μM dexamethasone (MP Biomedicals), 40 μg/mL L-proline (Acros Organics) and 50 μg/mL ascorbate 2-phosphate (Sigma-Aldrich) [68]. The scaffolds were cultured in 37° C and 5% CO_2 for 4 weeks and 250 ml of media changed weekly.

6.2.3 Mechanical Stimulation

After the 4 weeks of spinner flask culture, mechanical stimulation was applied to scaffolds using the Flexcell® Compression System. Scaffolds were moved to BioPress™ compression plates. Stationary platens were adjusted such that the bottom of the center screw just touched the top of the sample (assuming a sample height of 1.5 mm) and inserted into the wells of the culture plates. A loading regimen of three cycles of 1 hour on and 1 hour off dynamic compression following a sine waveform at 1 Hz was applied. An estimated peak stress of 177 kPa was applied to the scaffolds, corresponding to the lowest possible applied force using the Flexcell system. The experimental groups are shown in Error! Reference source not found.. In the long stimulation group, the dynamic compressive loading regimen was applied 5 days a week for 4 weeks. In the short stimulation group, scaffolds were cultured for an additional 2 weeks exclusively in a spinner flask before undergoing the loading regimen for 2 weeks. Corresponding control scaffolds from each group were also moved to compression plates with platens but were not subjected to mechanical stimulation. The two control groups were later combined into one static control group. When not undergoing static or dynamic loading (18

hours a day), all scaffolds were maintained in 100 ml spinner flasks and all constructs were cultured for a total of 8 weeks.

Table 8. Loading regimen

	0-4 weeks	**4-6 weeks**	**6-8 weeks**
Long Stimulation	250 ml spinner flask	Mechanical stimulation 4 hours/day 100 ml spinner flask 20 hours/day	Mechanical stimulation 4 hours/day 100 ml spinner flask 20 hours/day
Short Stimulation	250 ml spinner flask	100 ml spinner flask	Mechanical stimulation 4 hours/day 100 ml spinner flask 20 hours/day
Nonstimulated Control	250 ml spinner flask	Flexcell plates 4 hours/day 100 ml spinner flask 20 hours/day	Flexcell plates 4 hours/day 100 ml spinner flask 20 hours/day

6.2.4 Histology

Constructs (*n*=3 per group) were embedded in OCT freezing medium (Tissue-Tek) and flash frozen to -80°C. The samples were cryo-sectioned at 6 μm, fixed in cold acetone, and stained with picrosirius red for collagen staining and Safranin-O/Fast green for GAG staining [125]. Immunostaining for collagen types I and II was performed as previously described [127], using a Vectastain® ABC kit (Vector Laboratories), monoclonal anti-human collagen type I antibody produced in mouse (Sigma), and monoclonal anti-human collagen type II produced in mouse (MP Biomedicals) [100, 127]. Negative stains were also performed without applying the primary antibody.

6.2.5 Biochemistry

Constructs (*n*=6 per group, same used for mechanical testing) were dried on the SpeedVac overnight and digested in a 125 μg/ml papain solution in 50 mmol phosphate buffer containing 5 mmol N-acetyl cystein for 24 hours at 65°C [80]. The DNA content was measured using a PicoGreen® dsDNA quantitation kit (Molecular Probes, Inc., Eugene, Oregon). The total hydroxyproline content was assessed using the modified protocol of reacting the samples with chloramine T and dimethylaminobenzaldehyde that allows for a colorimetric comparison and compared against collagen standards [72]. The total amount of glycosaminoglycan was measured using a dimethymethylene blue colorimetric assay kit (Biocolor; Newtownabbey, UK).

6.2.6 Compression Testing

Unconfined compression testing and analysis was performed per our published methods (n=6 per group) [101]. Prior to testing, the scaffold diameter was measured using digital calipers. The scaffolds were placed on a compression platen using a thin layer of cyanoacrylate. To determine an approximate construct height, force was applied to the scaffold until reaching 0.02 N, at which point the crosshead position was noted and the platen was immediately removed. The water bath was then filled with PBS and the thermocouple was set to 37°C prior to testing. The MTS Insight® was used to measure changes in force throughout the test. The upper platen was lowered within 0.1 mm of the determined construct height and a preload of 0.05 N was applied for 30 minutes. The height at the end of the preload was taken to be the height of the construct and was utilized in subsequent calculations. The constructs then underwent 10 cycles of preconditioning at 9%/min until 10% strain was reached [78, 101]. Immediately following preconditioning, the samples were compressed until 10% strain was reached, and were allowed to relax for 60 minutes.

A tangent modulus was fit to the linear portion of the stress strain curve using Matlab®, defined as the last 2% of 10% strain. The percent relaxation was determined by evaluating the ratio of the stress of the relaxed specimen, with the specimen considered fully relaxed at 60 minutes, to the peak stress.

6.2.7 Statistical Analysis

A one-way ANOVA was used to assess differences for biochemical and biomechanical values between the three groups (static control, long mechanical stimulation, and short mechanical

stimulation) with $p<0.05$ defined as statistically significant. Tukey's post hoc testing was used to examine differences between groups. Outliers were defined as observations with values exceeding 2.5 times the mean (when removed from dataset) and were excluded from the analysis. All statistical analysis was performed using Minitab®. All data is reported as average ± standard deviation of the means.

6.3 RESULTS

6.3.1 Gross morphology

The representative gross morphology of the PGS scaffolds at 8 weeks is shown in **Figure 18**. Scaffolds from all groups maintained the same diameter throughout the 8 week study and were indistinguishable by opacity. The scaffolds in the long stimulation group had a significantly lower average thickness (1.45 ± 0.09 mm) when compared to the control group (1.75 ± 0.18 mm) after 8 weeks.

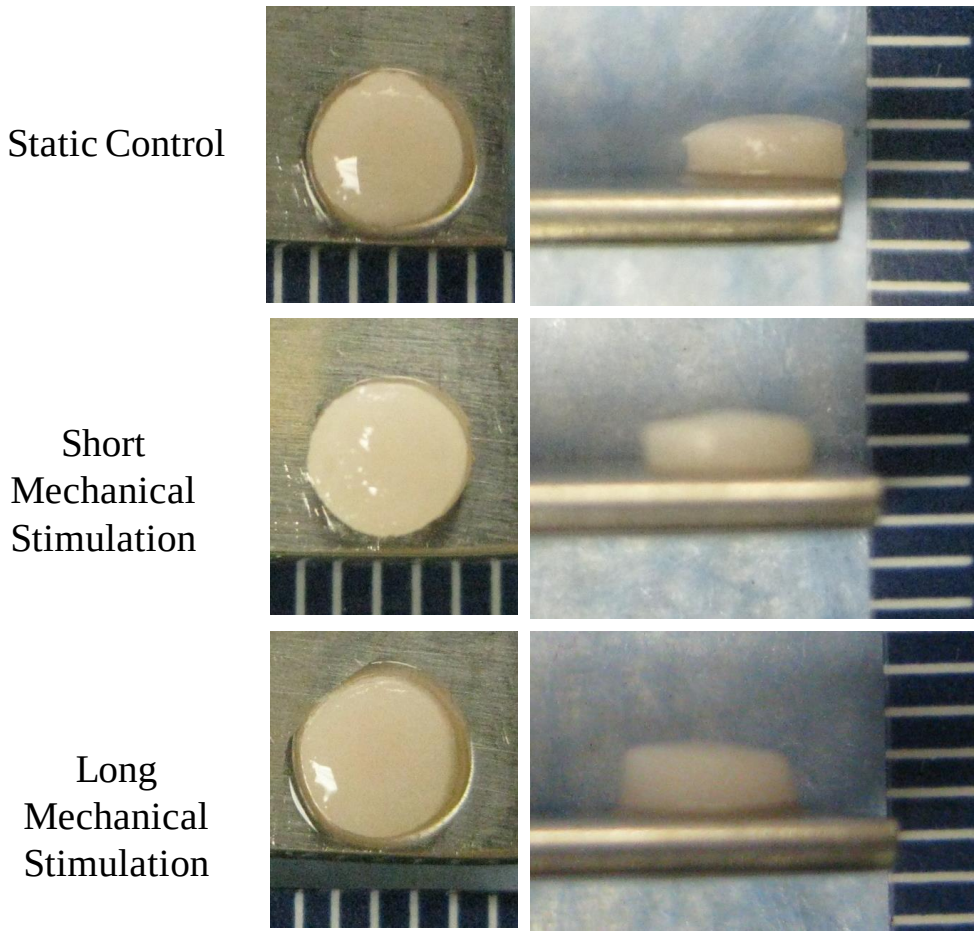

Figure 18. Gross morphology of the PGS scaffolds at 8 weeks. Scale bar is 1 mm.

6.3.2 Histology

The PGS scaffolds stained with hematoxylin and eosin are shown in **Figures 19 and 20.** The staining indicates homogenous distribution of cells and abundant ECM production in all groups. All groups stained positively for GAG at 8 weeks (**Figure 19**). In all groups there is a pattern of localization of GAG toward the middle of the scaffold. All groups stained positively for collagen at 8 weeks **(Figure 19)**. There were no noticeable differences between total collagen organization between the mechanically stimulated groups and the control.

All groups stained positively for both collagen type I and type II (**Figure 21**). In the short and long stimulation groups, there is a collagen type I shell that extends along the entire perimeter of the scaffolds. In the control group the collagen type I shell is confined to the short axis of the scaffold. All groups exhibited collagen type II staining throughout the scaffold with no noticeable differences in patterning between groups.

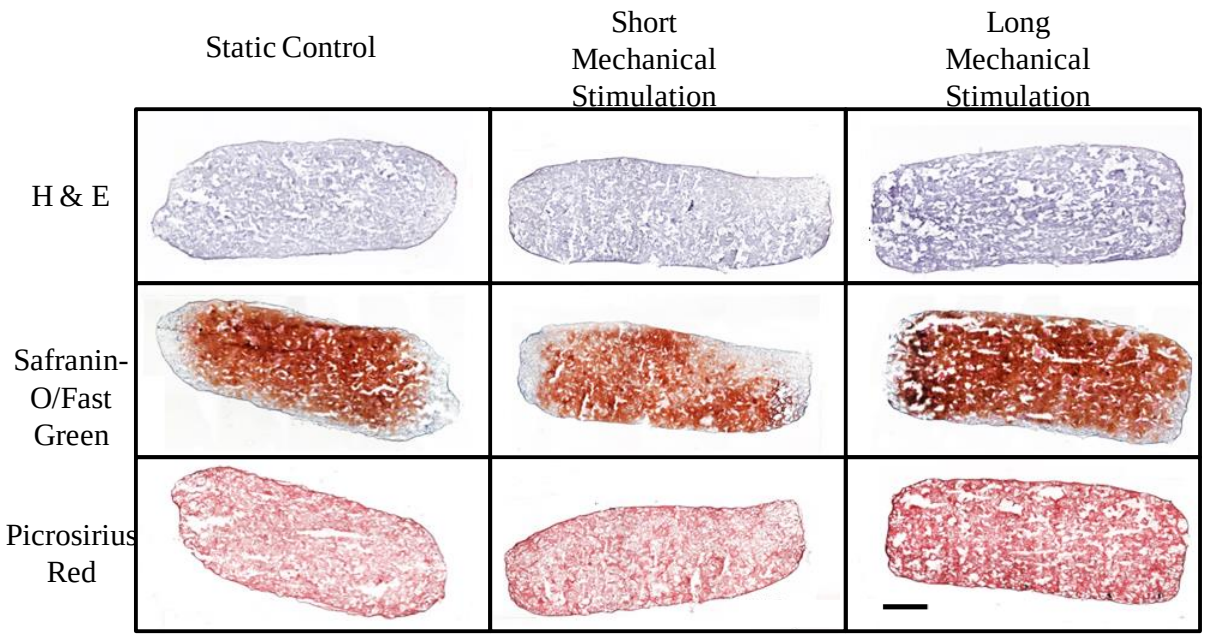

Figure 19. Histological staining of the PGS scaffolds at 8 weeks. Row 1: Hematoxylin and Eosin for cell nuclei. Row 2: Safranin O/Fast green stain for GAG. Row 3: Picrosirius red stain for collagen. Scale bar is 500 μm.

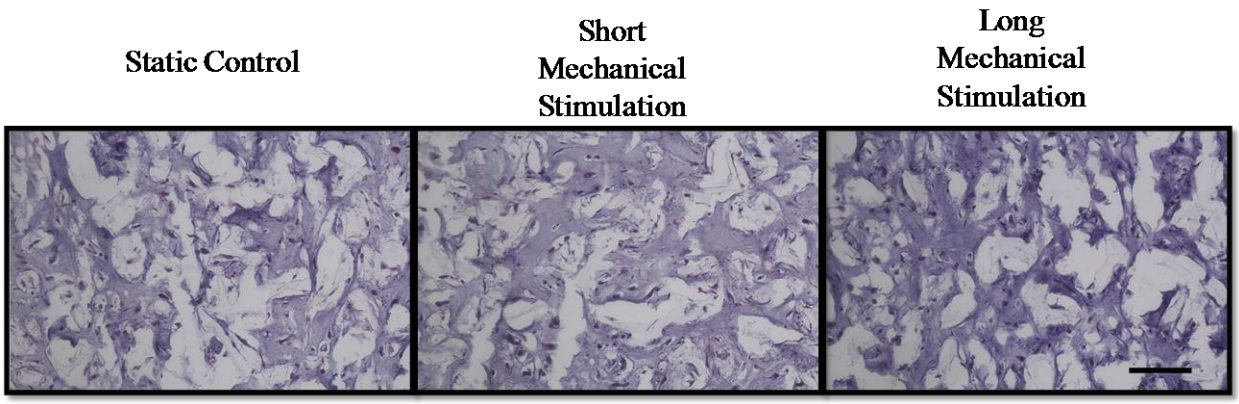

Figure 20. Hematoxylin and Eosin staining of the middle of the PGS scaffolds at 8 weeks.

Scale bar is 100 μm.

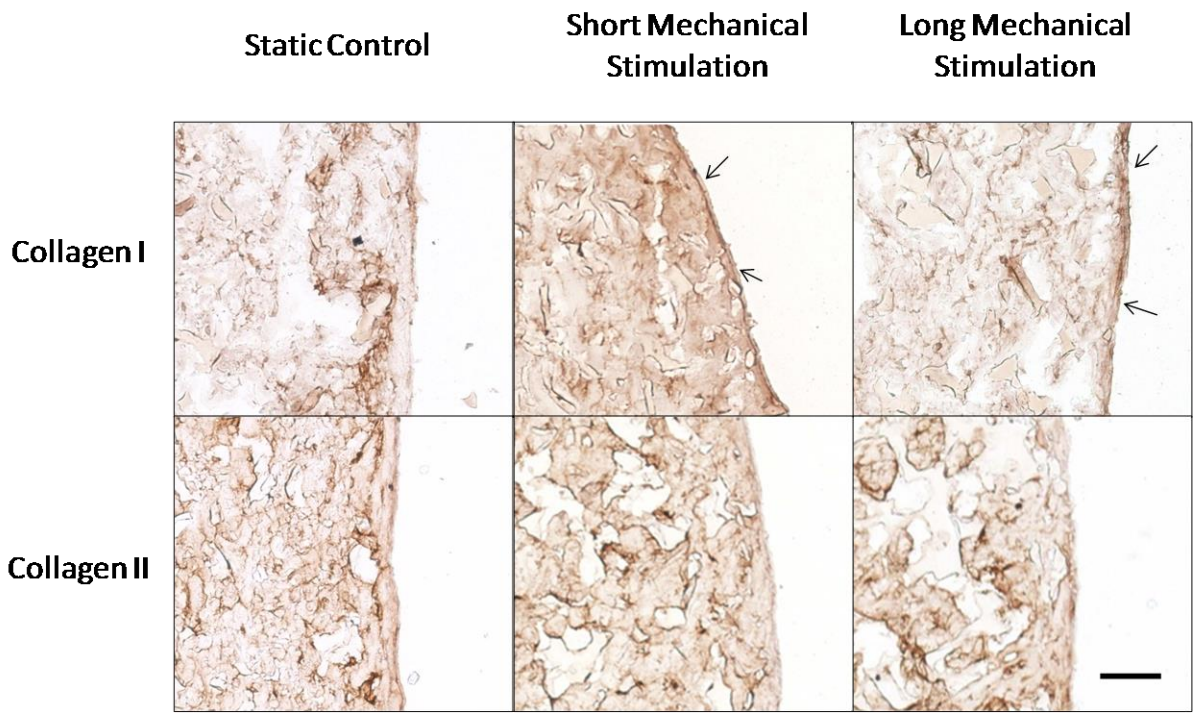

Figure 21. Immunostaining of the middle edge of PGS scaffolds at 8 weeks. Row 1: Collagen type I immunostain. Row 2: Collagen type II immunostain. Arrows point to collagen type I shell. Scale bar is 100 µm.

6.3.3 Biochemistry

The results from the biochemical assays are shown in **Figure 22**. **Figure 22a** shows the cellular content of the scaffolds. There was no significant difference in cellularity between the long and short stimulation groups and the control ($8.8 \times 10^5 \pm 1.3 \times 10^5$ cells per scaffold) at 8 weeks.

The amount of collagen per scaffold is shown in **Figure 22b**. There were no significant differences in collagen content between the long and short stimulation groups and the control (341 ± 84 µg per scaffold) at 8 weeks.

The amount of GAG per scaffold is shown in **Figure 22c**. Corresponding to the collagen results, there were no significant differences in GAG content between the long and short stimulation groups and the control (476 ± 170 µg GAG per scaffold) at 8 weeks.

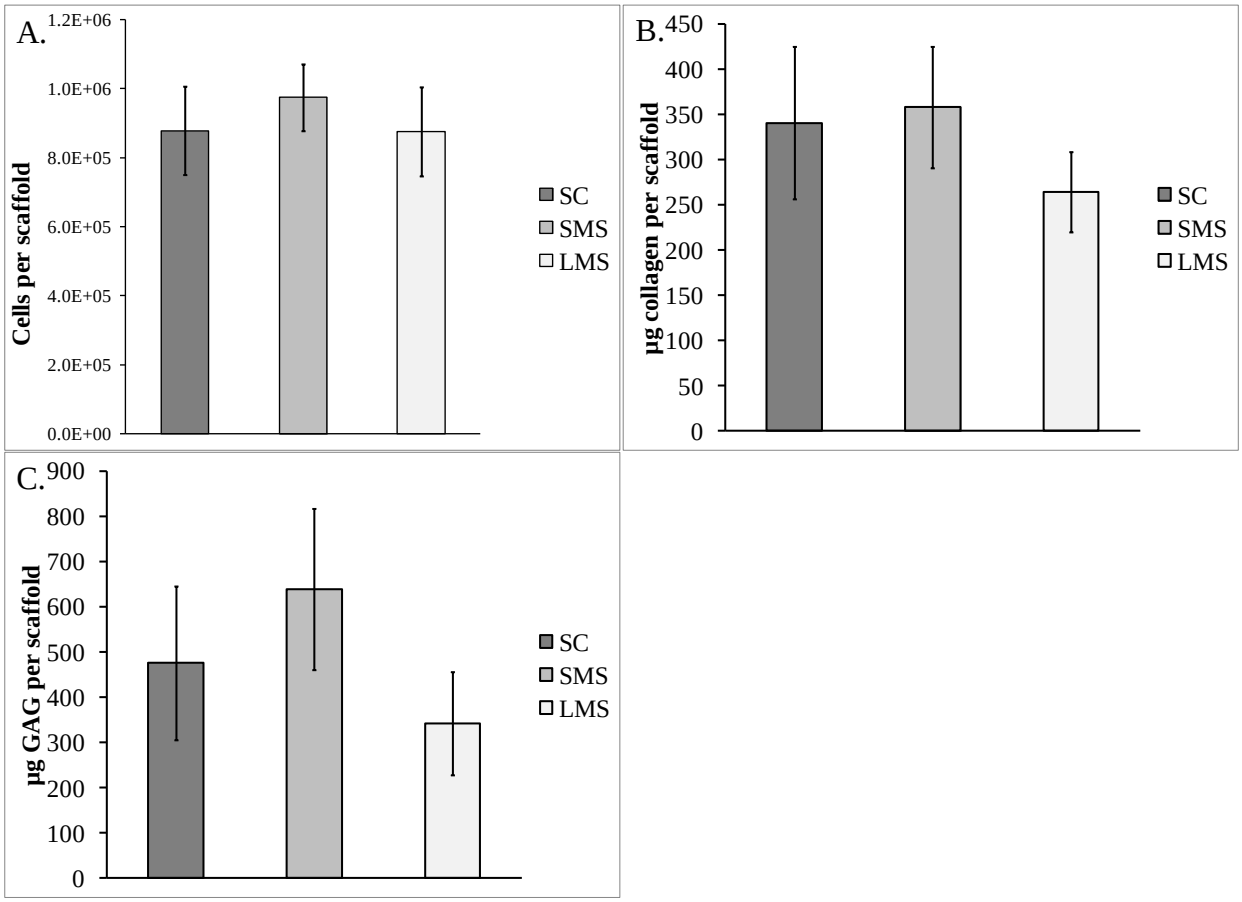

Figure 22. Biochemical properties static control (SC), short mechanical stimulation (SMS), and long mechanical stimulation (LMS) PGS scaffolds at 8 weeks. A. Cell content per construct, B. Collagen content per construct, and C. GAG content per construct. Error bars indicate average ± standard deviation.

6.3.4 Biomechanics

The results from the biomechanical analysis are shown in **Figure 23**. There were no significant differences in mechanical properties between mechanically stimulated groups and the control. The control scaffolds exhibited a peak stress of 49 ± 20 kPa, equilibrium stress of 16 ± 8 kPa, percent stress relaxation of 69 ± 5%, and tangent modulus of 667 ± 270 kPa.

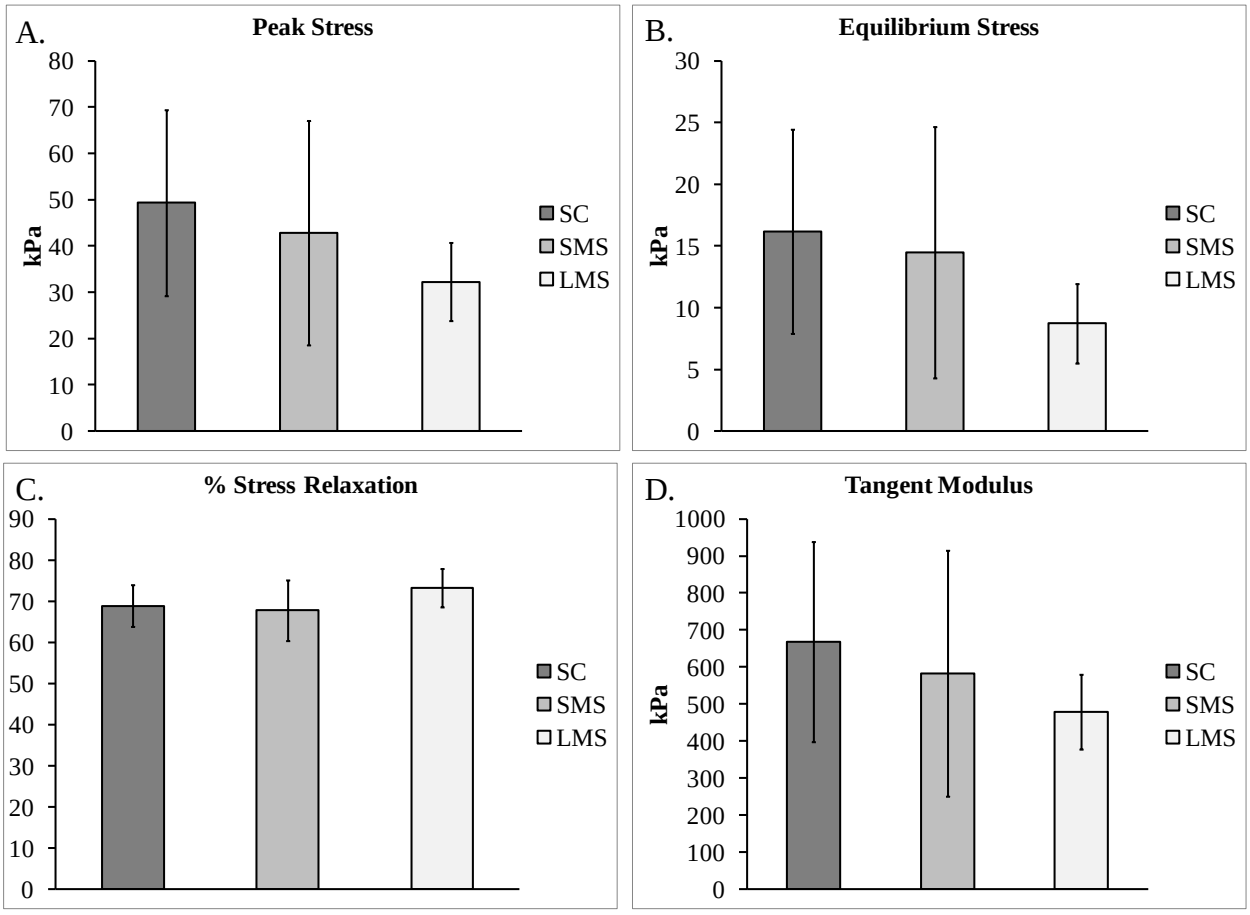

Figure 23. Biomechanical properties static control (SC), short mechanical stimulation (SMS), and long mechanical stimulation (LMS) PGS scaffolds at 8 weeks. A. Peak stress, B. Equilibrium stress, C. Percent stress relaxation, and D. Tangent modulus. Error bars indicate average ± standard deviation.

6.4 DISCUSSION

The results show that spinner flask culture allowed for high seeding efficiency, homogenous cell distribution, survival at the center of the scaffold, and abundant ECM production. Additionally, the application of mechanical forces did have an effect on the organization of regenerated ECM. The PGS scaffolds provided sufficient porosity which, combined with enhanced nutrient perfusion due to the bioreactor, allowed for cell survival and matrix production throughout the scaffold. This is a significant improvement from PGS cell seeding via injection which resulted in heterogeneous distribution of cells and extracellular matrix [125]. In contrast, our previous results with scaffoldless constructs formed by self-assembly of the same goat costal fibrochondrocytes resulted in cell death at the center of the scaffold, with a shell only spanning approximately 0.5 mm [128].

Histologically, it was shown that scaffolds from all groups exhibited a localization of GAG towards the middle of the scaffold. Furthermore, scaffolds in the groups undergoing both long and short mechanical stimulation had a type I collagen shell surrounding the scaffold, unlike the control. The differences in matrix organization between the mechanically stimulated and control groups indicate that there is a cellular response to compressive loading and that PGS scaffolds provide the necessary elastomeric properties to allow for transmission of forces from scaffold to cells. This loading mechanism could potentially be tailored to encourage ECM deposition in a ring-like pattern similar to the native TMJ disc. This could be accomplished by inserting a ring between the scaffold and loading platen to create a trampoline-effect on the PGS scaffold. This may result in a stress gradient that could encourage a ring-like organization of collagen.

Cells seeded on the PGS scaffolds in the spinner flask produced higher collagen content than PGS seeded via injection (9.1 ± 1.4 % compared to 3.5 ± 0.5 % per dry weight), as performed in our previous study [125]. (**Table 9**) While the amount of collagen produced by the goat fibrochondrocytes on PGS in this study exceeded that which has been reported using TMJ disc cells on PGA and PLLA scaffolds [112-114], there is still a need to reach levels closer to the native tissue, which are 45.7 ± 19.6% collagen per dry weight and 2.1 ± 1.2% GAG per dry weight of the goat TMJ disc [129]. Using chondroitinase to deplete GAG, allowing more room for collagen production, could be attempted in order to bring levels closer to those of the native tissue [130]. Additionally, combinations of growth factors such as transforming growth factor β1, platelet derived growth factor, and basic fibroblastic growth factor could be explored as a method to enhance collagen type I production in 3D [131].

A comparison between the mechanical properties of the PGS scaffolds at 8 weeks, PGS scaffolds seeded via injection, and scaffoldless constructs is outlined in Table 2. The tangent moduli of PGS scaffolds cultured in a spinner flask seem to have exceeded those using other seeding techniques. Additionally, the tangent modulus of the static control PGS scaffolds at 8 weeks (667 ± 270 kPa) is comparable to those of the native goat TMJ disc (304 ± 141 kPa) and mandibular condylar cartilage (205 ± 107 kPa) [119]. This indicates that the engineered devices could potentially withstand the compressive forces in the jaw. There was no difference between the mechanical properties of the stimulated groups and the static control group. This indicates that the collagen type I shell was not pronounced enough to have an effect on the compressive properties of the construct. Tensile testing will need to be performed in the future to ensure that the properties of the engineered tissue are similar to those of the native TMJ disc, which is hypothesized to mainly act in tension in the joint.

A limitation of this study was the failure to take into account changes in scaffold thickness over time. Scaffolds in the long stimulation group did have a significantly smaller scaffold thickness when compared to the control, indicating that the application of mechanical stimulation did have an effect on the shape of the constructs. This also supports our hypothesis that a longer free-swelling culture period in the spinner flask is necessary for scaffolds to mature enough to withstand mechanical stimulation, as scaffolds in the short mechanical stimulation group did not have thicknesses that were significantly different from the control group. Since loading platens were adjusted assuming a scaffold thickness of 1.5 mm, the decrease in scaffold height could have resulted in a decrease in actual load experienced by the scaffold over time. However, this did not have an effect on extracellular matrix production of cells seeded on the PGS scaffolds, as shown by the lack of quantitative differences in biochemical content. Additionally, the maximum stress of the 8 week control scaffolds at 10% strain was approximately 49 ± 20 kPa. The resolution of the Flexcell compression system allowed for a minimum stress of 177 kPa to be applied to the PGS scaffolds. It is likely that 10% strain was exceeded, perhaps considerably more in the less-mature constructs of the long mechanical stimulation group, which may have resulted in permanent deformation of the scaffold. Future studies should strive to optimize *in vitro* loading amplitude for tissue engineered scaffolds taking into account ECM maturity.

In conclusion, this study demonstrated that the spinner flask provides an ideal environment for both seeding and culturing fibrochondrocytes on PGS scaffolds. This was shown both qualitatively and quantitatively by homogenous cell distribution and high seeding efficiency. Furthermore, this enhanced environment allows for the production of more abundant ECM when compared to previous studies utilizing self-assembly or injection seeding (**Table 9**).

Mechanical stimulation does have an effect on extracellular matrix organization, and future studies are warranted to further explore this mechanism. Investigating various loading amplitudes, frequencies, and increments could provide more insight into how mechanical stimulation can most effectively be utilized to enhance fibrocartilage regeneration. PGS demonstrates great potential as a fibrocartilage scaffold material, which may provide TMD patients with a viable graft replacement option in the future.

Table 9. Comparison of average biochemical and biomechanical properties of goat costal fibrochondrocytes seeded on PGS and cultured using scaffoldless approach (± standard deviation). Biochemical and biomechanical values for each seeding technique were obtained using the same procedures outlined in the methods section.

	% Collagen per dry weight	**%GAG per dry weight**	**Tangent modulus**
Scaffoldless [128]	6.9 ± 1.1 %	16.5 ± 2.9 %	435 ± 115 kPa
Injection/Orbital Shaker [125]	3.5 ± 0.5 %	12.1 ± 2.3 %	124 ± 86 kPa
Spinner Flask	9.1 ± 1.4 %	11.1 ± 6.6 %	667 ± 270 kPa

7.0 PURE MAGNESIUM AND POLY (GLYCEROL SEBACATE) AT THE BONE-FIBROCARTILAGE INTERFACE OF THE MANDIBULAR CONDYLE: A PILOT STUDY

7.1 INTRODUCTION

Temporomandibular joint disorders (TMDs) are a significant public health problem afflicting millions of Americans [1]. Patients suffering from TMDs have a wide range of symptoms ranging from minor discomfort to severe joint pain, dysfunction, and deterioration of the articulating surfaces. Those with irreversible joint damage resulting from disease or trauma may be candidates for a total joint replacement system. The currently available temporomandibular joint (TMJ) replacement systems utilized by surgeons consist of a fossa component of ultra high molecular weight polyethylene and a condylar component of cobalt-chromium molybdenum. Both pieces are secured to the existing bone using titanium screws [93]. Non-degradable implant materials such as titanium have high mechanical strength but can harbor infection and contribute to stress-shielding effects. Furthermore, the expected lifetime of total joint replacement systems is 10-15 years, which is a major shortcoming considering that TMDs predominantly occur in premenopausal women between the ages of 20-40 [95, 96]. Methods for enhanced device fixation are currently being explored to increase the lifetime of these devices.

Magnesium has recently been investigated as a biodegradable orthopedic implant material. Witte *et al.* showed that magnesium implants promoted increased mineralized bone area in the femora of guinea pigs when compared to a degradable polymer control [98]. Our group has focused on the application of magnesium as a craniofacial implant material, specifically for the TMJ. We have demonstrated that fibrochondrocytes have a high resiliency to magnesium ion concentrations *in vitro,* indicating the potential of this material at the bone-fibrocartilage interface of the mandibular condyle [128]. Additionally, we have shown that magnesium screws implanted in the rabbit mandible helped promote new bone formation in the area surrounding the implant [132]. The osteoinductive properties of magnesium, as well as its similar mechanical properties to bone (i.e. density, elastic modulus [97]) make it a promising candidate for enhancing craniofacial device osseointegration.

Poly (glycerol sebacate) (PGS) is a biocompatible, biodegradable elastomeric polymer which has demonstrated potential as both a fibrocartilage [125] and bone [133] scaffold material. It is theorized that the load-transducing properties of this highly elastomeric material provide the appropriate mechanical environment for osteogenesis. This has been demonstrated *in vivo* in a rabbit ulna defect model which was repaired with PGS impregnated with allogenic bone marrow stromal cells. The implantation of cell-laden PGS resulted in a significant increase in bone volume and mechanical strength when compared to the empty defect control [133]. The study showed that PGS substrate acts as a niche for stem cells and allows for the transmission of mechanical load to cells, inducing osteogenesis and promoting mineralized bone deposition. However, this effect has not been tested for craniofacial applications.

In order to improve both implant fixation and longevity, the coupling of a material with high mechanical strength such as magnesium with a soft filler substance for cell infiltration and

matrix regeneration such as PGS is a potential avenue for exploration. However, the behavior of both magnesium and PGS in the mandibular bone needs to be investigated *in vivo* in order to determine the suitability of these materials for TMJ implants. Currently, the porcine model is regarded as the most anatomically relevant animal model for the TMJ [134-136]. Therefore, the objective of this study was to assess the biomaterials magnesium and PGS in the porcine mandibular condyle at one month post implantation in terms of new bone formation as assessed by micro-computed tomography (micro CT).

7.2 METHODS

7.2.1 Magnesium Rod Preparation

Commercially available pure magnesium was purchased from Goodfellow (Oakdale, PA). The magnesium was 99.9% pure. Magnesium rods were cut to size in the University of Pittsburgh Swanson School for Engineering Machine shop. After cutting to size, rods were sonicated in isopropanol to remove debris. The mg rods underwent stress relief heat treatment at 205°C for 1.5 hours in argon. Rods then underwent 3 cycles of sonication in isopropanol for 3 minutes each and were allowed to air dry. Rods were weighed and imaged prior to implantation. (**Figure 24**)

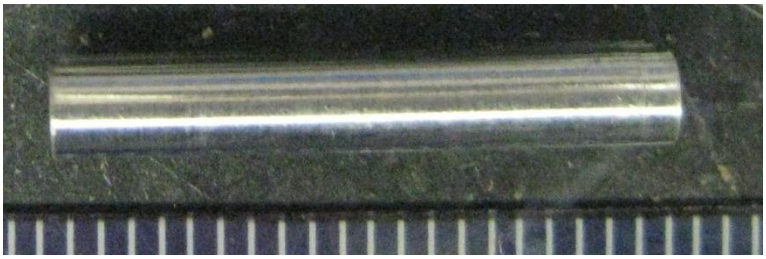

Figure 24. 99.9% Magnesium rod 20 mm length, 3.0 mm diameter. Scale bar is in mm.

7.2.2 PGS Scaffold Preparation

As previously described [133], PGS caffolds were synthesized by direct polycondensation of 1:1 glycerol/sebacid acid, and then dissolved in tetrahydrofuran (20%). The tubular scaffolds were then formed by salt fusion and the particulate leaching (pore size 75-150 μm) method as reported previously [117, 137]. The PGS scaffold is shown in **Figure 25**.

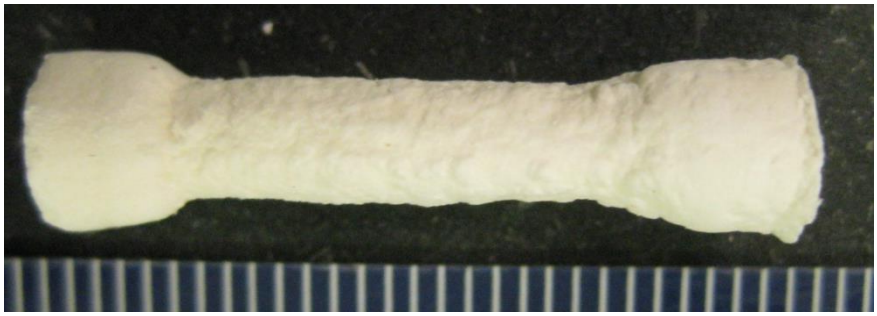

Figure 25. Tubular PGS scaffold. Scale bar is in mm.

7.2.3 Surgical Method

Three 3-month-old Yorkshire pigs were purchased from Wally Whippo (Enon Valley, PA). All animal procedures were approved by the Institutional Animal Care and Use Committee at the University of Pittsburgh in accordance with the National Institutes of Health guidelines for the use of laboratory animals.

Animals were sedated with ketamine and xylazine and intubated prior to surgery. Anesthesia was maintained with isoflurane. The surgical site was scrubbed with betadine and sterilely draped. An incision was made posterior to head of the mandibular condyle. The skin and fatty tissue were resected to reveal the bone. A sterile drill with a 2.99 mm diameter drill bit was used to drill a hole in the posterior aspect of the mandibular condyle. (**Figure 26**) The length of the resulting defect was measured and a 3.0 mm diameter magnesium implant with a

corresponding length was press fit into the defect. The same surgical procedure was repeated on the contralateral side, and defects were packed with PGS scaffolding material. After implantation, the tissue was sutured and skin closed using resorbable sutures.

Following surgery, pigs were extubated until recovered from anesthesia. Animals were monitored during the recovery period by the Division of Laboratory Animal Resources staff. Due to the similar density of magnesium and bone, x-rays could not be used to detect the implants. No hydrogen pockets were observed throughout the duration of the study. One month after surgical implantation, pigs were sedated with ketamine and xylazine, euthanized with intravenous injection of pentobarbital sodium, and condyles dissected.

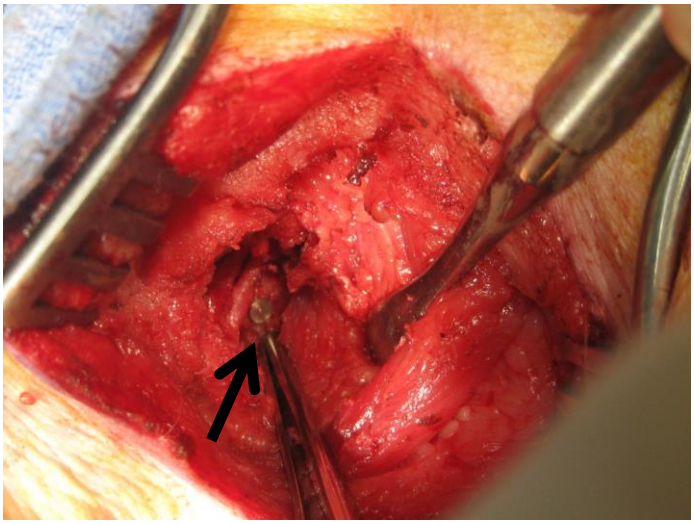

Figure 26. Surgical implantation of magnesium rods in the posterior aspect of the mandibular condyle. The arrow shows the magnesium rod press fit into the newly formed condylar defect.

7.2.4 Micro Computed Tomography Analysis

The condyles were excised, assessed grossly, cut and fixed in formalin for 3-7 days. The condyles were then transferred to 50 mL Falcon tubes containing 70% ethanol for micro CT analysis. Condyles were scanned on a SkyScan 1172 (Bruker-Skyscan, Contich, Belgium) at a 9.97 μm voxel size (70 kV, 141 μA). The scans were oriented, cropped, and analyzed using Skyscan DataViewer and CTAn software. As previously described [132], the rod volume fraction was determined for each visible rod.

For the condyles implanted with PGS, analysis was performed to quantify new bone formation. A region of interest corresponding to the diameter of the drill bit was created and extended along the visible length of the remaining bone tunnel. The number of voxels corresponding to bone within this cylindric region of interest was then quantified. A region of identical dimensions was then formed in an alternate portion of the condyle outside of the defect area. This was utilized to determine a baseline of bone per volume for comparison. The results are presented as a percentage of bone per volume.

7.3 RESULTS

7.3.1 Gross Morphology

In two of the three condyles implanted with magnesium there was no evidence of morphological damage to the mandibular condyle at the macroscopic level. In one specimen, the magnesium rod was visible on the posterior aspect of the condyle. (**Figure 27a**) In the same specimen, there

was also a defect observed on the anterior medial zone of the mandibular condyle corresponding to the path of the drill bit. (**Figure 27b**) There was no evidence of morphological damage to the TMJ disc in any of the three samples.

There was no evidence of morphological damage to the condyle or TMJ disc at the macroscopic level in any of the three of the condyles implanted with PGS.

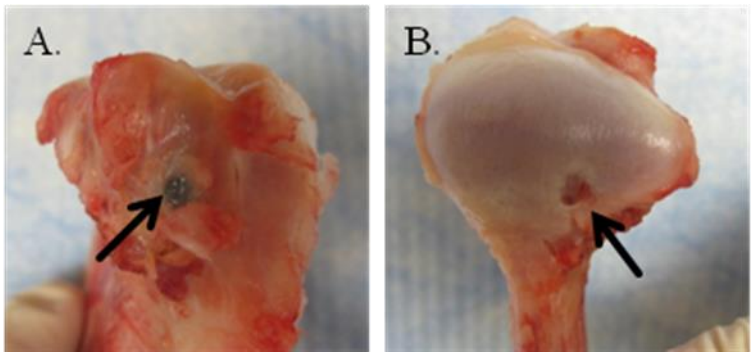

Figure 27. Gross morphology of porcine mandibular condyle at one month post surgery. a. Posterior aspect of right condyle. Arrow points to pure magnesium implant. b. Anterior surface of mandibular condyle. Arrow points to defect created in condylar cartilage by drill bit.

7.3.2 Micro CT

Micro CT imaging revealed magnesium rods and bone tunnels in the condyles of two of the three specimens. **(Figure 28**) In one condyle, there was no magnesium rod detected in the condyle. A 5.0% and 6.2% decrease in magnesium rod volume was observed in the two condyles where magnesium was present.

In the specimens with defects filled with PGS, the average percent of bone per volume at the defect site was 17±4%. (**Figure 29 and Figure 30**) In contrast, control non-defect regions had an average percent bone per volume of 38±10%. In defects implanted with PGS, over half of the loss in bone volume due to the defect was restored.

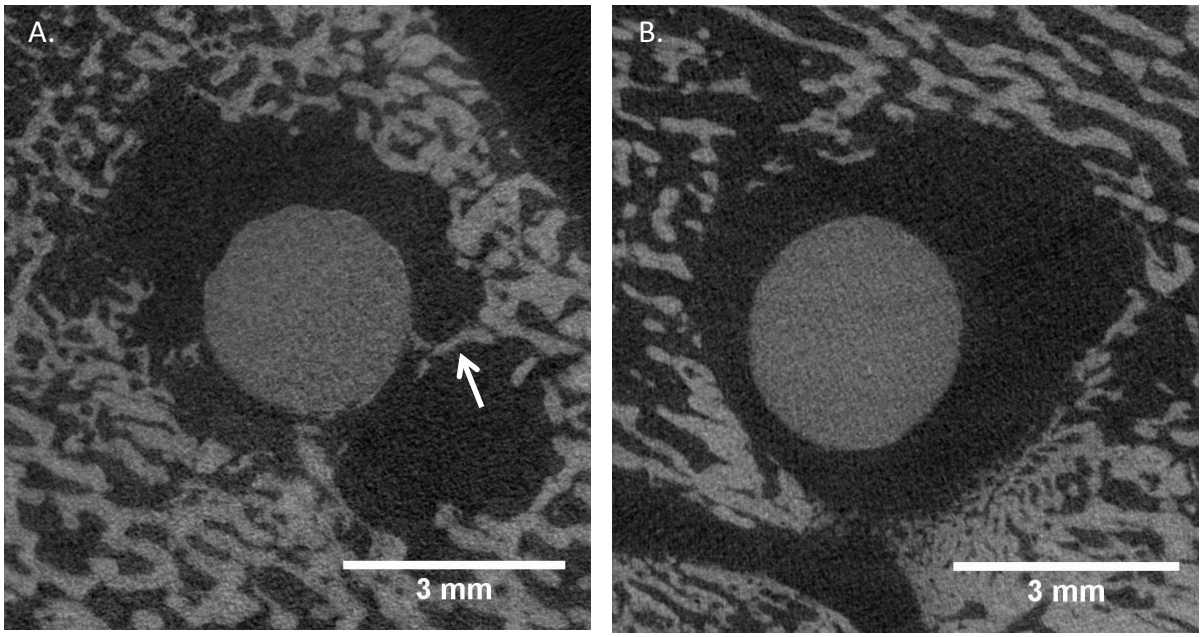

Figure 28. Micro CT images of rods in porcine condyles. Panels a. and b. are images of the magnesium rods in two different specimens. Arrow in a. points to possible new bone formation at the implant interface. Scale bar is 3 mm.

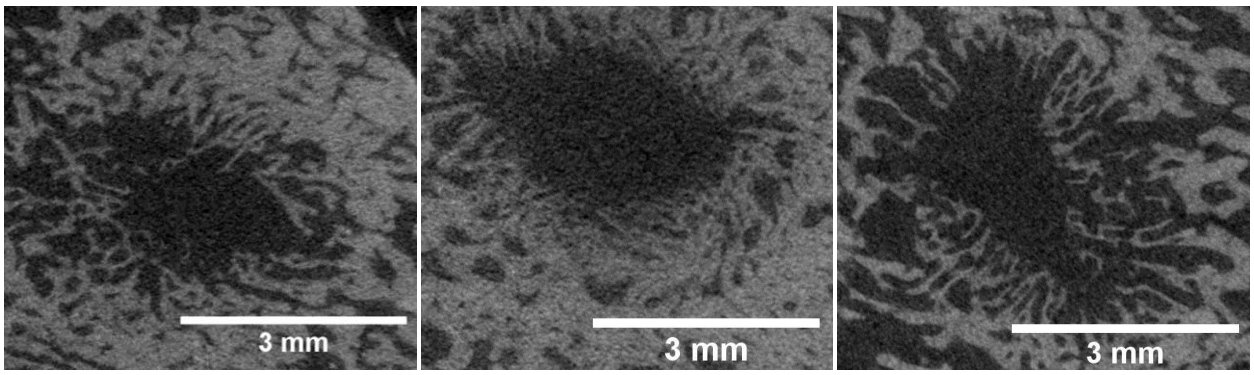

Figure 29. Micro CT images of three condyles with surgically implanted PGS. Scale bar is 3 mm.

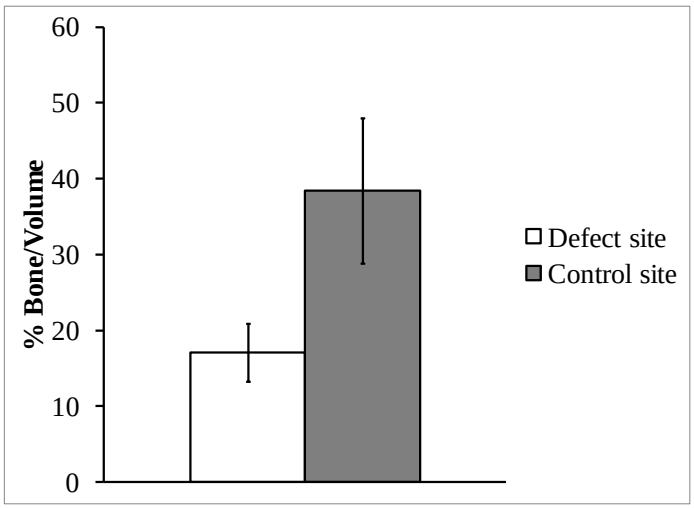

Figure 30. Average percent bone per volume in defect tunnels and control regions of condyles implanted with PGS. Error bars represent ± standard deviation.

7.4 DISCUSSION

The results of this pilot study demonstrate the feasibility of creating a surgical defect in the porcine mandibular condyle. In 5 out of the 6 surgically operated condyles, a defect was successfully created in the condyle and in one of the specimens there was visual evidence of the magnesium implant reaching the fibrocartilage surface of the condyle. The results of this study also indicate that pure magnesium (99.9%) degrades slowly and is still present in the porcine condyle at one month post implantation. Furthermore, micro CT analysis showed that PGS allows for new bone formation at the defect site.

A major challenge associated with the use of magnesium as an implant material is tailoring the degradation rate of the fixation device to be closely matched with the bone healing rate. The results show that there was 5-6% degradation of pure magnesium in the porcine mandibular condyle at one month after implantation. This slow degradation rate could potentially allow a suitable amount of time for bone healing. In contrast, pure magnesium screws implanted in the rabbit mandible experienced a 40% loss in volume over four weeks [132]. There was also a difference between the degradation rates of screws implanted in the cortical bone versus screws in contact with the marrow space [132]. As shown by the micro CT imaging, the rods in this study had little contact with the marrow space which may have contributed to their slow degradation rate.

The results show that PGS allowed for a considerable restoration of bone volume at the defect site. When compared to a non-defect control site, defects packed with PGS exhibited over half the native bone volume at one month post-surgery. This is consistent with a previous study which showed that PGS implanted in an ulnar defect resulted in a significant increase in flexural load of the bone at 8 weeks when compared to an empty defect control [133]. Future studies

should compare PGS-filled defects to empty surgical defects to verify that bone regeneration in the porcine mandibular condyle is indeed accelerated by the presence of PGS.

Currently, the porcine model is regarded as the ideal animal model for the TMJ. However, using Yorkshire pigs proved to be technically challenging due to the facial fatty tissue distribution, which limits access to the posterior portion of the mandibular condyle. Furthermore, the rapid growth rate of the animals could result in migration of implants from their original location. In order to improve the success rate in future studies, more feasible mammal models should be explored for craniofacial surgery, such as the goat. [19]

Based on the results of this pilot study, both pure magnesium and PGS do have potential as implant materials for the TMJ. As an initial step, magnesium could be used to better improve implant fixation. For instance, as magnesium coatings degrade, they could promote new bone formation and integration with both bone and the surrounding non-degradable device. This system would allow for a reduction in stress shielding between the condyle and implant, helping to extend the lifetime of the device. PGS could be used as a filler material, encased by magnesium, which allows for cell infiltration, differentiation, and matrix deposition. This system could also be applied to critical size defect repairs, eliminating the need for bone grafting and donor site morbidity. Future studies are warranted to better understand the behavior of both magnesium and PGS in the mandibular condyle both separately and as a composite system over time, and validate the potential of these materials as TMJ prosthetic components.

8.0 GENE EXPRESSION OF BONE MARROW STROMAL CELLS SEEDED ON ECM SCAFFOLDS SUBJECTED TO MECHANICAL STIMULATION

8.1 INTRODUCTION

The fibrocartilagenous temporomandibular joint (TMJ) disc is positioned between the mandibular condyle and fossa and helps to distribute both tensile and compressive forces in the joint during jaw movement [138]. Damage to the disc can disrupt the mechanical synchrony of the joint, cause pain and dysfunction, and lead to irreversible damage of the articulating tissues. Discectomy may relieve pain in some cases but can also lead to a cascade of degenerative changes in the joint. Alloplastic devices for TMJ disc replacement have a tumultuous history, marred by the use of Proplast/Teflon and Silastic implants, which fragmented in the joint space, resulting in an adverse immune response [139]. Autografts such as temporalis muscle flap, dermis, and auricular cartilage require increased donor site morbidity and have not demonstrated long-term efficacy [140-142]. Currently, long-term replacement options for patients with disc damage are limited and tissue engineered options are being explored as a means of restoring joint mechanics and preventing further tissue damage.

Scaffolds composed of xenogeneic extracellular matrix (ECM) have been shown to be inductive templates for musculoskeletal tissue regeneration [143]. Specifically, it has been shown that porcine urinary bladder matrix (UBM) TMJ disc scaffolds promote cell migration

and site-specific regeneration in a canine model [144]. At six months post surgery, scaffolds were morphologically, histologically, biochemically, and biomechanically similar to the native TMJ disc. In contrast, the contralateral side, where discectomy was performed without replacement, exhibited degenerative changes to the articulating surfaces. This study demonstrated that decellularized ECM scaffolds have the ability to remodel into a functional host tissue resembling the native TMJ disc, which prevented degeneration of the mandibular condyle.

While ECM has shown great promise as a TMJ disc replacement in-vivo, the mechanism of this remodeling process is not well understood. It is postulated that a regenerative immune response occurs following implantation in the joint space, then ECM scaffolds are populated by endogenous progenitor cells and undergo constructive remodeling. Due to the mechanosensitivity of TMJ fibrocartilage, it is also likely that this process is significantly impacted by the mechanical environment within the joint space upon implantation. However, the cellular response to compressive mechanical stimulus within the unique TMJ ECM scaffold environment remains unknown.

In order to help elucidate the mechanism of ECM scaffold tissue regeneration, the first step is to determine how human bone marrow stromal cells (hBMSCs) will respond to mechanical stimulation within the growth factor-rich environment of ECM scaffolds. It is hypothesized that compressive loading coupled with the bioactive milieu of ECM will provide the ideal niche to induce fibrochondrogenesis of hBMSCs. The objective of this study was to determine the effect of both chemical and mechanical stimulation on the gene expression of hBMSCs seeded on porcine small intestinal submucosa (SIS) scaffolds over time. Changes in gene expression of both fibrochondrogenic markers (collagen types I and II, aggrecan, and

decorin) and markers indicating multipotency (CD146 and NG2) were measured as indicators of differentiation of hBMSCS towards a fibrocartilage phenotype.

8.2 METHODS

8.2.1 SIS Scaffold Production

Scaffolds were prepared as previously described [145]. Briefly, SIS was harvested from market weight pigs. The external muscle and mucosal layers were mechanical removed. The tissue was then treated with 0.1% peracetic acid/ 4% ethanol to decellularize and disinfect the tissue. The tissue was washed in phosphate buffered saline and water. Tissue sheets were lyophilized and pulverized using a Wiley Mill. A hard plastic mold was machined to create a circular shaped depression. This depression was lined with two hydrated sheets of SIS and the pocket created by the depression packed with powdered SIS. Two additional hydrated sheets were placed over the top of the powder and the construct vacuumed until dry, forming a multilaminate pillow-like device. (Error! Reference source not found.) All constructs were sterilized using ethylene oxide.

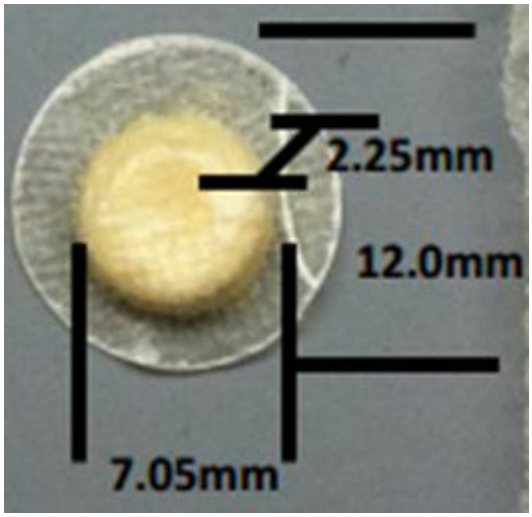

Figure 31. SIS Scaffold scaled to fit the Flexcell compression system. Pillow and sheet portions of the scaffold are labeled

8.2.2 Cell Culture and Scaffold Seeding

hBMSCs obtained from donor #7083 (male 24 years old) were provided by the Tulane Center for Gene Therapy/Institute for Regenerative Medicine at Scott & White. Cells were passaged four times in basal passaging media consisting of alpha minimum essential medium (αMEM) with L-glutamine (Invitrogen/GIBCO), 16% fetal bovine serum (Atlanta Biologicals), 1% L-glutamine (Invitrogen/GIBCO), and 1% penicillin G and streptomycin sulfate (Invitrogen). 9×10^5 cells/scaffold were injected into the middle of hydrated SIS scaffolds using a suspension volume of 30 µl of either basal passaging or chondrogenic medium with a 25 gauge needle and syringe. Two injection sites were used to improve cellular distribution. Chondrogenic media consisted of DMEM/high glucose (Thermo) supplemented with 1% penicillin-streptomycin (Lonza), MEM 1% non-essential amino acid solution (Thermo Scientific), 1% insulin-transferrin-selenium + premix (BD Biosciences), 0.1 µM dexamethasone (MP Biomedicals), 40 µg/mL L-proline (Acros Organics), 50 µg/mL ascorbate 2-phosphate (Sigma-Aldrich), and 10 ng/ml TGF β1 (Peprotech).[68, 146] Scaffolds were maintained in agarose-coated wells on a rocker at 30 rotations per minute overnight.

8.2.3 Mechanical Stimulation

Mechanical stress has been shown to cause an increase in chondrogenic gene expression of bone marrow stromal cells after one application for one hour [147]. Furthermore, cyclic stretching at a rate of 0.5 Hz has been shown to induce collagen I production of NIH 3T3 fibroblasts seeded on ECM scaffolds [148]. Similarly, constant hydrostatic pressure has been shown to cause an

increase in gene expression of collagen type I in TMJ disc cells [122]. Thus, 24 hours after seeding, scaffolds were exposed to different stimulation regimens one time for 4 hours.

Mechanical stimulation was applied to scaffolds using the Flexcell® Compression System. Scaffolds were moved to BioPress™ compression plates and divided into six groups: dynamic compressive loading to 10% strain, constant compressive loading to 10% strain, and free swelling control all with or without chondrogenic medium. (**Table 10**) Stationary platens were adjusted so that the bottom of the center screw just touched the top of the sample and were then inserted into the wells of the compression plates. In the dynamic compressive loading group, a loading regimen of dynamic compression following a sine waveform at 0.5 Hz was applied. An estimated peak stress of 180 kPa, corresponding to 1.63 lbs of air pressure, was applied to the scaffolds resulting in approximately 10% strain. This was estimated based on the reported compressive tangent modulus of UBM ECM scaffolds [149]. In the constant compressive loading group, a constant stress of 180 kPa was maintained. Scaffolds in the constant and dynamic compression groups underwent 4 hours of compressive culture in a Flexcell compression system. Free swelling control scaffolds were also moved to compression plates with platens but were not subjected to mechanical stimulation.

Table 10. Experimental groups

Free Swelling Control w/ Chondrogenic	Constant Compression to 10% Strain w/ Chondrogenic	Dynamic Compression to 10% Strain w/ Chondrogenic
Free Swelling Control w/ Basal	Constant Compression to 10% Strain w/ Basal	Dynamic Compression to 10% Strain w/ Basal

8.2.4 Histology

Scaffolds from the free swelling control group were embedded in OCT freezing medium (Tissue-Tek) and flash frozen to -80°C. The samples were cryo-sectioned at 6-10 μm, fixed in 10% neutral buffered formalin, and stained with hematoxylin and eosin to visualize cellular distribution throughout the scaffold. To detect apoptosis in seeded cells, scaffolds were also stained using the TACS® 2 TdT-DAB *In Situ* Apoptosis Detection Kit according to the manufacturer's instructions.

8.2.5 Gene Expression

Immediately following 4 hours of mechanical stimulation, samples were minced with a razor, submerged in Trizol® (life technologies™) and then further disrupted using a handheld tissue homogenizer (PRO scientific). 200 µl of methanol was added per 1 ml of Trizol and then samples were centrifuged at 12,000 RPM for 15 minutes at 4 ºC. The clear supernatant was removed and washed with 1:1 volume of 70% ethanol. RNA was then isolated using a RNeasy Mini Kit (Qiagen) according to the manufacturer's instructions. The RNA was treated on the column with DNase (Qiagen) to reduce genomic DNA contamination. The RNA concentration was measured using a spectrophotometer (Nanodrop 1000 Thermo Scientific). The RNA concentration of each sample was standardized to the least concentrated sample (40 ng/µl) and 10 µl of RNA from each sample was reverse transcribed using a First Strand cDNA synthesis kit (Thermo Scientific) according to the manufacturer's instructions. The resulting cDNA was then diluted 1:100 and stored at -80°C until real time polymerase chain reaction (RTPCR) was performed.

A 7900ht Fast Real-Time PCR System was used for detection of two housekeeping genes: 18s ribosomal RNA (18s) and hypoxanthine-guanine phosphoribosyltransferase (HPRT) and the target genes: collagen I (COL I), collagen II (COL II), decorin (DEC), aggrecan (AGC), CD146 (MCAM), and NG2. A forward primer, reverse primer, and SYBR® Green master mix (Thermo Scientific) were used for each gene. (**Table 11**) The real time analysis was performed by a 5 min activation step, followed by 40 cycles of 30 s at 95°C, 30 s at 60ºC, and 1 min at 72°C [122].

Each gene of interest was run simultaneously in the same plate with all samples. The efficiency of each well was calculated by examining the linear portion of the fluorescent signal

vs. cycle number curve and the cDNA abundance was normalized to the housekeeping gene. The data are expressed as the ratio of relative expression of the target gene to the housekeeping gene:

$$Relative\ Expression = 2^{-(C_{t,target} - C_{t,HPRT})}$$

Table 11. Primer sequences utilized in gene expression analysis.

Primer Name (Abbreviation)	Forward Sequence (5'-3')	Reverse Sequence (5'-3')	
Hypoxathine ribosyltransferase (HPRT)	*GGTCAGGCAGTATAATCCAAAGA*	*AGGCTCATAGTGCAAATAAACAGT*	*Taboas, 2004[150]*
18S ribosomal RNA (18s)	*GGCCCTGTAATTGGAATGAGTC*	*CCCAAGATCCAACTACGAGCTT*	*Taboas, 2004[150]*
Collagen I (COL1)	*TAAAGGGTCACCGTGGCT*	*CGAACCACATTGGCATCA*	*Taboas, 2004[150]*
Collagen II (COL II)	*CTGCTCGTCGCCGCTGTCCTT*	*AGGGGTCCCAGGTTCTCCATC*	*Taboas, 2004[150]*
Aggrecan	*GGGTCAACAGTGCCTATCAG*	*GGGTGTAGCGTGTAGAGATG*	*Taboas, 2004[150]*
Decorin	*AGAAGCTCTCCTACATCCGCATTG*	*CACATCTGAAGGTGGATGGCTGTA*	*Taboas, 2004[150]*
CD146	*GGGTACCCCATTCCTCAAGT*	*CAGTCTGGGACGACTGAATG*	*Pellegrinelli et al.[151]*
NG2	*CACGGCTCTGACCGACATAG*	*CCCAGCCCTCTACGACAGT*	*PrimerBank ID 4503099a1*

8.2.6 Statistics

A two-way ANOVA was used to examine differences in main effects and interaction effects of two independent variables (media type and mechanical stimulus) on the relative expression of target genes with $p < 0.05$ defined as statistically significant. Tukey's post hoc testing was used to examine differences between individual groups when significance was observed. All statistical analysis was performed using Minitab®. All data are reported as average ± standard deviation of the means.

8.3 RESULTS

8.3.1 Gross Morphology

The gross morphology of the SIS scaffolds is shown in **Figure 32**. The loading regimen had no visible effect on the mechanical integrity of the scaffolds, with scaffolds appearing intact and maintaining their original dimensions following 4 hours of both constant and dynamic stimulation.

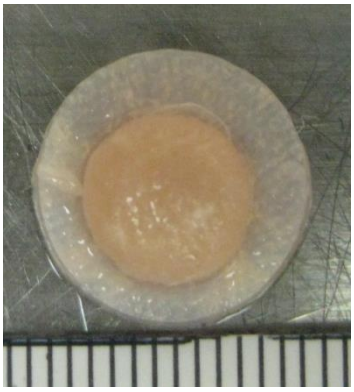

Figure 32. Gross Morphology of SIS scaffold in free swelling control group. Ruler marks are 1 mm apart.

8.3.2 Histology

The hematoxylin and eosin stain of the cell-seeded SIS is shown in **Figure 33a**. There was evidence of cell attachment on the periphery of the pillow portion of the SIS scaffold. Cells were distributed throughout the scaffold but in low numbers.

The apoptosis stain of the SIS scaffold is shown in **Figure 33b**. The stain was compared against both positive and negative control sections taken from the same sample. Few cells staining dark brown, indicating apoptosis, were identified amongst healthy cells in the SIS scaffold.

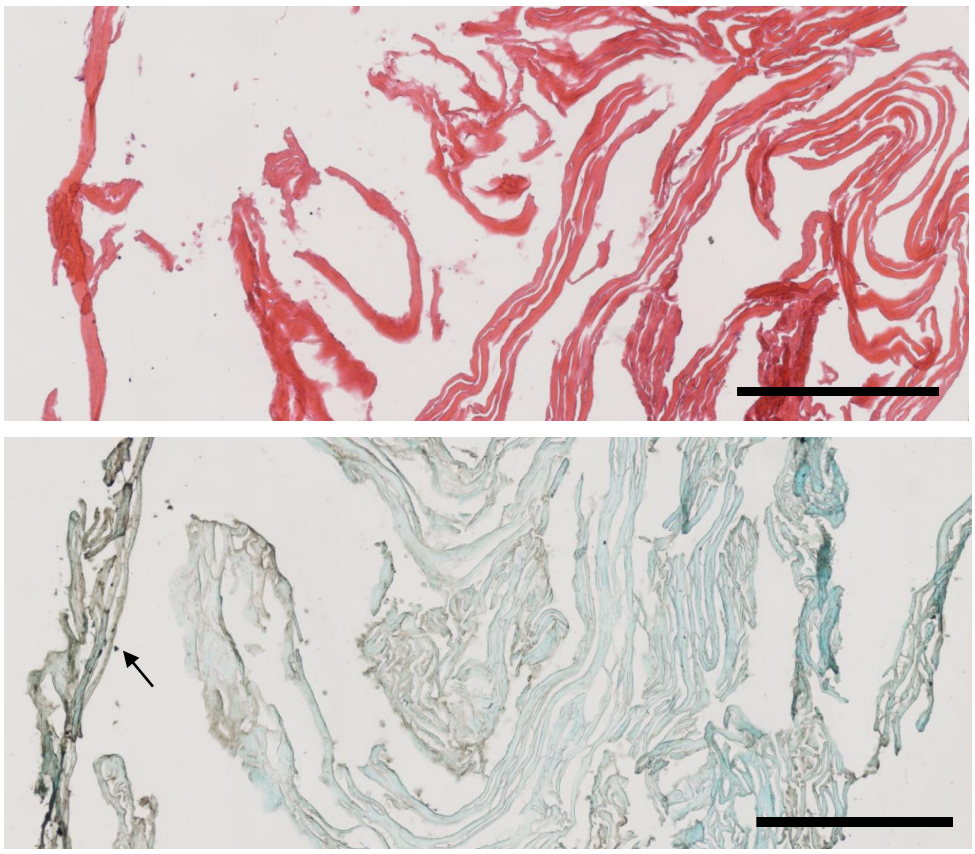

Figure 33. A. Hematoxylin and eosin staining and B. Apoptosis stain of free swelling SIS scaffold. Arrow points to darkened apoptotic cell in panel B. Scale bar is 500 µm.

8.3.3 Gene Expression

The results from the gene expression analysis are shown in **Figure 34**. Genes of interest were normalized to HPRT housekeeping gene, which showed the least variation in expression across groups when compared to 18s. A two-way ANOVA revealed no overall effect for mechanical stimulation or chemical stimulation on the relative expression of collagen type I **(Figure 34a**). There was a significant effect between the interaction of mechanical and chemical stimulation ($p < 0.05$) with post hoc testing showing a significant increase in collagen type I gene expression in the dynamic chondrogenic media group when compared to the constant chondrogenic media group (2.1 fold). There was also a significant increase in the dynamic chondrogenic media group compared to the dynamic basal medium group (1.8 fold). Gene expression for collagen type II was not detected in any group (threshold cycle >35).

Mechanical and chemical stimulation had no effect on the aggrecan gene expression of BMSCs seeded in ECM scaffolds **(Figure 34b**). There were also no significant interaction effects found between groups for relative aggrecan gene expression. There was a significant overall effect of chemical stimulation on decorin gene expression with chondrogenic media groups expressing 3.0 fold more decorin than basal medium groups regardless of form of mechanical stimulation (**Figure 34c**) ($p < 0.05$).

Chemical stimulation had a significant overall effect on CD146 gene expression (Fig. 4D) ($p < 0.05$). Post hoc testing revealed significantly higher expression of CD146 in the dynamic chondrogenic media group when compared to free swelling, constant, and dynamic basal medium groups (3.2, 2.3, and 3.6 fold, respectively). Both mechanical and chemical stimulation had an overall effect on NG2 relative expression (**Figure 34e**). Scaffolds in the dynamic groups expressed significantly more NG2 than those in the constant groups (1.6 fold) (*p*

< .05). Scaffolds in the chondrogenic media groups also expressed significantly more NG2 than those in the basal medium groups (2.9 fold) ($p < .05$). The interaction effect between mechanical and chemical stimulation was also significant. The dynamic chondrogenic group had significantly greater NG2 expression than the constant and free swelling chondrogenic groups (2.0 and 1.7 fold, respectively). Also, the dynamic chondrogenic group had significantly greater NG2 expression than the dynamic basal medium group (4.5 fold).

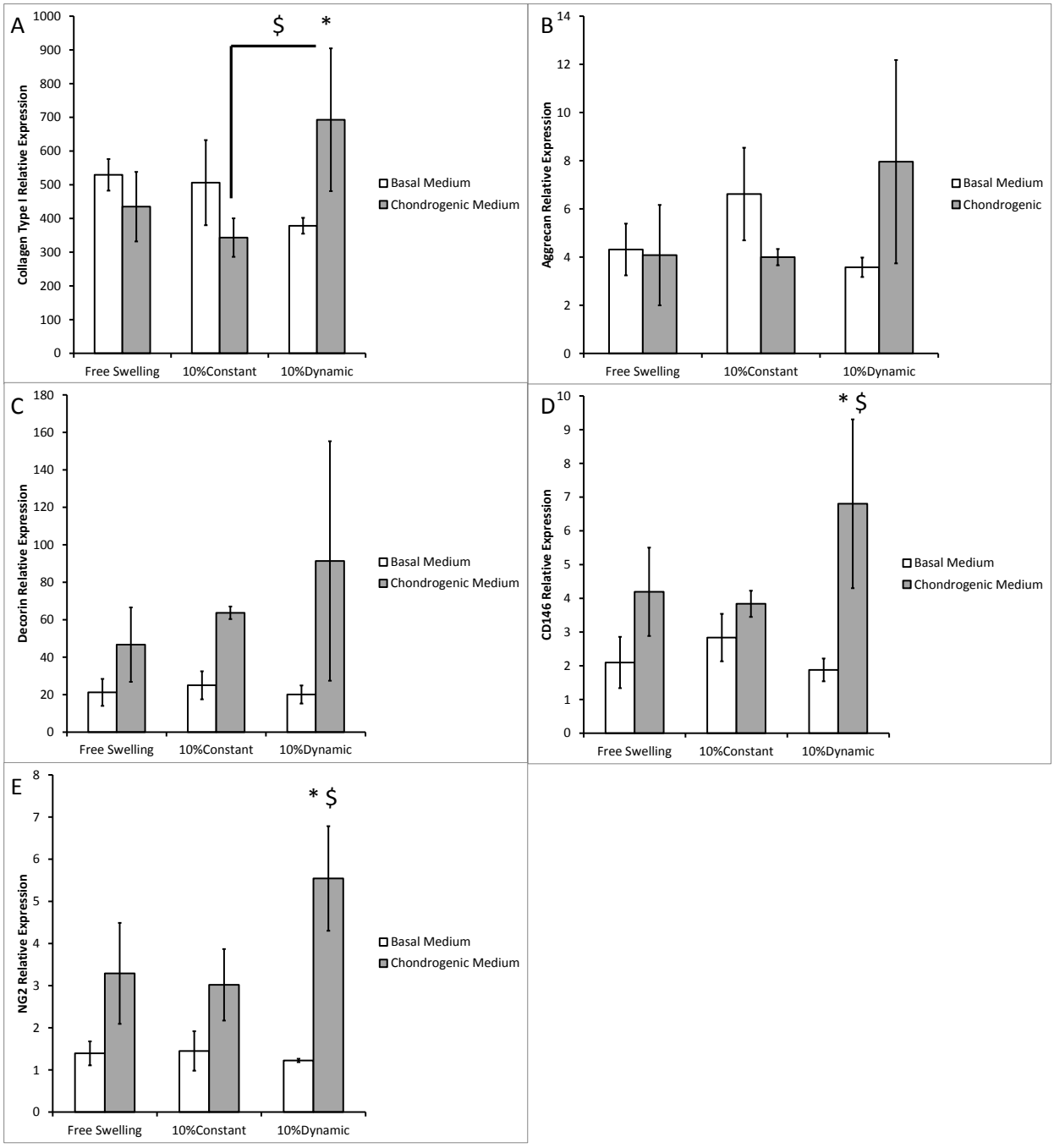

Figure 34. Relative gene expression of A. collagen type I, B. aggrecan, C. decorin, D. CD146, and E. NG2 to HPRT housekeeping gene. *=significant within mechanical stimulus group $p<0.05$ $=significant within chemical stimulus group $p<0.05$ Error bars are +/- standard deviation.

8.4 DISCUSSION

The results show that both chemical and mechanical stimulation do have a synergistic effect on hBMSC fibrochondrogenic differentiation within the ECM SIS scaffold environment. After four hours, there were differences in the relative expression of collagen type I, decorin, CD146, and NG2 in hBMSCs among scaffolds exposed to chondrogenic differentiation media and dynamic mechanical stimulation. The combination of dynamic mechanical stimulation and chondrogenic media caused the most significant increase in fibrocartilage gene expression. Within this system, these two stimuli work together to enhance cell differentiation.

Histology showed that cells were attached and distributed throughout the scaffold but in low numbers. Nevertheless, apoptosis staining revealed that the majority of cells within the scaffold were viable. The seeding technique utilized in this study was injection seeding, with scaffolds cultured on an orbital shaker overnight to improve nutrient diffusion and cell distribution. However, in order to improve on scaffold seeding efficiency for future studies, an optimized set of seeding parameters including suspension volume, cell number, scaffold hydration time, needle size, injection number, and seal reinforcement was identified. (**Table 12**) It was determined that the main contributor to reduction in seeding efficiency was fluid leaking from the scaffold where the sheet meets the pillow. (Error! Reference source not found.) In order to minimize this effect, the edges of the scaffold were sealed with cyanoacrylate. Additionally, using a smaller 30 gauge needle (from 25 gauge) and only one injection site minimized the loss of cells through the needle puncture point. Allowing a hydration time of 3-5 hours before seeding allowed for sufficient penetration of the needle (as opposed to seeding dry scaffolds) but minimized the loss of mechanical integrity due to degradation (after 12+ hours of hydration). Decreasing the suspension volume from 30 µl to 20 µl and increasing the cell

number (from 1 to 2 million) also resulted in an overall increase in scaffold cellularity. As shown in **Figure 35**, adjusting these cell seeding parameters allowed for a significant increase in scaffold cellularity which is critical for achieving more accurate and repeatable results in future studies.

While there were no overall effects of mechanical stimulation observed on the collagen type I, aggrecan, and decorin fibrochondrogenic markers in this study, the interaction between mechanical and chemical stimulation did prove to be influential. Specifically, collagen type I gene expression was enhanced by the synergistic effect of both dynamic compressive loading and treatment with chondrogenic media. This is consistent with results reported in the literature using progenitor cells on multiple types of scaffolds [152, 153]. There were no differences observed between the chondrogenic and basal medium groups in the constant loading group in this study. This could be attributed to limited nutrient diffusion in the constant and free swelling groups when compared to the dynamic loading group. Hydrostatic pressure, which has been shown to increase collagen type I production in TMJ disc cells [122], may be a more effective way of applying constant compressive loads. Worth noting, there was a slight difference in HPRT takeoff cycle between the dynamic loading group treated with chondrogenic media and all other groups (<1 cycle). Due to this variation, it must be recognized that the elevated gene expression levels in this group could be attributed to changes in cellular metabolism. Future studies should be performed to validate changes in fibrochondrogenesis as a result of chemical and mechanical stimulation.

Interestingly, stem cell markers CD146 and NG2 were both significantly upregulated by the introduction of chondrogenic media. It has been shown that osmotic pressure, glucose levels, and TGF may upregulate cell adhesion molecule (CAM) CD146 [154]. Similarly, NG2, which

also exhibited upregulation in response to mechanical stimulation, is associated with the onset of chondrogenesis in-vivo [155]. It is possible that within this experimental study, these markers for multipotency indicated an initial differentiation response. Longer term studies should be performed in the future to elucidate the effect of cellular differentiation on the expression of these markers over time.

Due to the vascularity of the discal attachments, it is hypothesized that perivascular stem cells (PVSCs) may be a more accurate model for studying the effect of loading on migrant progenitor cells in ECM scaffolds. A preliminary comparison between human PVSCs and hBMSCs was performed and it was shown that after several passages PVSCs had significantly higher NG2 and CD146 gene expression than hBMSCs. This suggests that PVSCs better maintain their differentiation potential through expansion, and may prove to be a more technically feasible cell source for future studies. PVSCs should be further examined in the ECM environment to determine how their response to mechanical and chemical stimulation compares to hBMSCs.

This study demonstrated the short term response of progenitor cells to both mechanical loading and chemical stimulation within the ECM TMJ disc scaffold environment. Mechanical stimulation does appear to have an effect on the early fibrochondrogenesis of hBMSCs in ECM scaffolds, possibly helping to explain the exceptional performance of these scaffolds in the loaded joint environment in-vivo. Based on the results of this study, we can conclude that after four hours both mechanical and chemical stimuli play a key role in the differentiation of multipotent stem cells towards a fibrocartilage lineage within the ECM scaffold milieu.

Table 12. Suspension volumes, cell numbers, hydration times, needle gauges, injection numbers, and reinforcement methods utilized to optimize scaffold seeding. Highlighted values indicate the optimum combination of variables for high cellularity as indicated by hematoxylin and eosin staining of scaffolds.

Suspension volume (µl)	Cell Number	Scaffold hydration time	Needle gauge	Number of injections	Seal reinforcement
30	$\approx 1 \times 10^6$	None	25	1	None
20	$\approx 2 \times 10^6$	3-5 hrs	30	2	Cyanoacrylate
		12 hrs		>2	
		24 hrs			

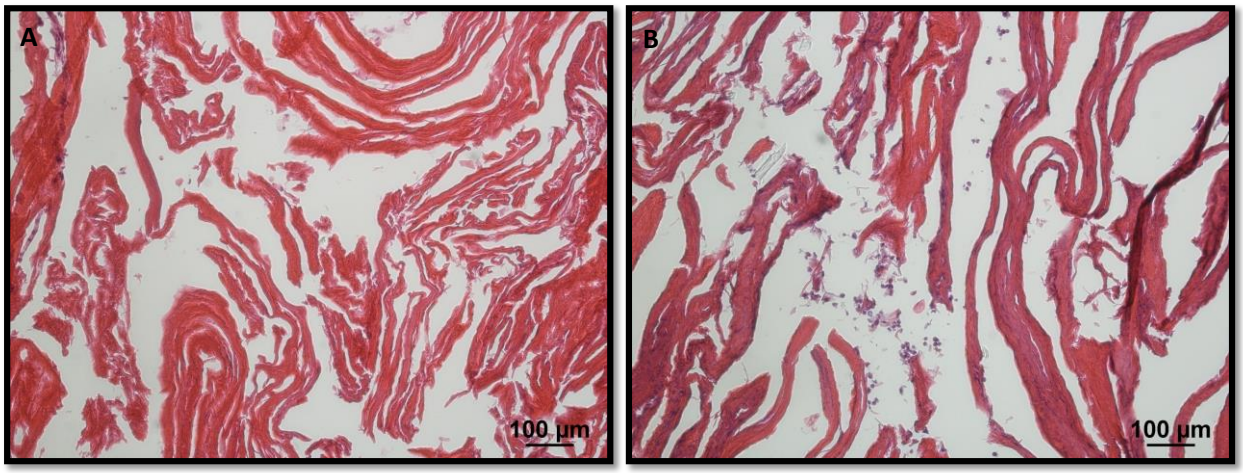

Figure 35. Hematoxylin and Eosin staining comparing non-optimized (A) to optimized (B) cell seeding using conditions outlined in Table 12.

9.0 CONCLUSION

The chief hypothesis of this thesis, that there is a set of culture conditions, including bioactive ions and/or compressive loading, and scaffolds that will stimulate cells to produce fibrocartilage has been demonstrated. At high concentrations, magnesium ions exhibit the ability to allow for fibrocartilage regeneration in-vitro. Poly (glycerol sebacate) (PGS) is a substrate conducive to fibrochondrocyte infiltration and extracellular matrix (ECM) regeneration. The mechanical properties of PGS also allow for the transmission of forces from the scaffold to the cells, impacting the patterning of collagen type I deposition. Within the bioactive environment of ECM scaffolds, compressive mechanical loading results in increased fibrochondrogenic gene expression of human bone marrow stromal cells (hBMSCs). The mechanical and biochemical properties of regenerated tissues have been compared against the characterized properties of the TMJ disc and condylar cartilage.

The compressive mechanical properties and biochemical content of the goat TMJ disc and mandibular condylar cartilage were determined (Chapter 3). It was shown that there is no statistical variation between the medial, lateral, and intermediate zone regions of either tissue type. The results indicated that the TMJ disc exhibits a significantly greater tangent modulus than the MCC from 20% to 50% strain with values ranging from 729 ± 267 to 2413 ± 406 kPa and 363 ± 169 to 1677 ± 538 kPa, respectively ($p < .05$). The collagen content of the TMJ disc was significantly greater than the MCC, while the opposite held for the glycosaminoglycan

(GAG) and DNA content. The mandibular condylar cartilage, despite having significantly higher GAG content, is significantly less stiff than the TMJ disc under compression. These results support the recent findings of Willard et al. [156], which determined that GAG abundance under 10% per dry weight does not necessarily correlate with compressive mechanical properties. The average compressive behavior of each tissue was successfully fit to the transversely isotropic biphasic model at strain levels ranging from 10-30%. The characterization of the mechanical and biochemical properties of the goat TMJ fibrocartilage provided the success criteria for tissue engineered fibrocartilage.

Magnesium was investigated for its effect on fibrocartilage regeneration potential (Chapter 4). The hypothesis that magnesium ions will allow for regeneration of fibrocartilage was confirmed, and at 4 weeks, there were no significant differences in compressive tangent modulus and total matrix production between constructs cultured in 20 mM Mg^{2+} and the 0.8 mM Mg^{2+} control (435 ± 47 kPa). Additionally, scaffoldless constructs cultured in 20 mM $MgSO_4$ group exhibited a significantly higher collagen type II/I ratio compared to the control. Fibrochondrocytes exhibited a high degree of resilience to increasing magnesium ion concentrations.

A pilot study was performed where pure magnesium rods were implanted in the porcine mandibular condyle (Chapter 7). After four weeks, the magnesium rods had degraded less than 10% and there was evidence of new bone formation at the implant interface. These results, coupled with the in-vitro findings which demonstrate the resilience of fibrocartilage to high magnesium concentrations, indicate the potential application of magnesium as a bioactive biomaterial that can be used for tissue engineering of the mandibular condyle.

PGS, an elastomeric biodegradable scaffold material, was also investigated for its potential as an in-vitro TMJ fibrocartilage scaffold. Goat costal fibrochondrocytes were seeded on PGS at three seeding densities (25, 50, 100 million cells/mL scaffold), respectively, and cultured for 24 hours, 2 weeks, and 4 weeks (Chapter 5). Histological staining revealed an abundance of both collagen and GAG throughout the highest seeding density scaffolds at 4 weeks. There was also a significant increase in the cellular content over the four week period, showing that the scaffolds promoted cell attachment and proliferation. The compression tangent modulus was significantly greater at 4 weeks than 24 hours (123.6 ± 86 kPa and 26.2 ± 5 kPa, respectively) (seeding density groups combined) ($p<0.001$), with no differences between seeding groups at each time point. After 4 weeks, the tangent modulus of the low seeding density group was in a similar range of the goat TMJ disc (180 ± 127 kPa compared to 304 ± 141 kPa, respectively). The results showed that cell seeding density and culture time do have an effect on both the biochemical and biomechanical properties of PGS scaffolds. These findings demonstrated that PGS has great potential as a scaffold material for TMJ disc engineering.

In order to improve upon cell seeding efficiency and also explore the effect of mechanical stimulation, PGS scaffolds were seeded with fibrochondrocytes using a spinner flask and then subjected to a mechanical loading regimen (Chapter 6). The results showed that spinner flask culture allowed for high seeding efficiency, homogenous cell distribution, cell survival at the center of the scaffold, and abundant ECM production. The hypothesis that PGS will allow for transmission of forces from the scaffold to the cells was validated. Mechanically stimulated scaffolds had a collagen type I shell extending along the perimeter of the scaffold. The compressive tangent modulus of the PGS scaffolds at 8 weeks reached 667 ± 270 kPa, exceeding near-native mechanical properties. The differences in matrix organization between the

mechanically stimulated and control groups indicated that there was a cellular response to compressive loading and that PGS scaffolds provide the necessary elastomeric properties to allow for transmission of forces from scaffold to cells.

A pilot study was performed where a defect in the posterior aspect of the porcine mandibular condyle was created and filled with PGS (Chapter 7). At four weeks, over half the loss in bone volume was restored in defects filled with PGS. Taken with the in-vitro findings, these results indicate the potential of PGS to be utilized at the bone-fibrocartilage interface of the mandibular condyle. Future studies should validate the utility of PGS as a mechano-transductive material that allows for cell infiltration and site-specific tissue regeneration.

Uniaxial loading was applied to hBMSCs seeded on ECM scaffolds (Chapter 8). The hypothesis that mechanical loading results in an increase in fibrochondrogenic gene expression of progenitor cells seeded on ECM scaffolds was proven. After four hours, there were differences in the relative expression of collagen type I, decorin, CD146, and NG2 of hBMSCs in scaffolds exposed to chondrogenic differentiation media and/or mechanical stimulation. The results showed that the combination of dynamic mechanical stimulation and chondrogenic media caused the most significant increase in fibrocartilage gene expression. Future studies should utilize perivascular stem cells to examine the effect of mechanical loading on fibrochondrogenic gene expression. Due to the vascularity of the discal attachments, it is speculated that perivascular stem cells may prove to be a more relevant multipotential cell model for determining the effect of mechanical loading on migrant progenitor cells in ECM scaffolds.

An important factor in the eventual success or failure of an implantable device is the host immune response. Constructive remodeling of a biologic implant material can be defined as the process of a material degrading and being replaced by site-appropriate tissue [157]. When

implanted decellularized ECM devices are surrounded by healthy tissue and subjected to appropriate mechanical loading, the success criteria includes a cascade of host immunological responses that results in the transition from a proinflammatory phenotype to a constructive, remodeling phenotype [157]. Therefore, the use of various biomaterials for TMJ tissue engineering applications will require that engineered constructs elicit the appropriate immune response that results in the regeneration of tissues with appropriate biomechanical and biochemical properties. Taking this into account, it is important that tissue-engineered devices not necessarily achieve the same properties as the native tissue upon implantation, but rather have enough mechanical integrity to withstand the local loading environment while the device remodels.

The results of this thesis prove that magnesium, PGS, and porcine-derived ECM all have the potential to be utilized in TMJ fibrocartilage tissue engineering applications. Future studies should validate the efficacy of using these materials in tandem as part of a composite replacement system. For example, in order to model the potential effectiveness of a magnesium-PGS regenerative device, cells seeded on PGS could be further stimulated with bioactive magnesium ions. Additionally, application of different loading patterns including tensile forces should be examined for their effect on fibrochondrocyte matrix synthesis. In conclusion, the work of this thesis has demonstrated the potential application of various biomaterials to restore form and function to the injured TMJ.

BIBLIOGRAPHY

1. NIH. *TMJ Disorders*. 2010 March 2010; Available from: http://www.nidcr.nih.gov/OralHealth/Topics/TMJ/TMJDisorders.htm.

2. Farrar, W.B. and W.L. McCarty, Jr., *The TMJ dilemma.* J Ala Dent Assoc, 1979. **63**(1): p. 19-26.

3. Almarza, A.J., C.K. Hagandora, and S.E. Henderson, *Animal models of temporomandibular joint disorders: implications for tissue engineering approaches.* Ann Biomed Eng, 2011. **39**(10): p. 2479-90.

4. Dimitroulis, G., *A critical review of interpositional grafts following temporomandibular joint discectomy with an overview of the dermis-fat graft.* Int J Oral Maxillofac Surg, 2011. **40**(6): p. 561-8.

5. Sato, S., S. Goto, and K. Motegi, *Changes of the collagen fibre arrangement of the rabbit temporomandibular joint following discectomy.* J Craniomaxillofac Surg, 2002. **30**(3): p. 178-83.

6. Dimitroulis, G. and J. Slavin, *The effects of unilateral discectomy and condylectomy on the contralateral intact rabbit craniomandibular joint.* J Oral Maxillofac Surg, 2006. **64**(8): p. 1261-6.

7. Sato, S., et al., *Changes of the elastic fibre network of the rabbit temporomandibular joint following discectomy.* J Oral Rehabil, 2002. **29**(9): p. 847-52.

8. Takatsuka, S., et al., *Histologic evaluation of auricular cartilage grafts after discectomy in the rabbit craniomandibular joint.* J Oral Maxillofac Surg, 1996. **54**(10): p. 1216-25; discussion 1225-6.

9. Feinberg, S.E. and E.J. McDonnell, *The use of a collagen sheet as a disc replacement in the rabbit temporomandibular joint.* J Oral Maxillofac Surg, 1995. **53**(5): p. 535-42; discussion 543.

10. Ioannides, C. and J.C. Maltha, *Lyophilized auricular cartilage as a replacement for the interarticular disc of the craniomandibular joint. An experimental study in guinea pigs.* J Craniomaxillofac Surg, 1988. **16**(7): p. 295-300.

11. Ioannides, C. and J.C. Maltha, *Replacement of the interarticular disc of the craniomandibular joint with fresh autogenous sternal or auricular cartilage. An experimental study in guinea pigs.* J Craniomaxillofac Surg, 1988. **16**(8): p. 343-9.

12. Gerstner, G.E. and J.B. Gerstein, *Chewing rate allometry among mammals.* Journal of Mammalogy, 2008. **89**(4): p. 1020-1030.

13. Yaillen, D.M., et al., *Temporomandibular joint meniscectomy--effects on joint structure and masticatory function in macaca fascicularis.* J Maxillofac Surg, 1979. **7**(4): p. 255-64.

14. Bjornland, T. and H.R. Haanaes, *Discectomy of the temporomandibular joint: an experimental study in monkeys.* J Craniomaxillofac Surg, 1999. **27**(2): p. 113-6.

15. Tucker, M.R., M.C. Kennady, and J.R. Jacoway, *Autogenous auricular cartilage implantation following discectomy in the primate temporomandibular joint.* J Oral Maxillofac Surg, 1990. **48**(1): p. 38-44.

16. Tong, A.C. and H. Tideman, *A comparative study on meniscectomy and autogenous graft replacement of the Rhesus monkey temporomandibular joint articular disc--Part I.* Int J Oral Maxillofac Surg, 2000. **29**(2): p. 140-5.

17. Thyne, G.M., et al., *Temporalis muscle as a disc replacement in the temporomandibular joint of sheep.* J Oral Maxillofac Surg, 1992. **50**(9): p. 979-87; discussion 987-8.

18. Tong, A.C. and H. Tideman, *A comparative study on meniscectomy and autogenous graft replacement of the rhesus monkey temporomandibular joint articular disc--Part II.* Int J Oral Maxillofac Surg, 2000. **29**(2): p. 146-54.

19. Herring, S.W., *TMJ anatomy and animal models.* J Musculoskelet Neuronal Interact, 2003. **3**(4): p. 391-4; discussion 406-7.

20. Holmlund, A.B., S. Axelsson, and G.W. Gynther, *A comparison of discectomy and arthroscopic lysis and lavage for the treatment of chronic closed lock of the temporomandibular joint: A randomized outcome study.* Journal of Oral and Maxillofacial Surgery, 2001. **59**(9): p. 972-977.

21. Nyberg, J., R. Adell, and B. Svensson, *Temporomandibular joint discectomy for treatment of unilateral internal derangements--a 5 year follow-up evaluation.* Int J Oral Maxillofac Surg, 2004. **33**(1): p. 8-12.

22. Miloro, M. and B. Henriksen, *Discectomy as the primary surgical option for internal derangement of the temporomandibular joint.* J Oral Maxillofac Surg, 2010. **68**(4): p. 782-9.

23. Bjornland, T. and T.A. Larheim, *Discectomy of the temporomandibular joint: 3-year follow-up as a predictor of the 10-year outcome.* J Oral Maxillofac Surg, 2003. **61**(1): p. 55-60.

24. Hall, H.D., et al., *Prospective multicenter comparison of 4 temporomandibular joint operations.* J Oral Maxillofac Surg, 2005. **63**(8): p. 1174-9.

25. Dimitroulis, G., *The use of dermis grafts after discectomy for internal derangement of the temporomandibular joint.* Journal of Oral and Maxillofacial Surgery, 2005. **63**(2): p. 173-178.

26. Dimitroulis, G., *Condylar morphology after temporomandibular joint discectomy with interpositional abdominal dermis-fat graft.* J Oral Maxillofac Surg, 2011. **69**(2): p. 439-46.

27. Dimitroulis, G., M. McCullough, and W. Morrison, *Quality-of-life survey comparing patients before and after discectomy of the temporomandibular joint.* J Oral Maxillofac Surg, 2010. **68**(1): p. 101-6.

28. Krug, J., et al., *Influence of discoplasty and discectomy of the temporomandibular joint on elimination of pain and restricted mouth opening.* Acta Medica (Hradec Kralove), 2004. **47**(1): p. 47-53.

29. Schellhas, K.P., *Internal derangement of the temporomandibular joint: radiologic staging with clinical, surgical, and pathologic correlation.* Magn Reson Imaging, 1989. **7**(5): p. 495-515.

30. Schellhas, K.P., C.H. Wilkes, and C.C. Baker, *Facial pain, headache, and temporomandibular joint inflammation.* Headache, 1989. **29**(4): p. 229-32.

31. Schellhas, K.P., et al., *The diagnosis of temporomandibular joint disease: two-compartment arthrography and MR.* AJR Am J Roentgenol, 1988. **151**(2): p. 341-50.

32. Schellhas, K.P., M.A. Piper, and M.R. Omlie, *Facial Skeleton Remodeling Due to Temporomandibular-Joint Degeneration - an Imaging Study of 100 Patients (Reprinted from Ajnr, Vol 11, Pg 541-555, 1990).* Cranio-the Journal of Craniomandibular Practice, 1992. **10**(3): p. 248-259.

33. Yabuta, N.H., et al., *Diagnostic arthroscopy of temporomandibular joint on outpatient. Review of 47 examinations, 40 cases.* J Osaka Univ Dent Sch, 1993. **33**: p. 58-64.

34. Takaku, S., et al., *A comparison between magnetic resonance imaging and pathologic findings in patients with disc displacement.* Journal of Oral and Maxillofacial Surgery, 1998. **56**(2): p. 171-176.

35. Chen, M.J., et al., *Synovial Chondromatosis in the Inferior Compartment of the Temporomandibular Joint: Different Stages With Different Treatments.* Journal of Oral and Maxillofacial Surgery, 2012. **70**(1): p. E32-E38.

36. Takaku, S., T. Sano, and M. Yoshida, *Long-term magnetic resonance imaging after temporomandibular joint discectomy without replacement.* Journal of Oral and Maxillofacial Surgery, 2000. **58**(7): p. 739-745.

37. Flygare, L., et al., *Cartilage matrix macromolecules in lavage fluid of temporomandibular joints before and 6 months after diskectomy.* European Journal of Oral Sciences, 1997. **105**(4): p. 369-372.

38. Takaku, S., et al., *Correlation of magnetic resonance imaging and surgical findings in patients with temporomandibular joint disorders.* J Oral Maxillofac Surg, 1995. **53**(11): p. 1283-8.

39. Schellhas, K.P., et al., *Mr of Osteochondritis Dissecans and Avascular Necrosis of the Mandibular Condyle.* American Journal of Roentgenology, 1989. **152**(3): p. 551-560.

40. Kirk, W.S., *Risk factors and initial surgical failures of TMJ arthrotomy and arthroplasty: A four to nine year evaluation of 303 surgical procedures.* Cranio-the Journal of Craniomandibular Practice, 1998. **16**(3): p. 154-161.

41. Petersson, A., L. Eriksson, and P.L. Westesson, *MR images mimic disc after discectomy.* Dentomaxillofacial Radiology, 2005. **34**(4): p. 237-239.

42. Persson, S., M.R. Gjerdet, and K. Tornes, *Metal fragment in the temporomandibular joint: a case report.* International Journal of Oral and Maxillofacial Surgery, 2003. **32**(6): p. 653-655.

43. Shibuya, T., et al., *Synovial osteochondromatosis accompanying an ossified articular disk in the temporomandibular joint: a case report.* Journal of Oral Pathology & Medicine, 2003. **32**(7): p. 441-442.

44. Shibuya, T., et al., *Synovial chondromatosis of the left temporomandibular joint superficially resembling chondrosarcoma: A case report.* Cranio-the Journal of Craniomandibular Practice, 2000. **18**(4): p. 286-288.

45. Mazzonetto, R. and D.B. Spagnoli, *Long-term evaluation of arthroscopic discectomy of the temporomandibular joint using the holmium YAG laser.* Journal of Oral and Maxillofacial Surgery, 2001. **59**(9): p. 1018-1023.

46. Eriksson, L. and P.L. Westesson, *Discectomy as an effective treatment for painful temporomandibular joint internal derangement: A 5-year clinical and radiographic follow-up.* Journal of Oral and Maxillofacial Surgery, 2001. **59**(7): p. 750-758.

47. Widmark, G., et al., *Diskectomy in temporomandibular joints with internal derangement - A follow-up study.* Oral Surgery Oral Medicine Oral Pathology Oral Radiology and Endodontics, 1997. **83**(3): p. 314-320.

48. Widmark, G., et al., *Radiographic morphology in the temporomandibular joint after diskectomy.* Cranio, 1996. **14**(1): p. 37-41.

49. Takaku, S. and T. Toyoda, *Long-term evaluation of discectomy of the temporomandibular joint.* J Oral Maxillofac Surg, 1994. **52**(7): p. 722-6; discussion 727-8.

50. Widmark, G., *On surgical intervention in the temporomandibular joint.* Swed Dent J Suppl, 1997. **123**: p. 1-87.

51. Eriksson, L. and P.L. Westesson, *Diskectomy in the treatment of anterior disk displacement of the temporomandibular joint. A clinical and radiologic one-year follow-up study.* J Prosthet Dent, 1986. **55**(1): p. 106-16.

52. Hansson, L.G., L. Eriksson, and P.L. Westesson, *Magnetic-Resonance Evaluation after Temporomandibular-Joint Diskectomy.* Oral Surgery Oral Medicine Oral Pathology Oral Radiology and Endodontics, 1992. **74**(6): p. 801-810.

53. Westesson, P.L., J.M. Cohen, and R.H. Tallents, *Magnetic-Resonance-Imaging of Temporomandibular-Joint after Surgical-Treatment of Internal Derangement.* Oral Surgery Oral Medicine Oral Pathology Oral Radiology and Endodontics, 1991. **71**(4): p. 407-411.

54. Schliephake, H., et al., *Long-term results of the use of silicone sheets after diskectomy in the temporomandibular joint: clinical, radiographic and histopathologic findings.* International Journal of Oral and Maxillofacial Surgery, 1999. **28**(5): p. 323-329.

55. Florine, B.L., et al., *Tomographic evaluation of temporomandibular joints following discoplasty or placement of polytetrafluoroethylene implants.* J Oral Maxillofac Surg, 1988. **46**(3): p. 183-8.

56. Spagnoli, D. and J.N. Kent, *Multicenter Evaluation of Temporomandibular-Joint Proplast-Teflon Disk Implant.* Oral Surgery Oral Medicine Oral Pathology Oral Radiology and Endodontics, 1992. **74**(4): p. 411-421.

57. Heffez, L., et al., *CT evaluation of TMJ disc replacement with a Proplast-Teflon laminate.* J Oral Maxillofac Surg, 1987. **45**(8): p. 657-65.

58. Westesson, P.L., L. Eriksson, and C. Lindstrom, *Destructive lesions of the mandibular condyle following diskectomy with temporary silicone implant.* Oral Surg Oral Med Oral Pathol, 1987. **63**(2): p. 143-50.

59. Lieberman, J.M., et al., *Dermal grafts of the temporomandibular joint: postoperative appearance on MR images.* Radiology, 1990. **176**(1): p. 199-203.

60. Wilkes, C.H., *Internal derangements of the temporomandibular joint. Pathological variations.* Arch Otolaryngol Head Neck Surg, 1989. **115**(4): p. 469-77.

61. Mejersjo, C. and L. Hollender, *Radiography of the temporomandibular joint in female patients with TMJ pain or dysfunction. A seven year follow-up.* Acta Radiol Diagn (Stockh), 1984. **25**(3): p. 169-76.

62. Zarb, G.A. and G.E. Carlsson, *Temporomandibular disorders: osteoarthritis.* J Orofac Pain, 1999. **13**(4): p. 295-306.

63. Tanaka, E. and T. van Eijden, *Biomechanical behavior of the temporomandibular joint disc.* Crit Rev Oral Biol Med, 2003. **14**(2): p. 138-50.

64. Hansson, T. and B. Nordstrom, *Thickness of the soft tissue layers and articular disk in temporomandibular*
joints with deviations in form. Acta Odontol Scand, 1977. **35**(6): p. 281.

65. Bibb, C., A. Pullinger, and F. Baldioceda, *Serial variation in histological character of articular soft tissue in young human adult temporomandibular joint condyles.* Arch Oral Biol, 1993. **38**(4): p. 343-352.

66. Pullinger, A., F. Baldioceda, and C. Bibb, *Relationship ofTMJ articular soft tissue to underlying bone in young adult condyles.* J Dent Res, 1990. **69**(8): p. 1512-1518.

67. Bosshardt-Luehrs, C. and H. Luder, *Cartilage matrix production and chondrocyte enlargement*
as contributors to mandibular condylar growth in monkeys (Macaca fascicularis). Am J Orthod Dentofacial Orthop, 1991. **100**(4): p. 362-369.

68. Anderson, D.E. and K.A. Athanasiou, *Passaged goat costal chondrocytes provide a feasible cell source for temporomandibular joint tissue engineering.* Ann Biomed Eng, 2008. **36**(12): p. 1992-2001.

69. Anderson, D.E. and K.A. Athanasiou, *A comparison of primary and passaged chondrocytes for use in engineering the temporomandibular joint.* Arch Oral Biol, 2009. **54**(2): p. 138-45.

70. Delatte, M., et al., *Primary and secondary cartilages of the neonatal rat: the femoral head and the mandibular condyle.* Eur J Oral Sci, 2004. **112**(2): p. 156-62.

71. Poikela, A., et al., *Unilateral masticatory function changes the proteoglycan content of mandibular condylar cartilage in rabbit.* Cells Tissues Organs, 2000. **167**(1): p. 49-57.

72. Almarza, A.J., et al., *Biochemical analysis of the porcine temporomandibular joint disc.* Br J Oral Maxillofac Surg, 2006. **44**(2): p. 124-8.

73. Mow, V.C., et al., *Biphasic creep and stress relaxation of articular cartilage in compression? Theory and experiments.* J Biomech Eng, 1980. **102**(1): p. 73-84.

74. Shengyi, T. and Y. Xu, *Biomechanical properties and collagen fiber orientation of TMJ discs in dogs: Part 1. Gross anatomy and collagen fiber orientation of the discs.* J Craniomandib Disord, 1991. **5**(1): p. 28-34.

75. Singh, M. and M.S. Detamore, *Tensile properties of the mandibular condylar cartilage.* J Biomech Eng, 2008. **130**(1): p. 011009.

76. Cohen, B., W.M. Lai, and V.C. Mow, *A transversely isotropic biphasic model for unconfined compression of growth plate and chondroepiphysis.* J Biomech Eng, 1998. **120**(4): p. 491-6.

77. Allen, K.D. and K.A. Athanasiou, *A surface-regional and freeze-thaw characterization of the porcine temporomandibular joint disc.* Ann Biomed Eng, 2005. **33**(7): p. 951-62.

78. Sergerie, K., et al., *Mechanical properties of the porcine growth plate and its three zones from unconfined compression tests.* J Biomech, 2009. **42**(4): p. 510-6.

79. Lepriere, B.M., *Poisson's ratio in orthotropic materials.* AIAA, 1968. **6**(11): p. 2226-2227.

80. Farndale, R.W., C.A. Sayers, and A.J. Barrett, *A direct spectrophotometric microassay for sulfated glycosaminoglycans in cartilage cultures.* Connect Tissue Res, 1982. **9**(4): p. 247-8.

81. Woessner, J.J., *The determination of hydroxyproline in tissue and protein samples containing small proportions of this amino acid.* Archives of Biochemistry and Biophysics, 1961(93): p. 440-7.

82. Kuboki, T., et al., *Viscoelastic properties of the pig temporomandibular joint articular soft tissues of the condyle and disc.* J Dent Res, 1997. **76**(11): p. 1760-9.

83. Allen, K.D. and K.A. Athanasiou, *Viscoelastic characterization of the porcine temporomandibular joint disc under unconfined compression.* J Biomech, 2006. **39**(2): p. 312-22.

84. Singh, M. and M.S. Detamore, *Stress relaxation behavior of mandibular condylar cartilage under high-strain compression.* J Biomech Eng, 2009. **131**(6): p. 061008.

85. Ateshian, G.A., et al., *Finite deformation biphasic material properties of bovine articular cartilage from confined compression experiments.* J Biomech, 1997. **30**(11-12): p. 1157-64.

86. Mak, A.F., W.M. Lai, and V.C. Mow, *Biphasic indentation of articular cartilage--I. Theoretical analysis.* J Biomech, 1987. **20**(7): p. 703-14.

87. Mow, V.C., et al., *Biphasic indentation of articular cartilage--II. A numerical algorithm and an experimental study.* J Biomech, 1989. **22**(8-9): p. 853-61.

88. Kim, K.W., et al., *Biomechanical tissue characterization of the superior joint space of the porcine temporomandibular joint.* Ann Biomed Eng, 2003. **31**(8): p. 924-30.

89. Kuo, J., et al., *The region-dependent biphasic viscoelastic properties of human temporomandibular joint discs under confined compression.* J Biomech. **43**(7): p. 1316-21.

90. Kalpakci, K.N., et al., *An interspecies comparison of the temporomandibular joint disc.* J Dent Res. **90**(2): p. 193-8.

91. Minarelli, A.M., M. Del Santo Junior, and E.A. Liberti, *The structure of the human temporomandibular joint disc: a scanning electron microscopy study.* J Orofac Pain, 1997. **11**(2): p. 95-100.

92. Athanasiou, K.A., et al., *Tissue Engineering of Temporomandibular Joint Cartilage*. 2009 Morgan & Claypool Publishers.

93. Ingawale, S. and T. Goswami, *Temporomandibular joint: disorders, treatments, and biomechanics.* Ann Biomed Eng, 2009. **37**(5): p. 976-96.

94. Hsu, J.T., et al., *Effect of screw fixation on temporomandibular joint condylar prosthesis.* J Oral Maxillofac Surg. **69**(5): p. 1320-8.

95. Kapila, S. and Y. Xie, *Targeted induction of collagenase and stromelysin by relaxin in unprimed and beta-estradiol-primed diarthrodial joint fibrocartilaginous cells but not in synoviocytes.* Lab Invest, 1998. **78**(8): p. 925-38.

96. Kuttila, M., et al., *TMD treatment need in relation to age, gender, stress, and diagnostic subgroup.* J Orofac Pain, 1998. **12**(1): p. 67-74.

97. Li, L.C., J.C. Gao, and Y. Wang, *Evaluation of cyto-toxicity and corrosion behavior of alkali-heat-treated magnesium in simulated body fluid.* Surface & Coatings Technology, 2004. **185**(1): p. 92-98.

98. Witte, F., et al., *In vivo corrosion of four magnesium alloys and the associated bone response.* Biomaterials, 2005. **26**(17): p. 3557-63.

99. Feyerabend, F., et al., *Unphysiologically high magnesium concentrations support chondrocyte proliferation and redifferentiation.* Tissue Eng, 2006. **12**(12): p. 3545-56.

100. Detamore, M.S., et al., *Quantitative analysis and comparative regional investigation of the extracellular matrix of the porcine temporomandibular joint disc.* Matrix Biol, 2005. **24**(1): p. 45-57.

101. Hagandora C.K., C.T.W., and Almarza A.J., *A Comparison of the Mechanical Properties of the Goat Temporomandibular Joint Disc to the Mandibular Condylar Cartilage in Unconfined Compression.* Journal of Dental Biomechanics, 2011. **2011**

102. Loeser, R.F., *Modulation of integrin-mediated attachment of chondrocytes to extracellular matrix proteins by cations, retinoic acid, and transforming growth factor beta.* Exp Cell Res, 1994. **211**(1): p. 17-23.

103. Lee, C.H., et al., *Intra-articular magnesium sulfate (MgSO4) reduces experimental osteoarthritis and nociception: association with attenuation of N-methyl-D-aspartate (NMDA) receptor subunit 1 phosphorylation and apoptosis in rat chondrocytes.* Osteoarthritis Cartilage, 2009. **17**(11): p. 1485-93.

104. Fischer, J., et al., *Interference of magnesium corrosion with tetrazolium-based cytotoxicity assays.* Acta Biomater. **6**(5): p. 1813-23.

105. Witte, F., et al., *In vitro and in vivo corrosion measurements of magnesium alloys.* Biomaterials, 2006. **27**(7): p. 1013-8.

106. Donzelli, P.S., et al., *Biphasic finite element simulation of the TMJ disc from in vivo kinematic and geometric measurements.* J Biomech, 2004. **37**(11): p. 1787-91.

107. Beek, M., et al., *Three-dimensional finite element analysis of the human temporomandibular joint disc.* J Biomech, 2000. **33**(3): p. 307-16.

108. Tanaka, E., et al., *Three-dimensional finite element analysis of human temporomandibular joint with and without disc displacement during jaw opening.* Med Eng Phys, 2004. **26**(6): p. 503-11.

109. Dimitroulis, G., *The use of dermis grafts after discectomy for internal derangement of the temporomandibular joint.* J Oral Maxillofac Surg, 2005. **63**(2): p. 173-8.

110. Lai, W.F., J. Bowley, and J.G. Burch, *Evaluation of shear stress of the human temporomandibular joint disc.* J Orofac Pain, 1998. **12**(2): p. 153-9.

111. Klompmaker, J., et al., *Porous implants for knee joint meniscus reconstruction: a preliminary study on the role of pore sizes in ingrowth and differentiation of fibrocartilage.* Clin Mater, 1993. **14**(1): p. 1-11.

112. Almarza, A.J. and K.A. Athanasiou, *Seeding techniques and scaffolding choice for tissue engineering of the temporomandibular joint disk.* Tissue Eng, 2004. **10**(11-12): p. 1787-95.

113. Almarza, A.J. and K.A. Athanasiou, *Effects of initial cell seeding density for the tissue engineering of the temporomandibular joint disc.* Ann Biomed Eng, 2005. **33**(7): p. 943-50.

114. Allen, K.D. and K.A. Athanasiou, *Scaffold and growth factor selection in temporomandibular joint disc engineering.* J Dent Res, 2008. **87**(2): p. 180-5.

115. Kalpakci, K.N., et al., *An Interspecies Comparison of the Temporomandibular Joint Disc.* J Dent Res, 2011. **90**(2): p. 193-198.

116. Wang, Y., Y.M. Kim, and R. Langer, *In vivo degradation characteristics of poly(glycerol sebacate).* J Biomed Mater Res A, 2003. **66**(1): p. 192-7.

117. Gao, J., P.M. Crapo, and Y. Wang, *Macroporous elastomeric scaffolds with extensive micropores for soft tissue engineering.* Tissue Eng, 2006. **12**(4): p. 917-25.

118. Hagandora, C.K., M.A. Tudares, and A.J. Almarza, *The effect of magnesium ion concentration on the fibrocartilage regeneration potential of goat costal chondrocytes.* Ann Biomed Eng, 2012. **40**(3): p. 688-96.

119. Hagandora, C.K., Chase, T.W., and Almarza, A.J., *A Comparison of the Mechanical Properties of the Goat Temporomandibular Joint Disc to the Mandibular Condylar Cartilage in Unconfined Compression.* J Dent Biomech, 2011. **2011**: p. 212385.

120. Allen, K.D. and K.A. Athanasiou, *Tissue Engineering of the TMJ disc: a review.* Tissue Eng, 2006. **12**(5): p. 1183-96.

121. Almarza, A.J. and K.A. Athanasiou, *Evaluation of three growth factors in combinations of two for temporomandibular joint disc tissue engineering.* Archives of Oral Biology, 2006. **51**(3): p. 215-221.

122. Almarza, A.J. and K.A. Athanasiou, *Effects of hydrostatic pressure on TMJ disc cells.* Tissue Eng, 2006. **12**(5): p. 1285-94.

123. Gunja, N.J. and K.A. Athanasiou, *Effects of Co-Cultures of Meniscus Cells and Articular Chondrocytes on PLLA Scaffolds.* Biotechnology and Bioengineering, 2009. **103**(4): p. 808-816.

124. Ingawale, S. and T. Goswami, *Temporomandibular Joint: Disorders, Treatments, and Biomechanics.* Annals of Biomedical Engineering, 2009. **37**(5): p. 976-996.

125. Hagandora, C.K., et al., *Poly (glycerol sebacate): a novel scaffold material for temporomandibular joint disc engineering.* Tissue Eng Part A. **19**(5-6): p. 729-37.

126. MacIntosh, R.B., *The use of autogenous tissues for temporomandibular joint reconstruction.* Journal of Oral and Maxillofacial Surgery, 2000. **58**(1): p. 63-69.

127. Hagandora, C.K., M.A. Tudares, and A.J. Almarza, *The Effect of Magnesium Ion Concentration on the Fibrocartilage Regeneration Potential of Goat Costal Chondrocytes.* Ann Biomed Eng.

128. Hagandora, C.K., M.A. Tudares, and A.J. Almarza, *The Effect of Magnesium Ion Concentration on the Fibrocartilage Regeneration Potential of Goat Costal Chondrocytes.* Annals of Biomedical Engineering, 2012. **40**(3): p. 688-696.

129. Hagandora, C.K., T.W. Chase, and A.J. Almarza, *A comparison of the mechanical properties of the goat temporomandibular joint disc to the mandibular condylar cartilage in unconfined compression.* J Dent Biomech. **2011**: p. 212385.

130. Natoli, R.M., C.M. Revell, and K.A. Athanasiou, *Chondroitinase ABC treatment results in greater tensile properties of self-assembled tissue-engineered articular cartilage.* Tissue Eng Part A, 2009. **15**(10): p. 3119-28.

131. Murphy, M.K., et al., *Enhancing post-expansion chondrogenic potential of costochondral cells in self-assembled neocartilage.* PLoS One. **8**(2): p. e56983.

132. Henderson, S.E., et al., *Magnesium alloys as a biomaterial for degradable craniofacial screws.* Acta Biomater.

133. Zaky, S.H., et al., *Poly(Glycerol sebacate) elastomer: a novel material for mechanically loaded bone regeneration.* Tissue Eng Part A. **20**(1-2): p. 45-53.

134. Berg, R., *Contribution to the applied and topographical anatomy of the temporomandibular joint of some domestic mammals with particular reference to the partial resp. total resection of the articular disc.* Folia Morphol (Praha), 1973. **21**(2): p. 202-4.

135. Bermejo, A., O. Gonzalez, and J.M. Gonzalez, *The pig as an animal model for experimentation on the temporomandibular articular complex.* Oral Surg Oral Med Oral Pathol, 1993. **75**(1): p. 18-23.

136. Strom, D., et al., *Gross anatomy of the mandibular joint and masticatory muscles in the domestic pig (Sus scrofa).* Arch Oral Biol, 1986. **31**(11): p. 763-8.

137. Lee, K.W. and Y. Wang, *Elastomeric PGS scaffolds in arterial tissue engineering.* J Vis Exp, (50).

138. Tanaka, E. and T. van Eijden, *Biomechanical behavior of the temporomandibular joint disc.* Critical Reviews in Oral Biology & Medicine, 2003. **14**(2): p. 138-150.

139. Wolford, L.M., *Temporomandibular joint devices: Treatment factors and outcomes.* Oral Surgery Oral Medicine Oral Pathology Oral Radiology and Endodontics, 1997. **83**(1): p. 143-149.

140. Dimitroulis, G., *Condylar Morphology After Temporomandibular Joint Discectomy With Interpositional Abdominal Dermis-Fat Graft.* Journal of Oral and Maxillofacial Surgery, 2011. **69**(2): p. 439-446.

141. Thyne, G.M., et al., *Temporalis Muscle as a Disk Replacement in the Temporomandibular-Joint of Sheep.* Journal of Oral and Maxillofacial Surgery, 1992. **50**(9): p. 979-987.

142. Tong, A.C.K. and H. Tideman, *A comparative study on meniscectomy and autogenous graft replacement of the rhesus monkey temporomandibular joint articular disc - Part II.* International Journal of Oral and Maxillofacial Surgery, 2000. **29**(2): p. 146-154.

143. Badylak, S.F., *Xenogeneic extracellular matrix as a scaffold for tissue reconstruction.* Transplant Immunology, 2004. **12**(3-4): p. 367-377.

144. Brown, B.N., et al., *Inductive, scaffold-based, regenerative medicine approach to reconstruction of the temporomandibular joint disk.* J Oral Maxillofac Surg. **70**(11): p. 2656-68.

145. Brown, B.N. and S.F. Badylak, *Extracellular matrix as an inductive scaffold for functional tissue reconstruction.* Transl Res.

146. Wang, L.M., et al., *A Comparison of Human Bone Marrow-Derived Mesenchymal Stem Cells and Human Umbilical Cord-Derived Mesenchymal Stromal Cells for Cartilage Tissue Engineering.* Tissue Engineering Part A, 2009. **15**(8): p. 2259-2266.

147. Li, J., et al., *The influence of delayed compressive stress on TGF-beta 1-induced chondrogenic differentiation of rat BMSCs through Smad-dependent and Smad-independent pathways.* Biomaterials, 2012. **33**(33): p. 8395-8405.

148. Gilbert, T.W., et al., *Gene expression by fibroblasts seeded on small intestinal submucosa and subjected to cyclic stretching.* Tissue Engineering, 2007. **13**(6): p. 1313-1323.

149. Brown, B.N., et al., *Inductive, Scaffold-Based, Regenerative Medicine Approach to Reconstruction of the Temporomandibular Joint Disk.* Journal of Oral and Maxillofacial Surgery, 2012. **70**(11): p. 2656-2668.

150. Taboas, J.M., *Mechanobiologic regulation of skeletal progenitor cell differentiation*. 2004. 1 v.

151. Pellegrinelli, V., et al., *Endothelial cells from visceral adipose tissue disrupt adipocyte functions in a three-dimensional setting: partial rescue by angiopoietin-1*. Diabetes. **63**(2): p. 535-49.

152. Haugh, M.G., et al., *Temporal and Spatial Changes in Cartilage-Matrix-Specific Gene Expression in Mesenchymal Stem Cells in Response to Dynamic Compression.* Tissue Engineering Part A, 2011. **17**(23-24): p. 3085-3093.

153. O'Conor, C.J., N. Case, and F. Guilak, *Mechanical regulation of chondrogenesis.* Stem Cell Res Ther. **4**(4): p. 61.

154. Wang, Z.Q. and X.Y. Yan, *CD146, a multi-functional molecule beyond adhesion.* Cancer Letters, 2013. **330**(2): p. 150-162.

155. Nishiyama, A., K.J. Dahlin, and W.B. Stallcup, *The Expression of Ng2 Proteoglycan in the Developing Rat Limb.* Development, 1991. **111**(4): p. 933-944.

156. Willard, V.P., et al., *The regional contribution of glycosaminoglycans to temporomandibular joint disc compressive properties.* J Biomech Eng. **134**(1): p. 011011.

157. Badylak, S.F., *Decellularized Allogeneic and Xenogeneic Tissue as a Bioscaffold for Regenerative Medicine: Factors that Influence the Host Response.* Ann Biomed Eng. **42**(7): p. 1517-27.